

Dist: A

AD-A284 959

N PAGE

Form Approved  
OMB No. 0704-0188

1

Public  
Information  
Center  
Dept. of  
Com. &  
Tech. Info.



How to use this form. (including the time for reviewing instructions, searching existing data sources, gathering of additional data, reviewing comments regarding the burden estimates or any other aspect of this report, including suggestions for reducing the burden.) Send comments regarding this burden estimate or any other aspect of this report, including suggestions for reducing the burden, to Washington Headquarters Services, Directorate for Information Operations and Reports, 1215 Jefferson Davis Highway, Suite 1204, Arlington, VA 22202-4302, and to the Office of Management and Budget, Paperwork Reduction Project (0704-0188), Washington, DC 20503.

1. AG

August 25, 1994

3. REPORT TYPE AND DATES COVERED

Interim April 1, 1993 to June 30, 1994

4. TITLE AND SUBTITLE

Study of the Compression Behavior of High Performance Fibers

ANAL

5. FUNDING NUMBERS

62102F  
2419/00

6. AUTHOR(S)

Satish Kumar et al.

7. PERFORMING ORGANIZATION NAME(S) AND ADDRESS(ES)

Georgia Tech Research Corporation  
Office of Contract Administration.  
Atlanta GA 30332-0420

8. PERFORMING ORGANIZATION REPORT NUMBER

AEOSR-TR- 94 0560

9. SPONSORING / MONITORING AGENCY NAME(S) AND ADDRESS(ES)

AFOSR/DEML  
Building 410, Bolling AFB DC  
20332-6448 D-LEE

10. SPONSORING / MONITORING AGENCY REPORT NUMBER

AFOSR-91-0194

11. SUPPLEMENTARY NOTES

12a. DISTRIBUTION / AVAILABILITY STATEMENT

Approved for public release distribution unlimited

A

12b. DISTRIBUTION STATEMENT

DTIC  
SELECTE  
SEP 23 1994  
S B D

13. ABSTRACT (Maximum 200 words)

Kink band analysis has been carried out in PBZT, methyl PBZT, and Kevlar samples. Methyl PBZT and methyl PBO samples heat treated to various times and temperatures have been studied using swelling behavior in 85% and 100% methane sulfonic acid. Raman spectroscopic studies have been carried out on PAN precursor fiber, and the fiber stabilized and carbonized at different temperatures ( 270, 400, 800, 1800, 2800°C). A study on the compression behavior of polymeric resins has been conducted. A review has been written on the compression behavior of polymeric materials. PBO/sulfuric acid interaction has been studied using thermogravimetric analysis, wide angle x-ray diffraction, and using <sup>13</sup>C solid state NMR.

14. SUBJECT TERMS

15. NUMBER OF PAGES

16. PRICE CODE

17. SECURITY CLASSIFICATION OF REPORT

u

18. SECURITY CLASSIFICATION OF THIS PAGE

u

19. SECURITY CLASSIFICATION OF ABSTRACT

u

20. LIMITATION OF ABSTRACT

u

1004

## Table of Contents

	page
Summary	2
I Compression Kink Band Analysis	5
II Crosslinking Studies	8
III Raman Spectroscopy on Carbon Fibers	14
IV Compression Behavior of Glassy Polymers	21
V Compression Behavior of Fibers	55
VI PBO/sulfuric acid interaction	110

<b>Accession For</b>	
NTIS GRA&I	<input checked="" type="checkbox"/>
DTIC TAB	<input type="checkbox"/>
Unannounced	<input type="checkbox"/>
Justification	
By _____	
Distribution/	
Availability Codes	
Dist	Avail and/or Special
A-1	

DTIC QUALITY INSPECTED 3

94-31006



115 P5

94 9 28 0 52

**Annual (Interim) Technical Report  
SUMMARY**

**Title: Study of the Compression Behavior of High Performance Fibers**

**Principal Investigator: Satish Kumar**

**Inclusive Dates: April 1, 1993 - June 30, 1994**

**Grant number: AFOSR-91-0194**

**Research Personnel:**

1. Dr. Victor Kozey - post-doctoral fellow
2. Vinay Mehta - Ph.D student
3. Xiaodong Hu - Ph.D. student

**Publications: In the third year of the project, the following papers have been published or submitted for publication/presentation:**

1. N. Venkatasubramanian, M.B. Polk, Satish Kumar, and L.T.Gelbaum, "Structural Investigations on Lewis Acid-Mediated Solubilization of poly (p-phenylenebenzobisthiazole) in an Aprotic Solvent". J. Polym. Sci. (Phys ed.), 31 (1993) p. 1965-1973.
2. V. V. Kozey and S. Kumar, "Compression Behavior of Materials: Part I - Glassy Polymers", accepted for publication in J. Mater. Res.
3. V. R. Mehta and Satish Kumar, Temperature Dependent Torsional Properties of High Performance Fibers and their Relevance to Compressive Strength " Accepted for publication in J. Mater. Sci.
4. M. Sahafeyan and Satish Kumar, "Tensile and Compressive Behavior of Poly(para-phenylene benzobisthiazole) fibers, Submitted for publication in J. Appl. Polym. Sci.
5. V. V. Kozey, H. Jiang, V. R. Mehta, and S. Kumar, " Compressive Behavior of Materials - part 2: High Performance Fibers", Submitted to J. Mater. Research.
6. C. P. Chang, S. C. Bhatia, and S. Kumar, "Investigation of Carbon Fibers and Charcoal Powder by FT-Raman Spectroscopy", Presented at Pittsburgh Conf., Chicago, March 1994.
7. B. Yang, V. R. Mehta, S. B. Warner, S. Kumar, and D. L. Vanderhart,

- "Rigid-rod Polymer Solvent Interaction", Presented at the Spring 1994 meeting of the Amer. Phys. Soc., Pittsburgh, March 1994.**
- 8. V. R. Mehta and S. Kumar, "On the Evidence of Crosslinking and its influence on Compressive Strength in Rigid-rod Polymers", Presented at the Spring 1994 meeting of the Amer. Phys. Soc., Pittsburgh, March 1994.**
  - 9. X. Hu, M. B. Polk, and S. Kumar, "Three Dimensionally Crosslinkable Rigid-rod Polymer Systems", Presented at the Spring meeting of the Materials Research Soc., San Francisco, April 1994.**
  - 10. V. R. Mehta and S. Kumar, "Crosslinking in Rigid-rod Polymers and its influence on Compressive Strength", Presented at the Spring meeting of the Materials Research Soc., San Francisco, April 1994.**
  - 11. S. Kumar, "Scattering Studies on Rigid-rod Polymeric Fibers", Invited paper presented at 1994 Denver X-ray Conference", Steamboat Springs (CO), August 1994.**

**In the third year of the project, work has been carried out in the following areas:**

**I. From the study of approximately 100 specimens tested in recoil for each type of fiber, it was observed that the average kink angle from the fiber axis was 57° in Kevlar 49, and 69° in 50:50 methyl PBZT and in 100% PBZT. Helical kink bands are observed in Kevlar 49, the percentage of fibers in which helical kink bands are observed increases from 0% at 0.30 GPa to 37% at 0.50 GPa. Preliminary data on the kink bands and kink band analysis is presented.**

**II. Methyl pendant PBZT and methyl pendant PBO fibers were heat treated for varying times and temperatures in air and in nitrogen. Attempts were made to characterize the degree of crosslinking by swelling studies and infra red spectroscopy. Preliminary data on this study is presented.**

**III. Raman spectroscopic studies have been carried out on PAN precursor, fiber stabilized at 270°C, and heat treated at 400, 800, 1700, and at 2800°C. Raman studies were also carried out on number of commercial fibers. Precursor fiber shows raman frequencies characteristic of PAN and the presence of C=O band from copolymers. Fiber stabilized at 270°C shows the presence of NH or NH<sub>2</sub>, aromatic CH, CH<sub>2</sub>, CHO, C=N, C=C=O, C=C or C-N groups, and vibrations corresponding to ring breathing or ring stretch. Fiber heat treated to 800°C exhibit a rather unique spectrum, with a very broad band in the range of 1000 to 1500 cm<sup>-1</sup> with a maximum at 1317 cm<sup>-1</sup>. Such a broad single band has previously not been reported for any of the carbon materials. However the fact that a distinct band at 1575 cm<sup>-1</sup> is not observed, also suggests that the graphitic structure has not yet began to form. Fibers heat**

treated to higher temperatures, show both the G (1575  $\text{cm}^{-1}$ ) and D (1320  $\text{cm}^{-1}$ ) line.

IV. A study on the compression behavior of polymeric resins was conducted. Conclusions from this study are summarized here: Both thermoset and thermoplastic glassy polymers exhibit yielding under compression. On yielding, localization of plastic deformation in the form of shear bands can occur if stress-strain diagram showed stress softening. Compressive yield strength of thermoplastic and thermosetting glassy polymers is proportional to their glass transition temperature and density. Compressive yield strength of glassy polymers does not exhibit a unique dependence on the tensile and shear modulus. Experimental data indicates that the compressive and tensile moduli of glassy polymers are equal. Compressive yield strength of thermosetting resins does not exhibit a unique dependence on tensile strength. Inclusion of rigid particles, short, or long fibers increases compressive yield strength of glassy polymers.

V. A review has been written (and submitted for publication) on the Compressive Behavior of Polymeric Materials - Part 2 (High Performance Fibers). A complete copy of this review is enclosed in this report.

VI. We have studied the interaction of PBO with sulfuric acid. Based on the TGA analysis, it was observed that PBO/sulfuric acid system vacuum dried at 160°C for three hours, only one molecule of sulfuric acid is present per PBO repeat unit. Based on WAXD, it was concluded that this molecule fits in the PBO lattice. Based on  $^{13}\text{C}$  Solid State NMR, it was observed that the field on the carbon atoms attached to the nitrogen was effected, while the carbon attached to the oxygen was not effected. This suggests that under these conditions sulfuric acid interacts with nitrogen and not with oxygen.

Work in the following areas is planned for the coming year:

1. Additional 100% methyl pendant PBZT has been synthesized at the Air Force Materials Laboratory. This will be spun into fibers. Heat treatment, crosslinking studies (both from swelling and from Spectroscopic studies), and compressive strength studies will be carried out on this fiber. Attempts will be made to quantify the degree of crosslinking.
2. Recoil kink band analysis, currently underway will be completed and submitted for publication.
3. Attempts will be made to synthesize the following structure into high molecular weight polymer. On completion of the polymer synthesis, crosslinking studies, fiber spinning, and fiber compression testing will be carried out.

## Part I.

### COMPRESSION KINK BAND ANALYSIS IN HIGH PERFORMANCE POLYMERIC FIBERS

Recoil tested fibers were mounted on SEM stubs and sputter coated with gold (coating thickness about 400 Å) and examined on Hitachi S-800 SEM. From SEM micrographs, angle of kink with the fiber axis (as shown in the schematic in figure 1), and the distance from the rigid clamp boundary at which the kink is observed are noted. Test results on the following fibers are reported in the present work:

Kevlar®49

As-spun MePBZT/PBZT (50:50)

MePBZT/PBZT (50:50), heat treated in N<sub>2</sub>

MePBZT (100 %), heat treated in air

Both the as spun and the heat-treated methyl pendant PBZT samples were received from the Air Force Materials Laboratory. Kevlar 49 fibers were obtained from DuPont Co.

The compressive strength values based on recoil failure probability of 0.5 are given in Table 1.

Table 1 : Recoil Compressive Strength for different polymeric fibers

Fiber	Compressive Strength (GPa) (50 % recoil failure probability)
Kevlar®49	0.37
pristine PBZT <sup>+</sup>	0.27
as-spun MePBZT (50:50)	0.40

Comparison with the literature data on pristine PBZT shows that the compressive strength of as-spun methyl PBZT (0.4 GPa) is almost 50 % higher than that of pristine PBZT (0.27 GPa).

**Types of Kink Geometries :** Under recoil compression, various kink geometries are observed which can be broadly classified into five categories:

- Shear type of failure with kink angle generally different than 45°
- plastic deformation in shear with angle  $\neq$  45°
- splitting or the fibrillation in the kinked region
- intersecting (two or more) kinks
- helical kinks

Kevlar®49 fiber often exhibit helical kinks, while no helical kinks were observed in MePBZT. One possible clue in understanding this behavior may be the flexibility in

Kevlar<sup>®</sup>49 due to CONH (amide group).

Kink Band Analysis: Table 2 shows the analysis of kinks in various systems. The distance at which first kink is observed for both the types of fibers with wide variation in diameters are similar (about 0.3 mm). The kink angle values are also given in Table II.

Table 2 : Kink band analysis for various polymeric fibers

Fiber (No. of Kinks/ No. of Total Observations)	Ave. diameter ( $\mu\text{m}$ )	Range of kink angles with the fiber axis ( $^{\circ}$ )	Ave. angle of kink with the fiber axis ( $^{\circ}$ )	Ave. distance of first kink from glued end (mm)
Kevlar <sup>®</sup> 49 (66/127)	13.0	32 - 90	57	0.27
As spun MePBZT/PBZT (50:50) (65/147)	33.0	40 - 90	69	0.30
MePBZT/PBZT (50:50), HT at 500 $^{\circ}$ C in N <sub>2</sub> (28/90)	31.0	40 - 90	69	0.45
MePBZT (100 %), HT in air at 500 $^{\circ}$ C (44/89)	31.0	44 - 90	69	0.34

In Kevlar 49 we monitored the distance at which the first kink is observed as a function of the applied stress. Table 3 gives this data and suggests that the applied stress level does not systematically influence the distance at which the first kink is observed. Number of kinks in Kevlar 49 are helical and percentage of helical kinks increases with increasing compressive stress as shown in Table 3.

This supports the energy based compression failure mechanism since it is believed that helical kinks provide an efficient mechanism for dissipation of strain energy due to development of large surface area.

Table 3 : Data for Kevlar®49

---

Compr. Stress (GPa)	No. of Data pts.	Ave. Distance at which First Kink is observed (mm)	Percentage of Helical Kinks Observed
0.30	4	0.25	0.0
0.35	12	0.16	14.0
0.40	15	0.36	15.0
0.45	21	0.21	30.0
0.50	14	0.36	37.0

---

Summary: Analysis of a large number of kinks suggests that kinks develop at angle of 30-90°, a rather large range but the average angle observed for Kevlar®49 is 57° whereas that for MePBZT it is 69°. Various kink geometries are observed but helical geometry is typical for Kevlar®49 amongst others which is not observed in case of MePBZT. As-spun MePBZT has almost 50 % higher recoil compressive strength (0.4 GPa) over that of unmodified heat treated PBZT (0.27 GPa).

## Part II

### CROSSLINKING STUDIES

Crosslinking studies have been carried out on pristine PBZT, PBO, and methyl PBZT and methyl PBO fibers heat treated at 400 and 500°C for various times. The possible crosslinking mechanism in the presence of air and in nitrogen is shown in Figure 1 a and b respectively. The swelling studies have been carried out in 85% methane sulfonic acid and the swelling results are presented in Figures 2 a and b. The 85% methane sulfonic acid was used, in order to follow the swelling quantitatively, as in 100% methane sulfonic acid fiber dissolution in some cases is rather fast. From the limited results presented in Figure 2, following observations are made.

Methyl PBZT fiber heat treated for 1 hour exhibit no swelling. Moderate swelling was observed in the fiber heat treated at 400°C for one hour. Other fibers swell significantly. However the swelling front was delayed on increasing heat treatment time. This suggest the formation of skin and core structure. If the lack of swelling is due to crosslinking, then the observation of delayed front suggest that in the early stages of heat treatment crosslinking has occurred in skin of the fiber and not in the core. Decrease in the fiber diameter after few hours, in the fibers that do exhibit swelling, is a result of the beginning of the fiber dissolution. Photographs taken on the optical microscope, during the swelling process confirm this. However, no change in the fiber diameter was observed, even after 1000 minutes in methane sulfonic acid, in the methyl pendant PBZT fiber heat treated at 500°C for one hour. Methyl PBZT fiber heat treated at 500°C for one hour exhibited swelling in 100% methane sulfonic acid, but did not dissolve after two days. However we must point out here that a pristine PBZT fiber also heat treated at 500°C for one hour did not dissolve in 100% MSA after two days. The question, therefore is, if the lack of dissolution in pristine PBZT is due to crosslinking , as generally attributed to the case of methyl PBZT, or is a result of enhanced order. Our experiments in this regard using WAXS, elemental analysis, and FTIR suggest that the lack of swelling in pristine PBZT is a result of enhanced order and not that of crosslinking. We would

like to confirm this result by further studies. At the same time this raises the question, whether the lack of swelling in the methyl system is really due to crosslinking? Therefore, the direct evidence of crosslinking from spectroscopic technique is sought.

A rather surprising result was observed on as spun PBO, which did not swell at all in 85% methane sulfonic acid, yet dissolved rather quickly in 100% MSA. this result suggests that the minimum concentration of MSA in water required for PBO dissolution is above 85%, while that for as spun PBZT is below 85%. This suggests that there are intrinsic differences in the dissolution characteristics of the two polymers (PBO and PBZT).

# Possible Mechanisms of Crosslinking

(I)

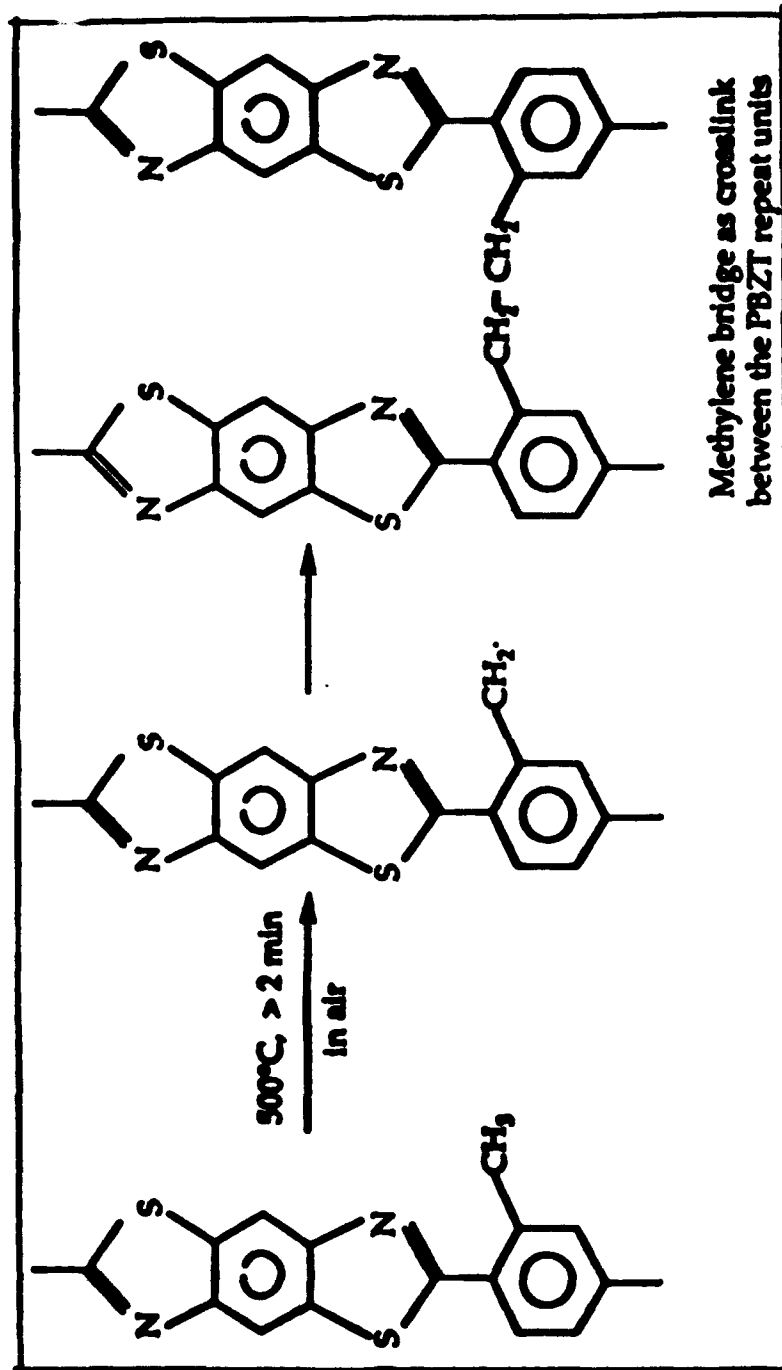


Figure 1a

(II)

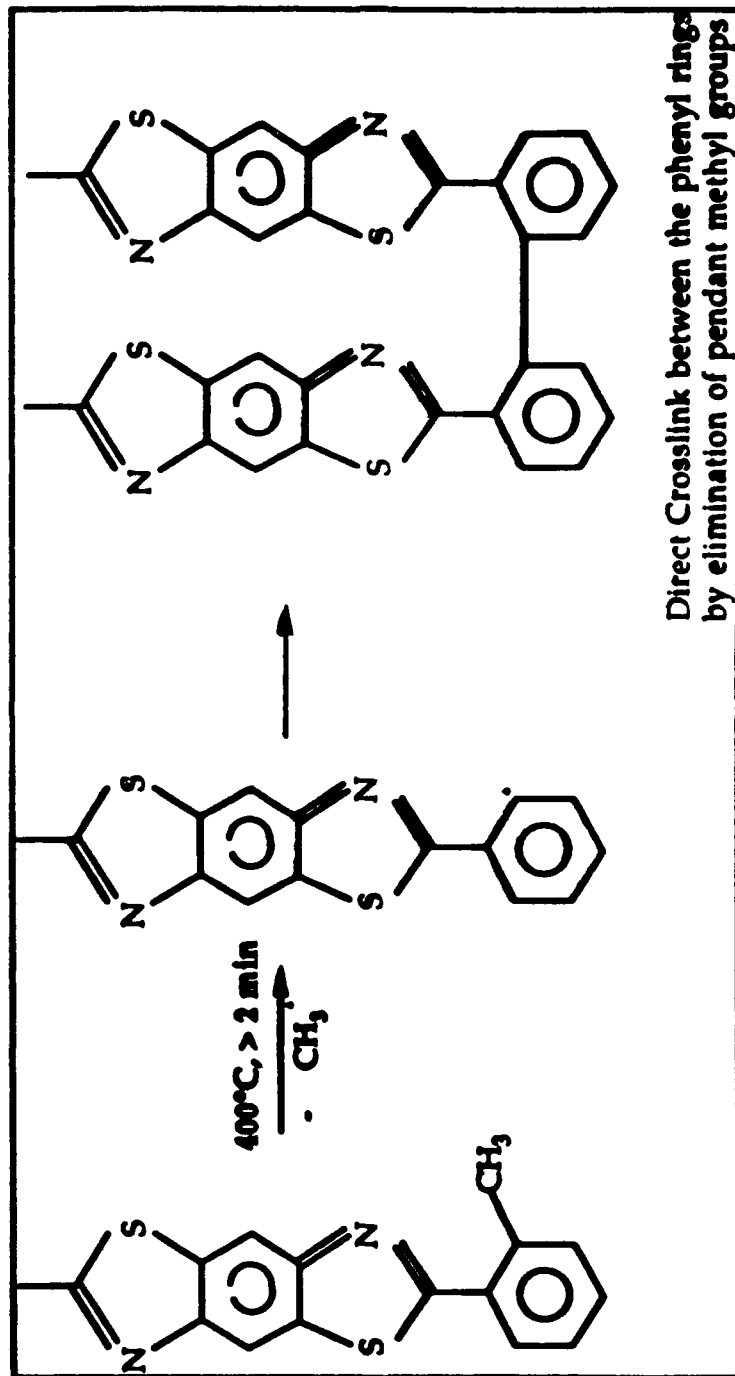


Figure 1b

# Swelling Behaviour of MePBZT

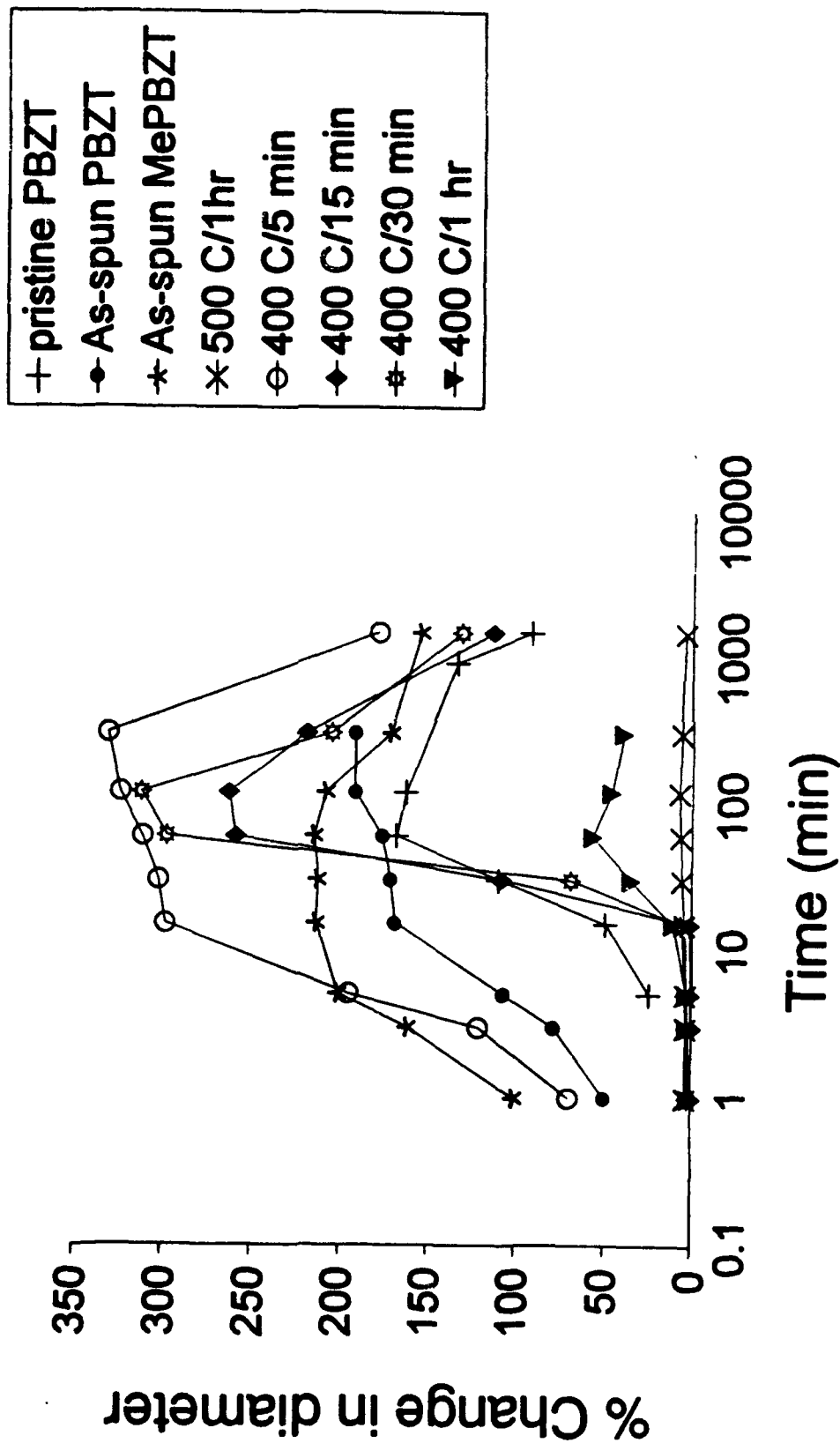


Figure 2a . Swelling agent used is Methane Sulfonic Acid (MSA) <sup>85%</sup>

# Swelling behavior of MePBO

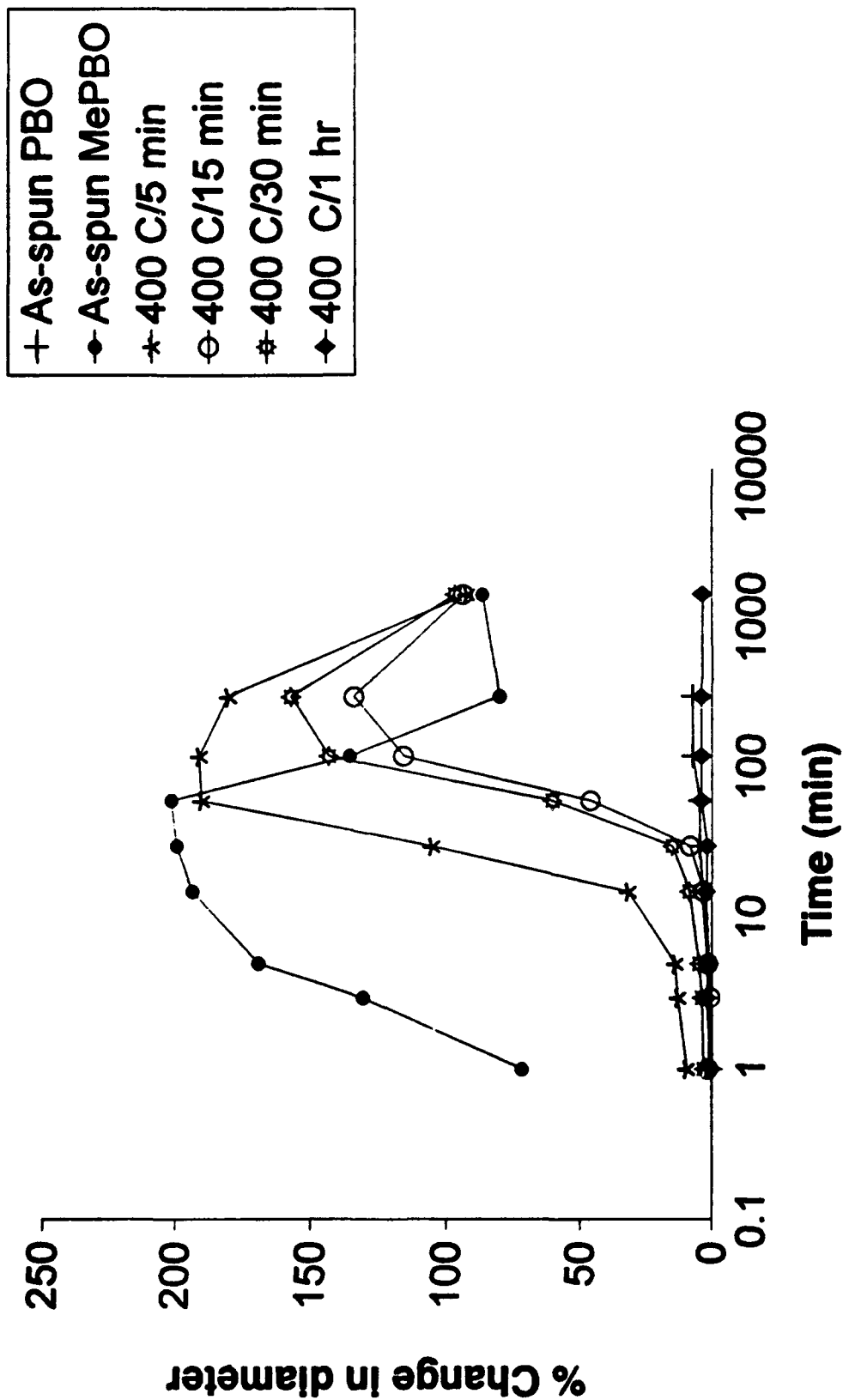


Figure 2b Swelling agent used is 5% Methane Sulfonic (MSA)

### Part III

## RAMAN SPECTROSCOPIC STUDIES ON CARBON FIBERS

The detailed Raman spectroscopic study of experimental and commercial carbon fibers are reported in a recent M.S. thesis[1]. Raman Spectroscopic study was carried out on experimental carbon fiber samples received from courtalids. Spectra were obtained on fiber samples in KBr pellets using Nicolet FT Raman 950 system. The Nicolet raman system utilized a near infra red excitation source, neodymium:yttrium aluminum garnet ( $\text{Nd}^{3+}$ :YAG) laser, with its primary emission at  $1.064 \mu\text{m}$  ( $9393 \text{ cm}^{-1}$ ). The system was allowed to stabilize for thirty minutes before data collection was started. The laser output used for the present study ranged from 0.2 to 0.6 W.

Raman Spectra of fibers heat-treated to 400, 800, and  $1700^\circ\text{C}$  are given in Figures 1 to 3. For comparison, the raman spectra of single graphite crystal, and that of the diamond is given in Figures 4 and 5 respectively. At  $400^\circ\text{C}$ , the fusion of heterocyclic ring occurs. At  $400^\circ\text{C}$  the absorption corresponding to aromatic CH stretch ( $3183 \text{ cm}^{-1}$ ), ring breathing ( $900 \text{ cm}^{-1}$ ) and the CH deformation ( $650 \text{ cm}^{-1}$ ) have vanished. Heat treatment temperature of  $800^\circ\text{C}$  represents the early stage of carbonization. At this temperature dramatic changes have occurred in the raman spectrum. A very broad band is observed in the  $1600$  to  $1000 \text{ cm}^{-1}$  region with a maximum at  $1317 \text{ cm}^{-1}$ . The observation of broad band has been reported by Richter et al. [2] for various amorphous carbon films. These broad bands were observed in the  $1700$  to  $1000 \text{ cm}^{-1}$  region with a maxima at  $1530$  -  $1565 \text{ cm}^{-1}$  depending on the amorphous carbon film type. They suggest that this band is a composite of two overlapping bands, the G ( $1530$ - $1565 \text{ cm}^{-1}$ ) and the D ( $1325$  -  $1345 \text{ cm}^{-1}$ ) bands. With the maximum a approximately  $1565 \text{ cm}^{-1}$ , Richter et al. proposed that the carbon atoms in the amorphous carbon films were dominated by  $\text{sp}^2$  type hybridization (80 - 94%). However the peak observed in our sample (Figure 2) peaks at  $1317 \text{ cm}^{-1}$  and not at  $1530 \text{ cm}^{-1}$  as seen in Richter's samples and is in the  $1000$  to  $1600 \text{ cm}^{-1}$  range as opposed to  $1000$  -  $1700 \text{ cm}^{-1}$  range in their. These comparison point to the fact that the band observed in our spectrum is distinctly different from the one reported by

Richter et al. The band in our sample is clearly D line dominated.

Knight and White[3] have studied various type of diamond and diamond like carbon films and observed that the raman spectra of cut single crystal diamond and polycrystalline diamond have a sharp band at  $1319\text{ cm}^{-1}$  which has been assigned to small regions of hexagonal diamond or satellite faults. The geometry of hexagonal regions in diamond is unknown. The location and broadness of this band indicates that most of the carbon atoms may have  $sp^3$  hybridization, but the arrangement of carbon atoms is not tetrahedral as in a diamond crystal. The broadening effect is also observed when the synthetic diamond films are formed from dehydrogenation of organic material. Based on these literature observations, the broad band observed in  $800^\circ\text{C}$  carbon fiber can be attributed to hexagonal diamond type structure, the broadness of the band may be due to disorder in the structure.

Figure 6 gives the fiber compressive strength vs the relative integrated intensities of the G and the D bands for various carbon fibers. This Figure shows that the compressive strength increases with decreasing integrated intensity ratio ( $A_G / A_D$ ). This suggest that increased graphitic order (increase in the G line intensity and decrease in the D line intensity, either due to diamond like bonding or due to disorder) decreases compressive strength.

1. C. P. Chang, M. S. Thesis, Georgia Institute of Technology, 1994.
2. A. Richter, H. J. Scheibe, W. Pompe, K. W. Brzezinka, and I. Muhling, *J. non-cryst. Solids*, Vol. 88 (1986) p. 131.
3. D. S. Knight and W. B. White, *J. Mater. Res.* Vol 4 (1989) p. 385.

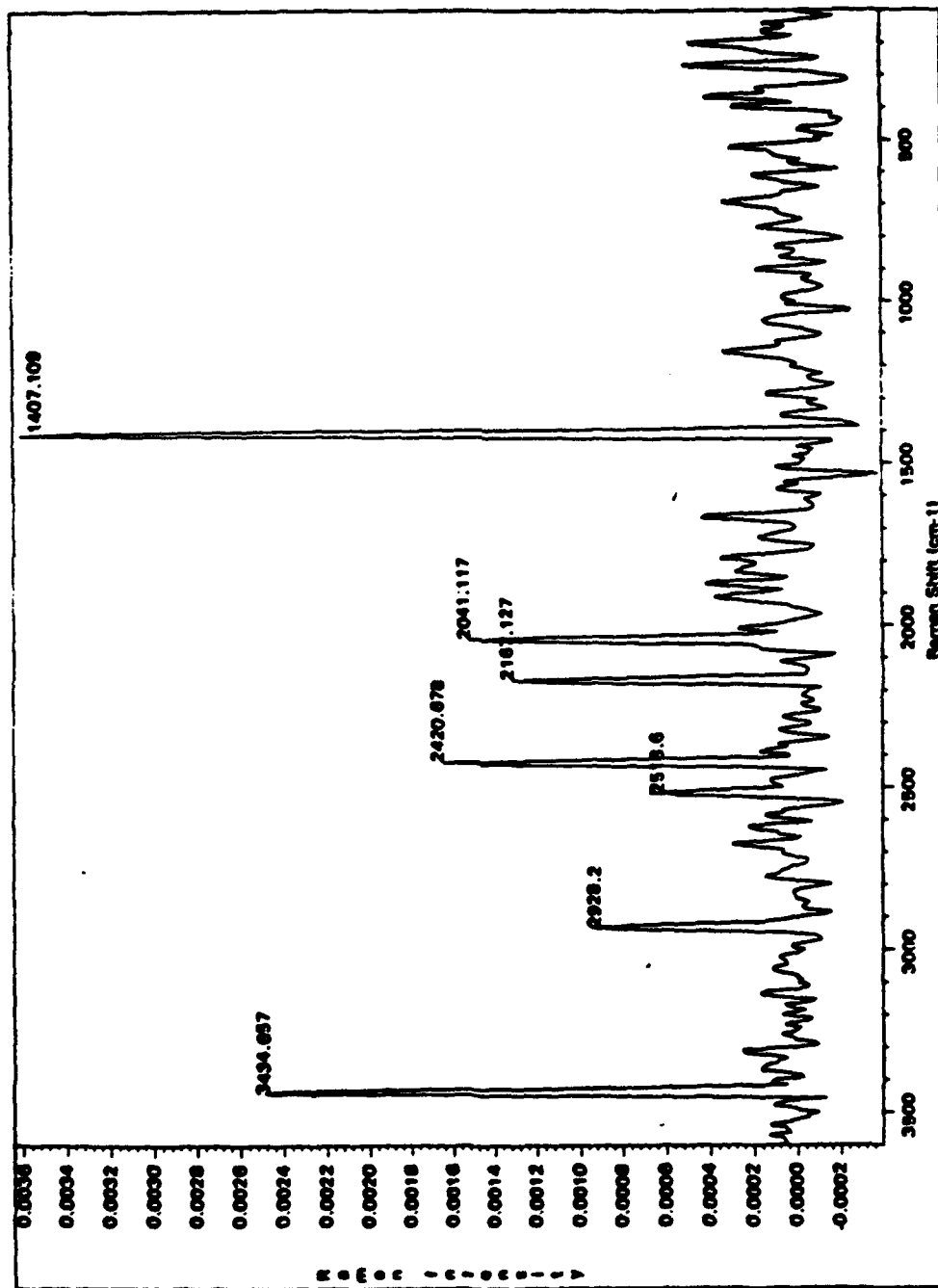


Figure 1. Raman spectrum of PAN fiber heat-treated to 400°C (NMR tube).

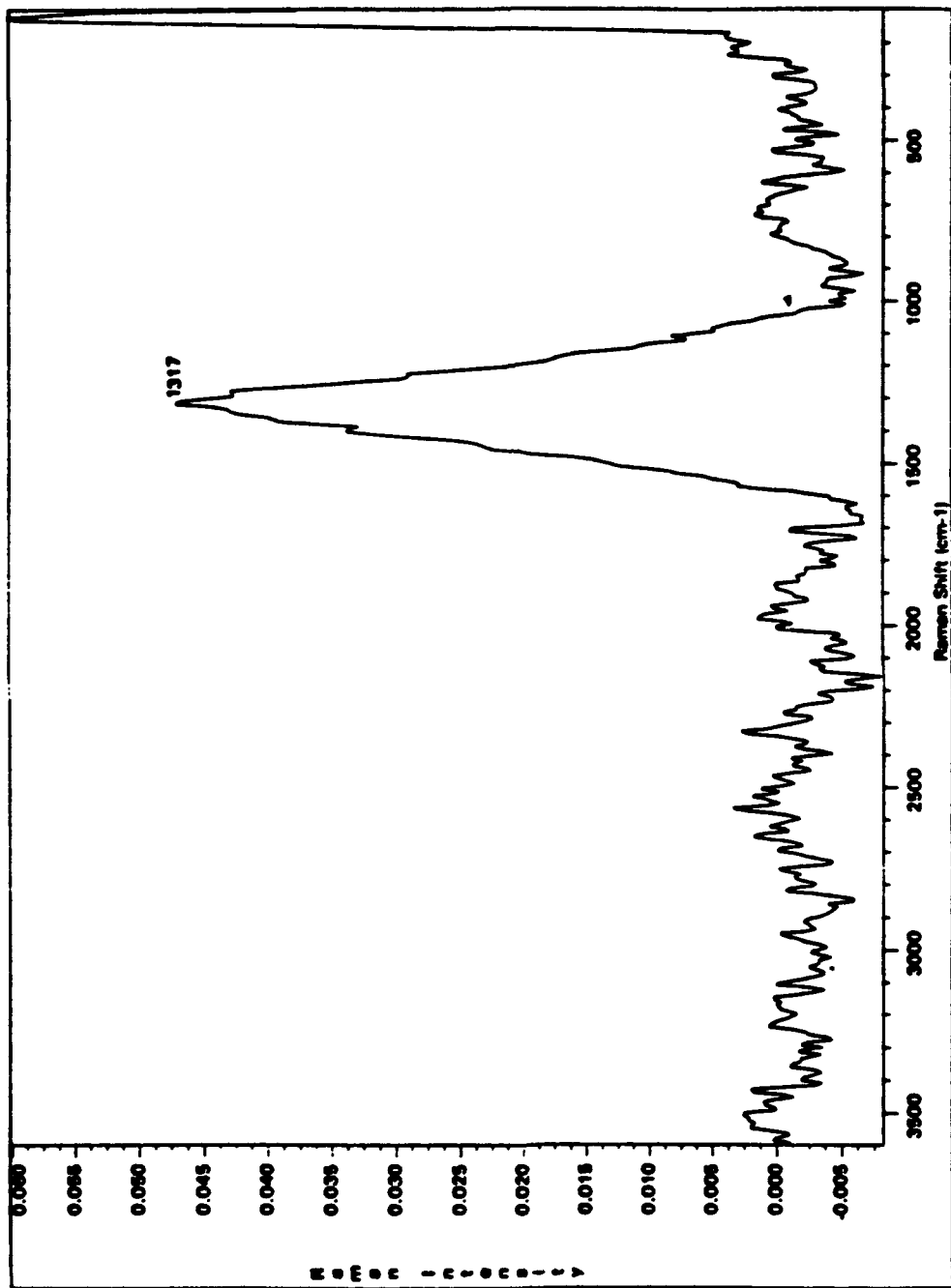


Figure 2 Raman spectrum of PAN fibers heat-treated to 800°C (KBr pellet).

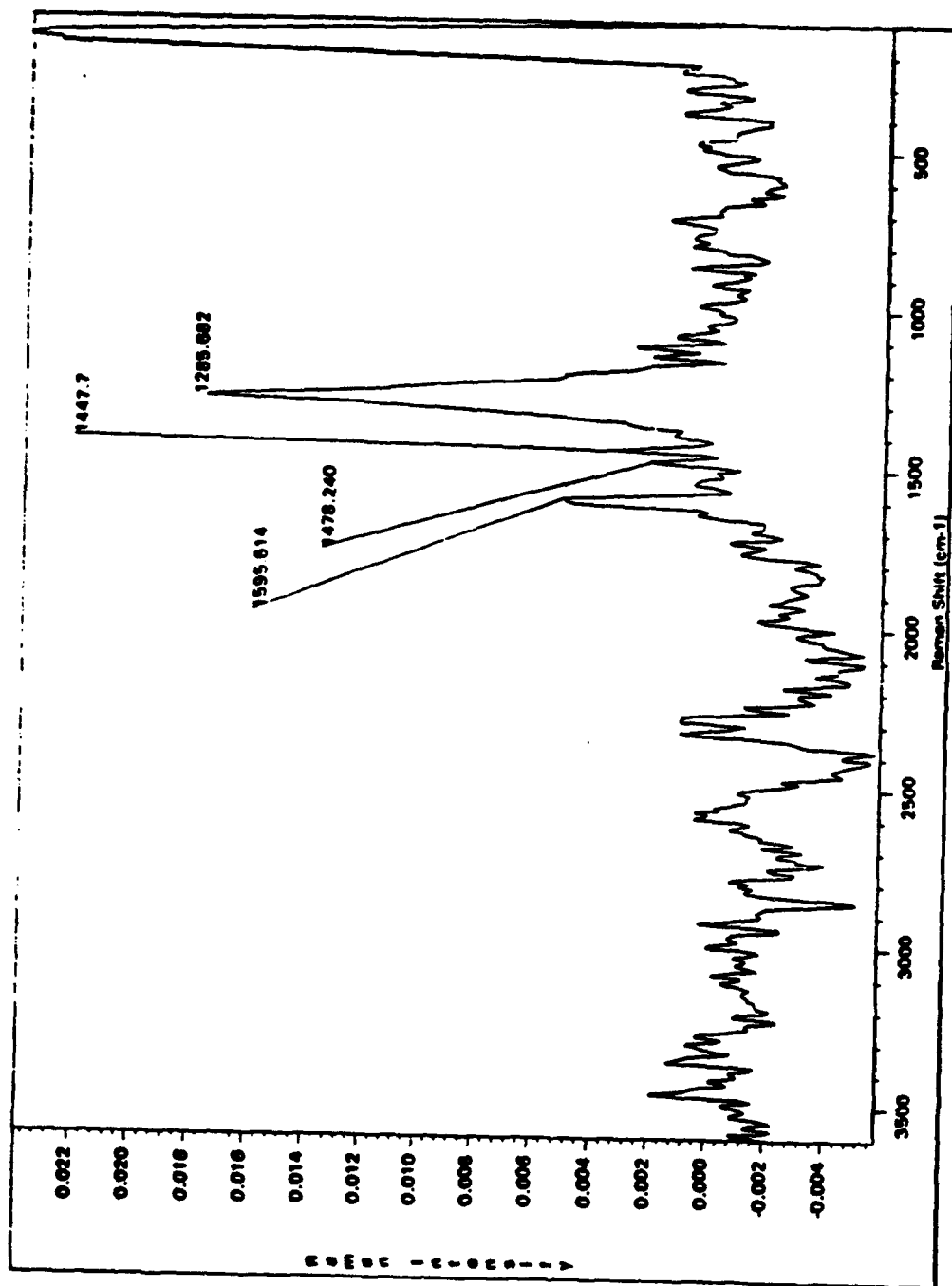


Figure 3. Raman spectrum of PAN fibers carbonized at 1700°C in nitrogen (KBr pellet).

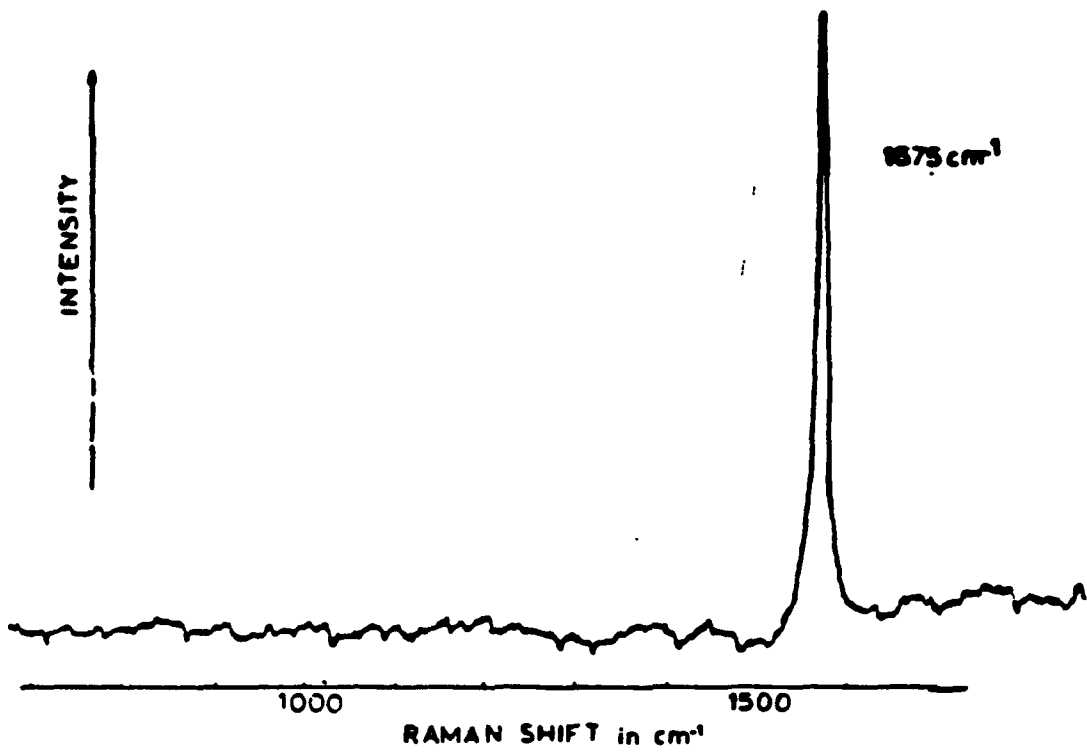


Figure 4. Raman spectrum of a single graphite crystal<sup>6</sup>.



Figure 5. Raman spectrum of a diamond crystal<sup>9</sup>.

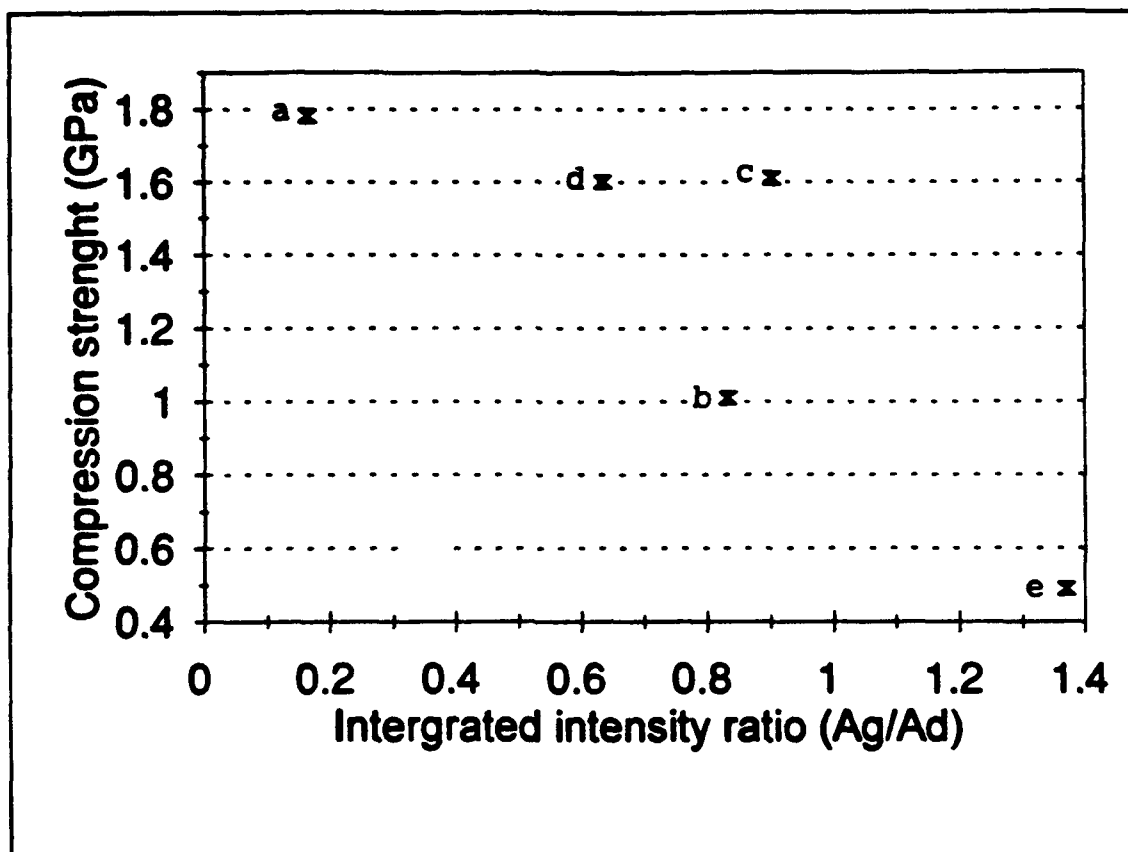


Figure 6. Compression strength Vs  $A_c/A_D$  for various carbon fibers; (a) CF1700°C, (b) CF2800°C, (c) T-50, (d) G50-300 and (e) P-100.

**COMPRESSION BEHAVIOR OF MATERIALS: . GLASSY POLYMERS**

**Victor V. Kozey and Satish Kumar**

**School of Textile & Fiber Engineering,  
Georgia Institute of Technology,  
Atlanta, GA 30332-0295, USA**

**ABSTRACT**

**In this three part series the compressive behavior of (i) glassy polymers, (ii) high performance polymeric and carbon fibers, and (iii) polymeric matrix composites has been addressed. The glassy polymers exhibit plastic yielding in compression. The dependence of compressive yield strength on factors such as tensile modulus, glass transition temperature, density, and free volume has been examined. Failure theories for yielding in glassy polymers have been reviewed. Compression behavior of high performance fibers and that of the composites is discussed in parts II and III respectively.**

**KEY WORDS: compression; glassy polymers; resins; compressive strength; yielding; failure modes, glass transition temperature.**

## LIST OF SYMBOLS

$\sigma_y^-$  = compressive yield strength

$\sigma_y^+$  = tensile yield strength

$\tau$  = shear yield strength

$T_g$  = glass transition temperature

$T_\beta$  =  $\beta$ -relaxation temperature

$E$  = tensile modulus;

$G$  = shear modulus

$\nu$  = Poisson's ratio

$\dot{\gamma}$  = strain rate

## INTRODUCTION

Recent research efforts on compressive strength have been mostly due to the poor axial compressive strength of the high performance polymeric and pitch based carbon fibers as well as their composites. Despite the continuing interest, compressive behavior of the materials in general and of high performance fibers in particular still remains a much misunderstood subject. Compressive failure in modern composites is affected by compressive failure of fibers, yielding of polymer matrix, or failure at the fiber-matrix interface. Therefore, it is important to recognize compressive failure mechanisms in polymer matrices, high-performance fibers, and in the polymeric matrix composites. This series of papers consists of three parts. In part I compression behavior of glassy polymers, and its dependence on structural and mechanical parameters has been discussed. Compression test methods for single fibers, dependence of compressive strength on various structural parameters, and failure modes of high performance polymeric and carbon fibers have been discussed in Part II. Various issues involved in compression failure of polymeric matrix composites containing polymeric, carbon and glass fibers have been addressed in Part III.

Many aspects of compressive failure observed in bulk polymers, fibers, and composites are also observed in other materials. For example, the kinking failure mechanism discussed in Parts II & III of this series is observed not only in anisotropic fibers and fibrous composites, but also in metallic crystals, wood and rocks. From this point of view, significant discussion on failure mechanism is of a general nature. Table 1 compares typical compressive strength values for various structural materials.

### **COMPRESSIVE YIELD BEHAVIOR**

**STRESS-STRAIN BEHAVIOR:** Bulk polymers generally exhibit plastic yielding in compression. Typical compressive stress-strain curves for different thermosetting epoxy resins and thermoplastic PVC are given in Figure 1. This Figure indicates that thermosetting epoxy resins, which generally have brittle failure under tension, undergoes considerable plastic deformation in compression. After yielding, some thermosetting epoxy polymers show a stress drop or so-called "stress-softening". Usually three main types of compressive stress-strain diagrams are observed in glassy polymers (Figure 1): Type 1 is characterized by a distinct peak on the stress-strain diagram after which stress softening occurs. The feature of the type 2 is a plateau in the stress-strain diagram. The type 3 is characterized by continuous stress increase with a significant slope change near the yield point. In this case yield strength is taken to be at the point where the stress-strain curve departs from elastic linearity by 0.2% [2]. In case of the type 1 behavior the "upper" and "lower" yield strengths can be defined as given by points A and B respectively in Figure 1 [1,3,4]. Finally, all three types of samples result in significant stress increase and the phenomenon is termed as "stress hardening" resulting from transforming cylindrical shape samples into a barrel-like ones [1,5,6] (Figure 1). As a result of the barrelling split, cracks appear leading to crushing the sample. The crushing strength calculated as a crushing load per unit of final cross-section was found to be very

close to yield strength [1].

**SHEAR BANDS:** Compressive deformation often manifests via development of shear bands at the yield point. Scanning electron micrographs of some of the shear bands are shown in Figure 2. The localization of axial deformation into shear bands directly depends on the stress softening effect [7,8]. In the epoxies exhibiting the stress-strain diagrams of the type 2 and 3 under compression no shear bands propagating across the specimen were observed [1]. In such systems a more uniform plastic deformation appears to occur. However, samples exhibiting all three types of stress-strain diagrams, result in short bands ( $< 1 \mu\text{m}$ ) intersecting at  $90^\circ$  as shown in Figure 2c, and we will call these "cross bands". Epoxy exhibiting type 1 stress-strain diagram, the shear band was found to propagate across the area rich with "cross bands". However, the presence of crosses on the surface is not a requirement for the development of shear bands[1,9,10], as the crosses may be located somewhere inside the sample and not on the surface.

The experimental observation of shear bands have been reported in many glassy thermoplastics[11-13] such as poly(methyl methacrylate), polystyrene, polycarbonate, as well as in thermosets[14,15]. The local deformation in shear bands is quite high - up to 40% in epoxies [15], and from 65% to 130% in polystyrene[16]. It has been reported that the localization of deformation into shear bands is a gradual process, and that the inhomogeneous plastic strain in polymers is preceded by homogeneous plastic strain producing softening[14,17]. Such form of plastic deformation inhomogeneity, as crazing, does not occur in compression because it is a free volume-dependent process needing dilatation conditions [5,9]. The shear bands have been reported both in compression as well as in tension resulting from shear stresses developing in the polymer sample[18]. A mechanism of the deformation localization in shear bands have been examined by Bowden[7] and Argon & Bessonov [8] as a process of unstable development of an initial strain-rate perturbation in the polymer undergoing stress softening. The perturbation may

arise near the cross bands. Initial strain-rate inhomogeneity will develop into deformation band when shear deformation becomes concentrated, at the same time that the deformation rate in the material outside the shear bands gradually decreases to zero. The larger the initial strain-rate inhomogeneity, the larger is the degree of stress softening, and more rapid the strain localization. Mathematically, localization of deformation in shear bands can be treated as instability of an uniform strain-rate field [19]. Such instability occurs only if a polymer exhibits stress softening [19].

**COMPRESSIVE YIELD STRENGTH:** Compressive yield strength values of most linear and crosslinked polymers in the bulk form generally vary from 50 to 200 MPa, with the exception of polyethylene and high temperature polymeric resins [5,6,8]. The value for bulk polyethylene is generally lower than 50 MPa, and for high-temperature high-performance polymers including polyimides and polybenzimidazole (PBI)-resin is generally greater than 200 MPa. There have been number of attempts to link yield strength of polymers with various other properties such as free volume, tensile modulus, radius of the polymer unit, and the degree of crosslinking in thermosets [20-23].

The relationship between compressive yield strength and density for crosslinked epoxy resin is presented in Figure 3a [1]. An increase in density reflects an decrease in free volume in a glassy polymers. A linear correlation between yield strength and density for epoxies has been also been reported by other workers[17,24]. Epoxy density increases with increasing degree of crosslinking[22,23]. This suggests that free volume in the polymers is decreasing as crosslinking density increases. This effect may explain the observed increase in compressive yield strength with the degree of crosslinking for thermosets[22,23,25,26]. The yield strength vs density for polyethylene are plotted in Figure 3b [27]. However in the polyethylene case the effect of crystallinity on density should also be taken into account. Thermal treatments of epoxies also affect density, free volume, and yield strength [1,3,4,23-25].

For the epoxies showing the stress softening, the sub- $T_g$  aging does not affect lower yield strength, while upper yield strength is affected as shown in Table 2. This indicates that the structure of the glassy polymer in the upper state is not in equilibrium, and therefore can be effected by thermal aging. The aged thermoplastics [28] and thermosets [4] exhibit an endothermic peak in the differential Scanning Calorimetry scans at a temperature slightly above the glass transition temperature. No endothermic peak was observed in the un-aged sample. The DSC peak has been attributed to more perfect structure of glass (and not crystallization) in the aged specimens which needs an excess of heat to jump from the glass to the rubbery state[4,28].

Northolt[21], reviewing the data on a wide spectrum of materials including bulk polymers, fibers, and inorganic solids, obtained an empirical dependence of compressive strength on  $(T_g)^2$ . The compression failure mechanisms in glassy polymers, fibers, and in inorganic materials are not the same [29,30], and therefore this generalization is probably inappropriate, nevertheless this gives useful insight in the compression failure process. Comparison of compressive strength vs some physical property only within a group of materials for which the compression failure mechanisms are same, will be on a sounder footing. For this reason we have compared the compressive yield strength and glass transition temperature relationship for glassy polymers only (Figure 4). A best fit line through the data in Figure 4 yields the following relationship:

$$\sigma_y^- \text{ (MPa)} \approx 0.8 T_g \text{ (}^\circ\text{C)} \quad (1)$$

Figure 4 also includes limited data on tensile strength of those epoxies which have a yielding behavior in tension. This suggests that the yield behavior both in tension and compression follows the relationship given by equation (1). Some authors [31,32] believe that the secondary relaxation temperature ( $T_\beta$ ) correlates with yielding better than  $T_g$ . For many glassy polymers it has been shown that  $T_\beta \text{ (K)} \approx 0.75 T_g \text{ (K)}$  [33-35]. Such relationship works especially well for the polymers in which  $\beta$ -relaxation involves motion about the chain backbone of a small number of

monomer units (1-2) coupled with the motion of side groups, examples of such systems being: polypropylene, poly (vinyl chloride), polystyrene, poly(methyl methacrylate), and some epoxies.

Compressive yield strength of glassy polymers decreases almost linearly with increasing test temperatures up to  $T_g$ [18,36]. Such plot for PBI-resin [37,38] is presented in Figure 5. Compressive strength increases with increasing strain rate [1,32,36] (Table 3). These facts indicate that yielding in glassy polymers is an activated process characterized by an activation energy and activation volume[39]. Estimation of the activation volume for yielding made from the stress - relaxation experiments gives the values ranged from 0.4 to 1.0 nm<sup>3</sup> for epoxies [32,40] and corresponds to 1-3 monomer units in the polymer chain. It points out that yielding is indeed a very localized process and that the crosslinking in thermosets does not affect molecular motions involved in yielding process.

Brown[20] has proposed a correlation between yield strength of polymers and their tensile modulus. Such a relationship ( $\sigma_y = 0.04 E$ ) has been reported for compressive yield strength of thermosetting polyester resins[41]. However, the examination of numerous experimental data for thermosetting resins[6,42] and glassy thermoplastics[5,38,43] in Figure 6 indicates that there is no general correlation between compressive yield strength and their tensile modulus in glassy state. In contrast to rubbery modulus, modulus of thermosetting resins in glassy state does not change significantly with the degree of crosslinking[23,25,44]. There are literature reports indicating that the compressive moduli in glassy state can be higher[45,46] or lower[42] than the tensile moduli, however the data in Figure 7 for epoxy resins indicate that both compressive and tensile moduli values are comparable.

A comparison of compressive yield strength and tensile strength (brittle failure in tension) of thermosetting resins in Figure 8 indicates the independent nature of the two properties. This finding can be attributed to brittle failure of the thermosetting resins in tension in contrast to their yielding behavior in

compression [1,47,48]. However, some thermosets can also exhibit plastic yielding in tension[47,48] and their values compare to the compressive yield strength as shown in Figure 4. Highly-crosslinked high- $T_g$  epoxies and other thermosets usually have much lower fracture toughness than low- $T_g$  epoxies[49] and therefore exhibit brittle failure in tension. Compressive yield strain of glassy polymers is in general proportional to their compressive yield strength as shown in Figure 9.

Compressive strength of glassy polymers increases with the addition of hard fillers such as silica or aluminum particles[6]. Similar trends have also been reported for (i) polyester resin/short glass fiber system[50] and (ii) epoxy resin/long polymeric fibers[51]. Compressive yield strength of epoxy/long polymeric fibers system linearly increased with fiber content as shown in Figure 10 [51]. In this experiment the fibers were not load-bearing elements as the compressive loading was in the transverse direction to the fiber axis. Shear bands were also observed in such filled epoxies. If the loading is along the fiber axis, the compressive strength of the fiber/epoxy system is naturally higher than for the pure epoxy, as in this case the fibers became load-bearing elements of the structure[51]. The increase in compressive yield strength on incorporating rigid particles or fibers may be a result of yielding being constrained by hard obstacles. Similar effect has also been observed in metals reinforced with fibers and particles [52]. It was postulated that hard obstacles prevent dislocation motion in the metals. In glassy polymers hard obstacles can decelerate the motion of shear bands [10].

Compressive yield strength of oriented glassy polymers seems to have very little dependence on orientation with respect to loading direction. Figure 11 illustrate, that the compressive yield strengths of anisotropic glassy polystyrene[53] of draw ratio 2.6 and of poly(vinyl chloride) (PVC) [54] of draw ratio 5.0, remain practically constant as the angle ( $\phi$ ) between orientation axis and the loading direction increases from 0 to 90°. The independence of the yield strength on orientation supports the idea that the local defects/structure is responsible for yielding in glassy polymers. At higher draw ratios the molecular orientation will be

higher and at high orientations compressive strength may depend more strongly on orientation.

### MODELLING THE YIELD BEHAVIOR

A number of theories have been proposed to relate compression yielding in glassy polymers to their microstructure and molecular motion[55-59]. Earlier models [55,56] have suggested that processes in glassy state are similar to the ones in rubber-like state i.e. associated with conformational motions of macromolecular coils. The theory assumes that the dimensions of the coil change on yielding. This effect has recently been observed using small-angle neutron scattering experiments[16,60]. However, molecular motions in polymeric glasses occur much slowly than in rubbers or liquids, and needs free volume. It was assumed[55,56] that the free volume increased with growing dilatation component of stresses under tension. But now it is well established that non-dilatation shear component of stresses causes yielding under tension and compression [58,61,62]. Therefore, Robertson [57] proposed that shear-stress field indirectly causes the increase in free volume in the following manner. The shear stress results in an increase in the fraction of backbone bonds that are not in the lowest energy conformation state. It was argued that the increased fraction of flexed bonds additionally leads to the free volume increase, resulting in a polymer structure resembling that of the liquid at some temperature above the glass transition. The similar model for glass transition has been introduced by Gibbs and DiMarzio [63]. Using above considerations along with several empirical relations, Robertson [57] successfully calculated the temperature dependencies of yield strengths for polystyrene and poly (methyl methacrylate). In the calculation, Robertson used the WLF equation [64] which describes the viscosity of polymers in the vicinity of glass transition temperature. This seems to limit the applicability of his theory to the temperature region near  $T_g$ . Robertson also assumed that the backbone bond motion is affected only by the intramolecular forces. In other words only the energy between cis- and trans- conformations in an

isolated coil are taken into account and the intermolecular interactions are not considered[57]. In polymeric glasses molecular motion is strongly affected by the intermolecular forces[65], which can be reflected by Lennard-Jones potential [66]. The calculations using this potential[67] showed that the rotational motion of the backbone segments can be dominated by intermolecular rather than intramolecular forces. In our opinion both intermolecular and intramolecular energy barriers for local motions of polymer chains during yielding should be taken into account. Naturally, the ratio of intermolecular to intramolecular energies will depend on (i) the mean distance between neighboring segments which are going to rotate. The distance is dictated by the available free volume in the polymer. The lower the distance between neighboring segments, lower is the free volume, and higher the barrier due to intermolecular forces[66]; (ii) the rigid segments (such as phenyl group) in the backbone especially coupled with bulky side groups are known to hinder molecular rotational motion in polymers[34]. The long rigid segments in high  $T_g$  polymers need more free volume for motions than short flexible backbone segments in low  $T_g$  polymers. In high density polymers with rigid backbones, thermally treated in such a way as to reduce the free volume, both inter and intramolecular motions would be suppressed resulting in high values of  $T_g$  and high compressive yield strengths. This conclusion is illustrated by the experimental correlations presented in Figures 3 and 4.

Argon's concept [58] is based on an idea that yielding is dominated only by intermolecular interactions. Local molecular motions were modelled via so-called "double molecular kinks". The energy stored in the kink was calculated using the formulas for a wedge disclination loop. It was arbitrarily assumed that the activation energy necessary for yielding is half of the energy stored by the double kink. This theory provides the following expressions for the shear yield strength ( $\tau$ ) or compressive yield strength ( $\sigma_y = \sqrt{3}\tau$ ) versus temperature (T), strain rate, and molecular parameters [58]:

$$(\tau/G)^{5/6} = A - B (T/G) \quad (2)$$

where the parameter A depends only on the Poisson's ratio; the parameter  $B = \ln(\gamma_0/\gamma)/(\omega^3 a^2)$ , where  $\gamma_0 = 10^{13} \text{ sec}^{-1}$ ;  $\omega$  is the net angle of rotation of a molecular kink between the initial and the activated configurations;  $a$  is the mean radius of a polymer unit, and  $T$  is the absolute temperature. The equation (2) contains two adjustable parameters:  $\omega$  and  $a$ . The equation (2) predicts that a plot of  $(\tau/G)^{5/6}$  vs  $(T/G)$  should be linear. Such a linear relationship has been observed for epoxy at temperatures  $T < 0.7T_g$  [36,68]. However, as the glass transition temperature approaches,  $(\tau/G)^{5/6}$  becomes independent of  $(T/G)$  [36]. Similar behavior has also been reported for various glassy thermoplastics[8,58]. This means that this theory applies at temperatures upto approximately 0.7 of  $T_g$ . The values of the Argon's model parameters for thermosetting epoxy resins are comparable to those for glassy thermoplastics [36,68].

The idea of using dislocations approach for glassy polymers has been introduced by Gilman[69] and further developed by Bowden and Raha [59]. It was proposed that plasticity in polymeric glasses is a result of local motions similar to dislocations with Burgers vectors of fluctuating magnitude. The dislocation approach for yielding in polymeric glasses is based on the several experimental findings: (i) The ideal yield strength in glassy materials was calculated by Frenkel[70] to be 10-20% of the shear modulus ( $G$ ), and compares well with the experimental magnitude of yield strength, which is approximately 4 to 8% of the shear modulus [71]. (ii) Pressure dependence of yield strength in polymers is found to be paralleled by the pressure-dependence of shear modulus [20]. (iii) The temperature dependence of yield strength is paralleled by the temperature dependence of shear modulus [11]. (iv) Shear bands observed in glassy polymers during yielding, look like Luders lines observed in polycrystalline metals[72]. It is assumed that the shear band deformation on macroscale reflects shear-like molecular rearrangement in coils at microscale similar to dislocation loop in metals. However, there are certain experimental observations which appears to contradict the above view, and are listed here: (i) For all glassy polymers the Poisson's ratio is about the same ( $\nu \approx 0.33$ ), therefore the

shear modulus ( $G = E/[2(1+ \nu)]$ ) should be proportional to their elasticity modulus. However, as illustrated in Figure 6, there is no general correlation between yield strength and E and hence with G. (ii) No significant pressure dependence of shear modulus has been observed for polycarbonate[73] or for poly(ethylene terephthalate)[74] (iii) No correlation has been observed between specimen deformation in a shear band and the molecular deformation of coils at microscale measured using neutron scattering[16]. (iv) shear bands have been observed not only in polycrystalline metals but also in amorphous metallic glasses [75]. In addition, it must be pointed out that there is no experimental evidence for the existence of dislocations in glassy polymers.

### Conclusions

1. Both thermoset and thermoplastic glassy polymers exhibit yielding under compression. On yielding, localization of plastic deformation in the form of shear bands can occur if stress-strain diagram showed stress softening.
2. Compressive yield strength of thermoplastic and thermosetting glassy polymers is proportional to their glass transition temperature and density.
3. Compressive yield strength of glassy polymers does not exhibit a unique dependence on the tensile and shear modulus. Experimental data indicates that the compressive and tensile moduli of glassy polymers are equal.
5. Compressive yield strength of thermosetting resins does not exhibit a unique dependence on tensile strength.
6. Inclusion of rigid particles, short, or long fibers increases compressive yield strength of glassy polymers.

## **REFERENCES**

1. V.V.Kozey, S.Kumar, SAMPE Proc. (1994). (To appear).
2. ASTM D 695-77 Standard; Annual book of ASTM standards, ASTM, Philadelphia, 1975, part 35.
3. C.G'Sell, G.B.McKenna, Polymer 33, 2103-2113, (1992).
4. T.-D.Chang, J.O.Brittain, Polym.Eng.&Sci. 22, 1221-1227, (1982).
5. I.Narisawa, "Strength of polymeric materials", OHMSHA Publisher, Tokyo, 1982.
6. Shell Epon Resin Structural Reference Manual, (1990).
7. P.B.Bowden, Phil.Magaz.22, 455-462 (1970).
8. A.S.Argon, M.I.Bessonov, Polym.Eng.Sci. 17, 174-179 (1977).
9. C.B.Bucknall, "Toughened Plastics", Applied Science Publisher, London, 1977.
10. J.C.M. Li, in "Plastic Deformation of amorphous and semi-crystalline materials", edited by B. Escaig & C. G'Sell, Les Houches, France, (1982), p. 359-373.
11. A.S.Argon, R.D.Andrews, J.A. Godrick, W. Whitney, J. Appl. Phys. 39, 1897-1906 (1968).
12. T.E. Bradey, G.S.Y. Yeh, J.Mater.Sci. 8, 1083-1094 (1973).
13. P.B. Bowden, S. Raha, Phil Magaz. 23, 463-470 (1970).
14. F.M. Kong, C.M.Walkup, R.J. Morgan, in "Epoxy Resin Chemistry- II" , edited by R.S. Bauer, ACS, (1983), p 211-225.
15. S.Bandyopadhyay, V.M.Silva, in Proc. 6-th Intern. Confer. on Fracture, edited by S.R.Valluri, Oxford Press, (1984), p 2971-2978.
16. J.M.Lefebvre, B.Escaig, G.Coulon, C.Picot, Polymer, 26, 1807-1813 (1985).
17. E.J.Kramer, J. Macrom. Sci., Phys.B10, 191-203 (1974).
18. P.B.Bowden, J.A.Jukes, J.Mater.Sci. Z, 52-61 (1972).
19. N.S.Grineva, A.A.Berlin, DAN SSSR 266, 384-387 (1982).
20. N.Brown, Mater.Sci.& Eng. 8, 69-73 (1971).
21. M.G.Northolt, J. Mater. Sci. Lett., 16, 2025-2028 (1981).
22. T.-D.Chang, S.H.Carr, J.O.Brittain, Polym.Eng.Sci., 22, 1213-1220 (1982).
23. M.Fisher, Advances in Polym. Sci., 100, 313-355 (1992).

24. E.S. Solodisheva, E.F.Oleinik, B.A.Rozenberg, *Vysokomol. Soedin.* **A22**, 1645-1649 (1980).
25. E.F.Oleinik, *Advances in Polym. Sci.*, **80**, 49-99 (1986).
26. X.Caux, G.Coulon, B.Escaig, *Polymer*, **29**, 808-813 (1988).
27. H.V.Boening, "Polyolefins". Elsevier. N.Y., (1966).
28. S.Petrie, *J.Macromol.Sci.-Phys.*, **B12** (1976) 225.
29. M.F.Ashby, D.R.H.Jones, "Engineering materials I & II", Pergamon Press, N.Y., (1980).
30. J.E. Gordon, "The science of structures and materials", Scientific American Library, N.Y., (1988).
31. B.Escaig , in "Plastic Deformation of amorphous and semi-crystalline materials", edited by B.Escaig , C. G'Sell, Les Houches, France, (1982) p 187-225.
32. J.M.Lefebvre, B.Escaig, *J.Mater.Sci.*, **20**, 438-442 (1985).
33. R.F.Boer, "Polymeric materials-Relationship between structure and mechanical behavior", ASM Publisher, Metals Park, (1974).
34. R.F. Boer, *J.Polym.Sci. Symp.*, **50**, 189-195 (1975).
35. S. Matsuoka, Y. Ishida, *J.Polym.Sci.* **C14**, 297-305 (1966).
36. S.Yamini, R.J.Young, *J. Mater.Sci.* **15**, 1814-1822 (1980).
37. S. Kumar, T.E.Helminiak, in "The Materials Science & Engineering of Rigid-rod Polymers" editors W. W. Adams, R. K. Eby, and D. E. McLemore, MRS Symp. *Proced.* **134**, 363-374 (1989).
38. B.C.Ward, in *Proceed. of 33 Inter. SAMPE Conf.*, edited by G.Carrillo, E.D.Newell, W.D.Brown, P.Phelau, **33**, 146-150 (1988).
39. H.Eyring, *J.Chem.Phys.*, **4**, 283-290 (1936).
40. S.A. Artemenko, Ph.D. Thesis, Institute of Chemical Physics, (Moscow, 1985).
41. M. R. Piggott and B.Harris, *J.Mater.Sci.*, **15**, 2523-2531 (1980).
42. J.King, M.Chaundhari, G.Disalvo, in *Proceed. of 32 Intern. SAMPE Conf.*, edited by R.Carson, M.Burg, K.J.Kjoller, F.J.Riel, **32**, 59-64 (1987).
43. D. C. Sherman, C.Y.Chen, J.L.Cercena, in *Proceed. of 33 Intern SAMPE Conf.*,

- edited by G. Carrillo, E.D.Newell, W.D.Brown, P.Phelau, 33, 134-137 (1988).
44. J.Heijboer, *British Polym. J.* 1, 3-14 (1969).
  45. V.V.Potapov, G. Neshvolodova, E.V.Prut, *Vysokomol. soedin.* A25, 585-589 (1983).
  46. I.P.Zemliakov, *Mechanics of polymers*, 1, 47-49 (1965).
  47. J.A. Schroeder, P.A.Madsen, R.T.Foister, *Polymer*, 28, 929-940 (1987).
  48. M.A. Markevich, *Mechanics of composite materials*, 35 (1992) 615.
  49. V.V.Kozey, B.A. Rozenberg, *Polymer Science* 34, 919-962 (1992).
  50. *Modern plastics encyclopedia*, *Modern Plastics*, 56, 503-539 (1979).
  51. V.V.Kozey, Ph.D. Thesis, Moscow Institute of Physics & Technology, Moscow, (1990).
  52. A. Kelly, N.H.MacMillan, "Strong Solids", Oxford Sci.Publisher, (1986), p. 207.
  53. L. Hoare, Ph.D. Thesis, University of Liverpool, Liverpool, UK, (1975).
  54. E.F. Rawson, J.G.Rider, *J.Polym.Sci. A-2*, 7 (1969) 829.
  55. J.D.Ferry, R.A. Stratton, *Kolloid Z.* 171, 107-114 (1960).
  56. S.Newman, S.Strella, *J.Appl. Polym. Sci.* 9, 2297-2304 (1965).
  57. R.E. Robertson, *J. Chem. Phys.* 44, 3950-3956 (1966).
  58. A.S.Argon, *Phil. Magaz.* 28, 839-865 (1973).
  59. P.B.Bowden, S.Raha, *Phil. Magaz.* 29, 149-166 (1974).
  60. J.M.Lefebvre, B.Escaig, G.Coulon, C.Picot, *Polymer*, 23, 1751-1757 (1982).
  61. Y.S.Lazurkin, *J.Polym.Sci.*, 30, 595-605 (1958).
  62. R.E. Robertson, *J.Appl.Polym.Sci.* 7, 443-451(1963).
  63. J.H.Gibbs, E.A. DiMarrzio, *J.Chem. Phys.* 28, 373-379 (1958).
  64. J.D.Ferry, "Viscoelastic properties of polymers", Jon Wiley, N.Y, (1961).
  65. I.V.Yannas , in "Proc. Intern.Symp. on Macromol". at Rio de Janeiro, edited by E.V.Mano, Elsevier Publisher, Amsterdam, (1975).
  66. J.E.Lennard-Jones, *Proc.Roy.Soc.* A196, 463-467 (1924).
  67. I.V.Yannas, A.C.Lunn, *Polym. Prepr. (ACS)*, 16, 564-569 (1975).
  68. S.M. Lee, *Proc. of Polym. Mat. Sci. & Engr. (ACS)*, 56, 253-255 (1987).

69. J.J. Gilman, in "Dislocation Dynamics", edited by. by A.R. Rosenfield, John Wiley, N.Y., (1968), p 55-92.
70. J.Frenkel, Z.Phys. 37, 572-576 (1926).
71. M.Kitagawa, J.Polym. Sci. Phys., 15, 1601-1611 (1977).
72. J.C.Bauwens, in "Plastic Deformation of amorphous and semi-crystalline materials", edited by B. Escaig, C. G'Sell, Les Houches, France, (1982), p.175-186.
73. A.W.Christiansen, Phil.Magaz. 24, 451-459 (1971).
74. S.Rabinowitz, I.Ward, J.Mater.Sci. 5, 29-37 (1970).
75. C.A.Pampillo, J.Mater.Sci. 10, 1194-1227 (1975).
76. A.W.Simpson, P.H.Hodkinson, Nature, 237, 320-332 (1972).
77. A.S.Argon, Acta Metallurgica, 27, 47-58 (1979).

**Table 1. Typical compressive strength values of various materials.**

<b>Material</b>	<b>Compressive Strength (MPa)</b>
Brick	10-70
Cast Iron	300-1,400
Stone	50-300
Wood	30-70
Thermosetting and thermoplastic polymeric resins	50-400
Graphite single crystal (perpendicular to c-axis)	100
Diamond	14,000
High performance polymeric fibers	100-500
Carbon fibers	400-5,000
Glass fibers	1,000-7,000
Alumina fiber	7,000
Boron fiber	6,000

Table 2. Compressive yield strength (MPa) of Epon 828/D400-70% epoxy system [1]

Quenched	Quenched and aged at $T=T_g-15^{\circ}\text{C}=40^{\circ}\text{C}$ for 20h	Annealed
Upper: 45	Upper: 47	Upper: 51
Lower: 42	Lower: 42	Lower: 42

Table 3. Compressive yield strength at various test speeds for the epoxy Epon<sup>R</sup> 828/ V40 (140%) [1].

Test speed (mm/min)	Yield strength (MPa)	Type of stress-strain diagram
5	26	type 2
25.4	31	types 2&3
254	37	type 2

## FIGURE CAPTIONS

- Figure 1.** Stress-strain curves for glassy polymers (1) Epoxy - Epon 828/D400 (50%), (2) Epon 828/D400 (50%) - tension, (3) Epon 828/Z (post cured at 130°C), (4) Epon 828/Z (post cured at 130°C), (5) Epon 828/Z (no post curing), (6) poly (vinyl chloride). All curves in compression except curve no. 2[1].
- Figure 2.** Scanning electron micrographs of shear bands in epoxy resins tested in compression; (a) a single shear band, (b) intersection of shear bands, and (c) "crosses" on the surface of epoxy[1].
- Figure 3.** (a) Compressive yield strength vs density of epoxy (Epon 828/ D-400) [1].
- Figure 3.** (b) Compressive yield strength vs density of polyethylene[27].
- Figure 4.** Yield strength vs glass transition temperature for polymers. (Data from ref 1, 5,6,38,41,42,43).
- Figure 5.** Compressive yield strength as a function of temperature for PBI resin[37,38].
- Figure 6.** Compressive yield strength vs compressive modulus for polymers [data from 1,5,6,38,41,43].
- Figure 7.** Compressive vs tensile moduli for epoxy resins [data from 1,6].
- Figure 8.** Compressive yield strength vs tensile strength for thermosetting resins that have brittle failure in tension [data from 1,6,38,41-43].
- Figure 9.** Compressive yield strength vs compressive yield strain for epoxy resins [data from 1,6].
- Figure 10.** Transverse compressive yield strength vs fiber content for epoxy / Kevlar™ fiber system[51].
- Figure 11.** Compressive yield strength as a function of angle between loading direction and the orientation angle for (a) polystyrene of draw ratio 2.6 [53] and (b) poly (vinyl chloride) of draw ratio 5 [54].

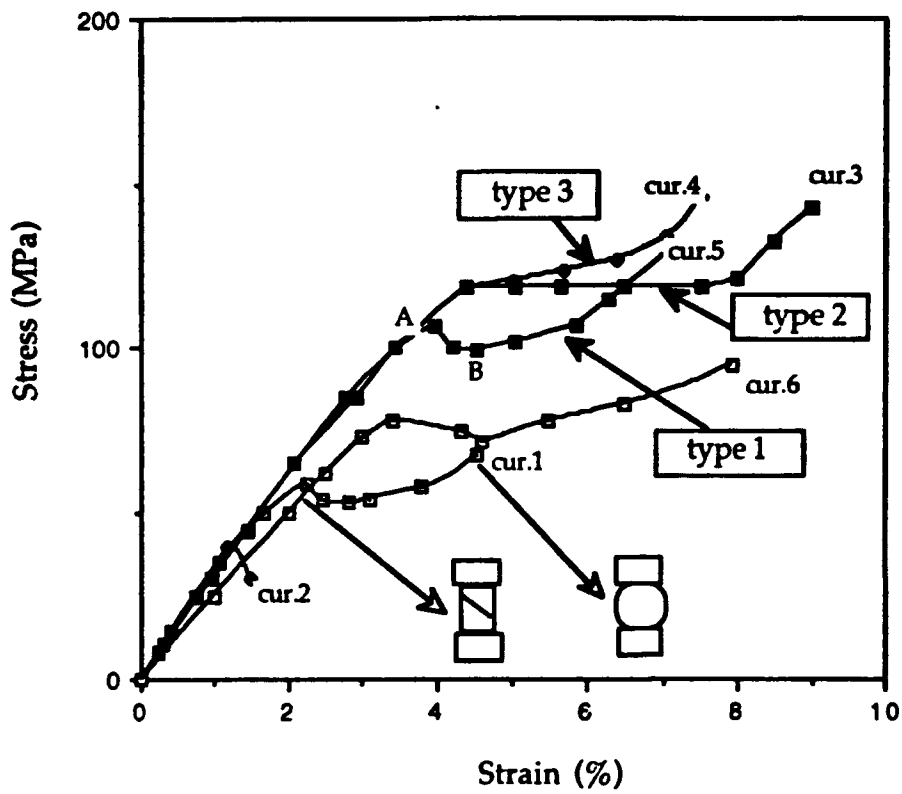
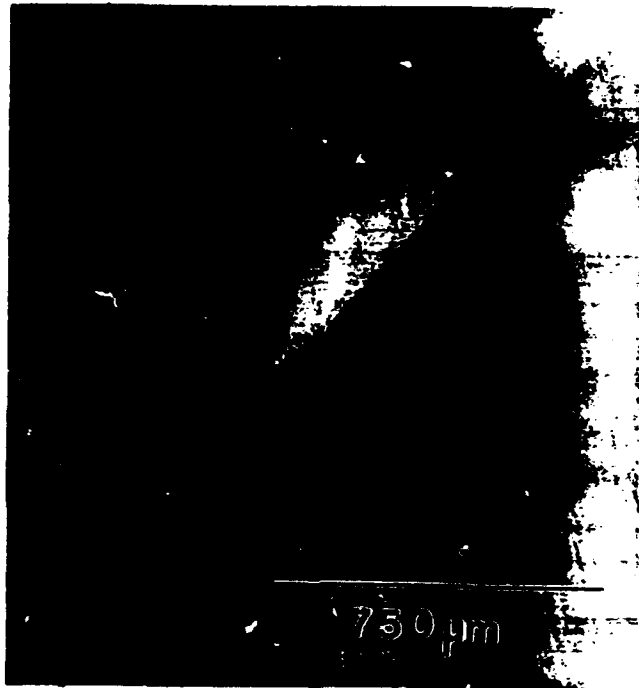
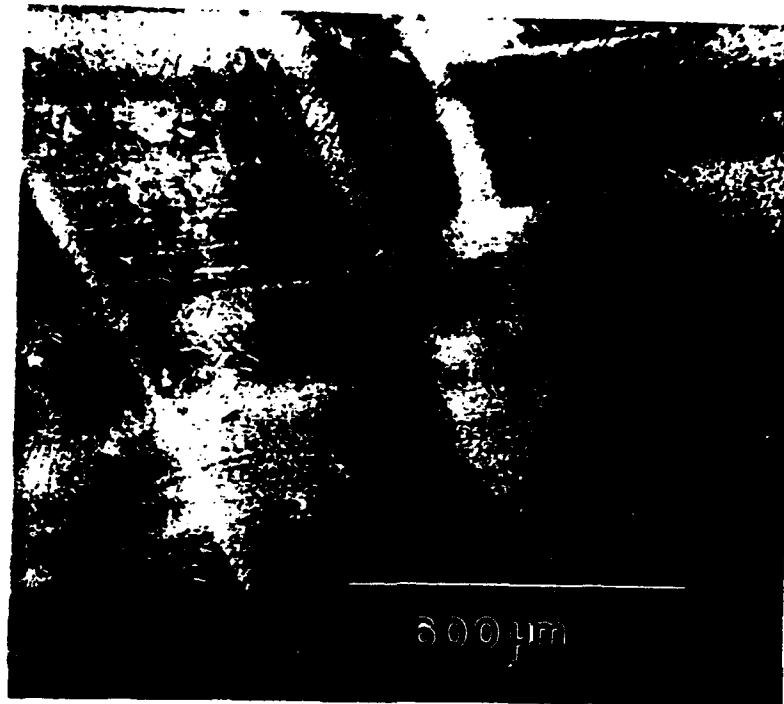
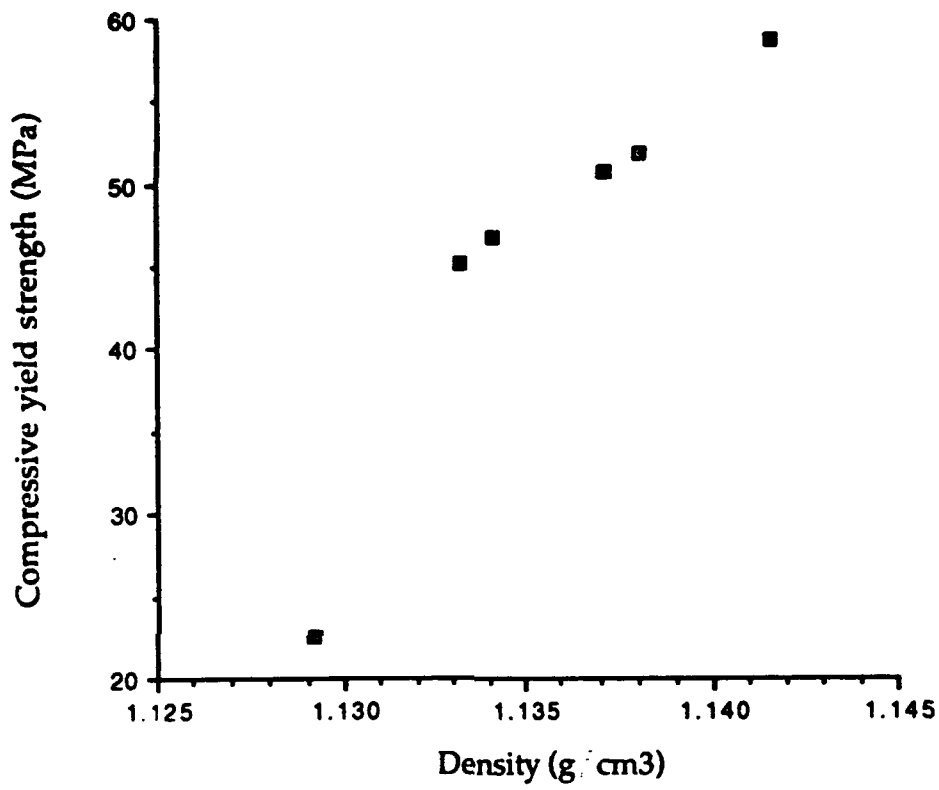


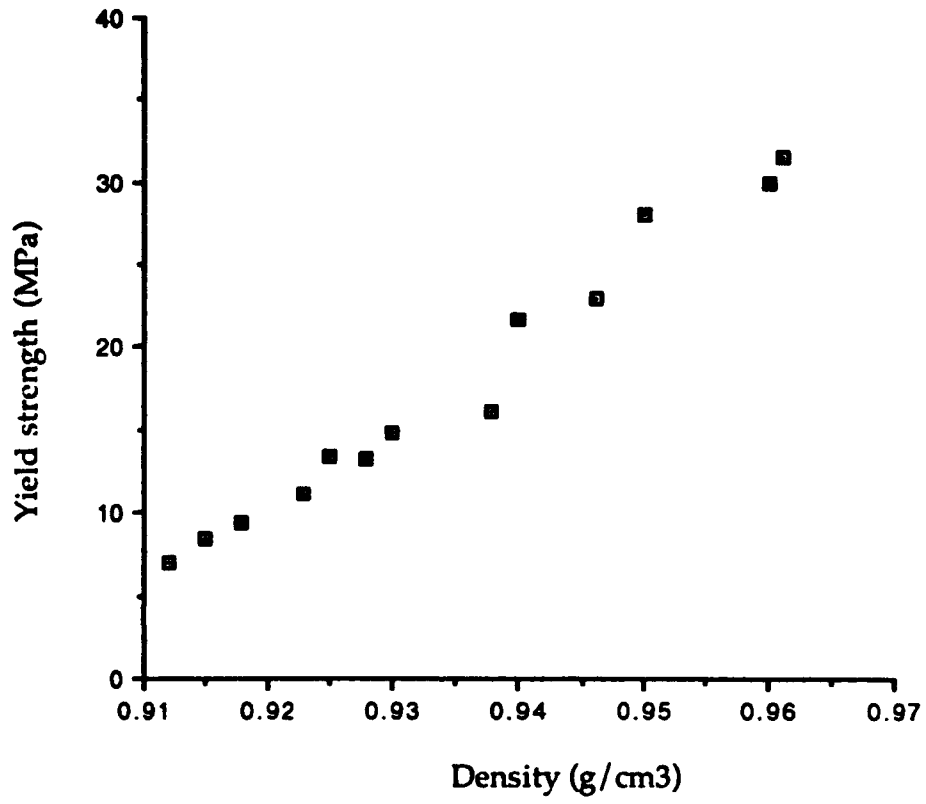
figure 1

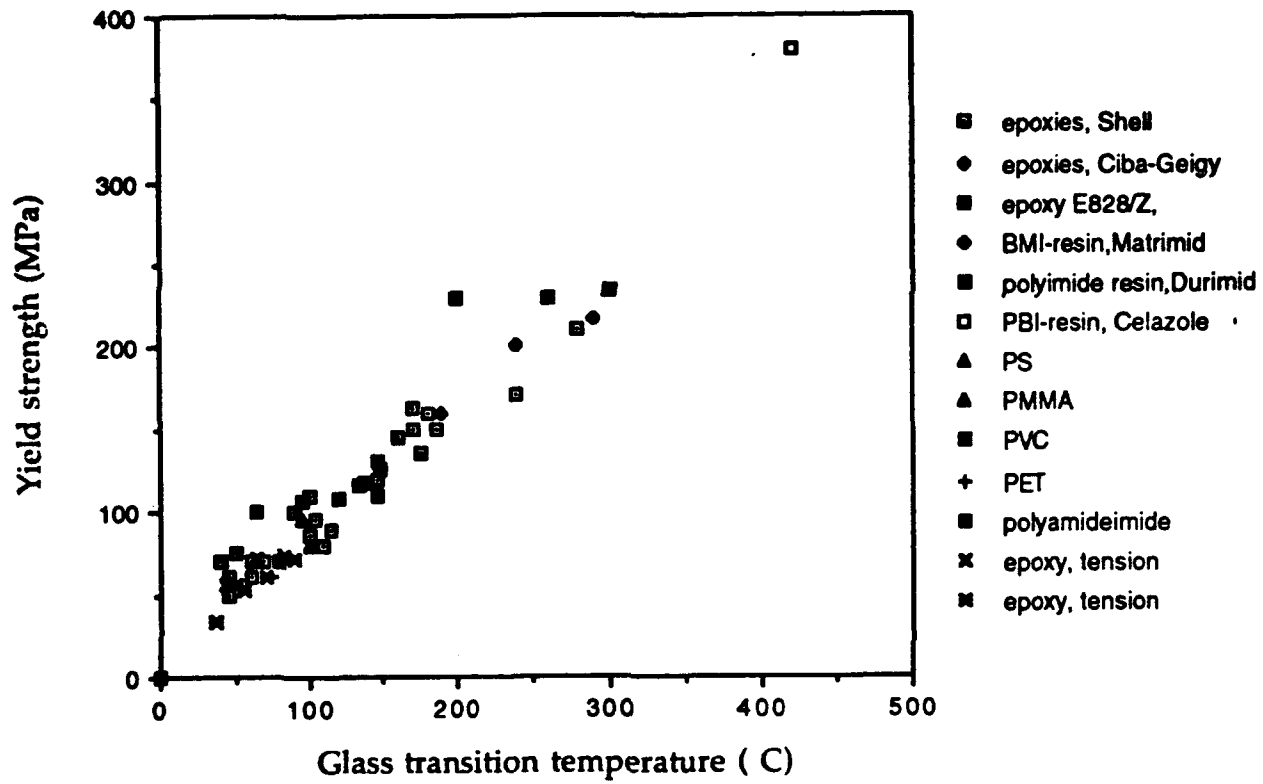


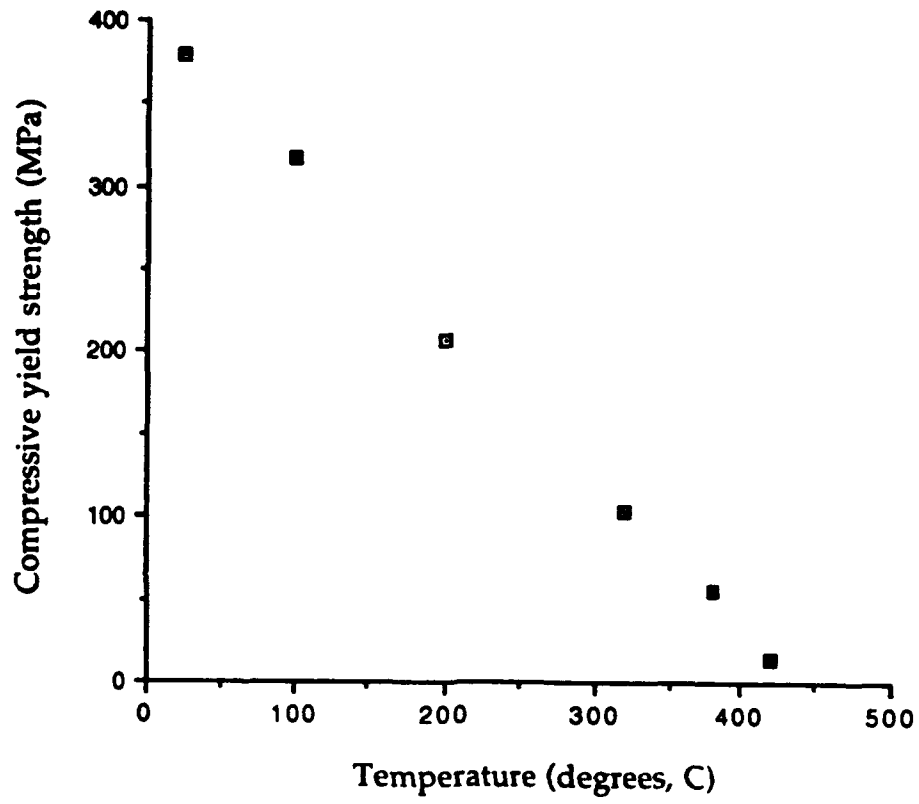












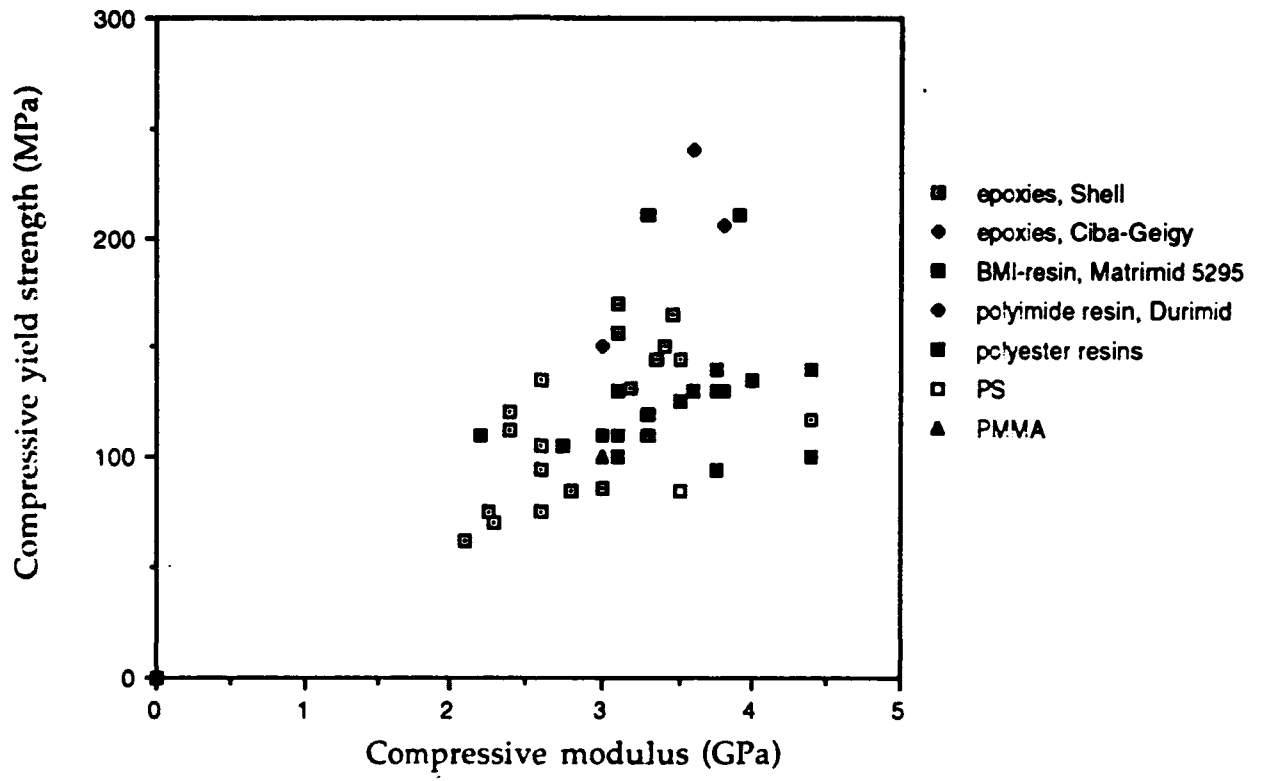
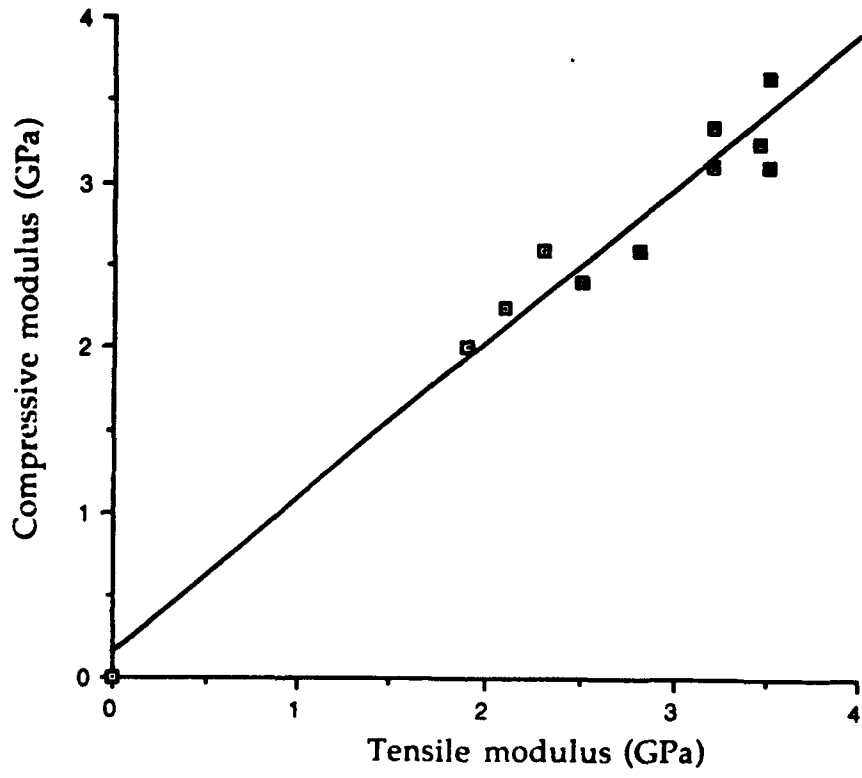
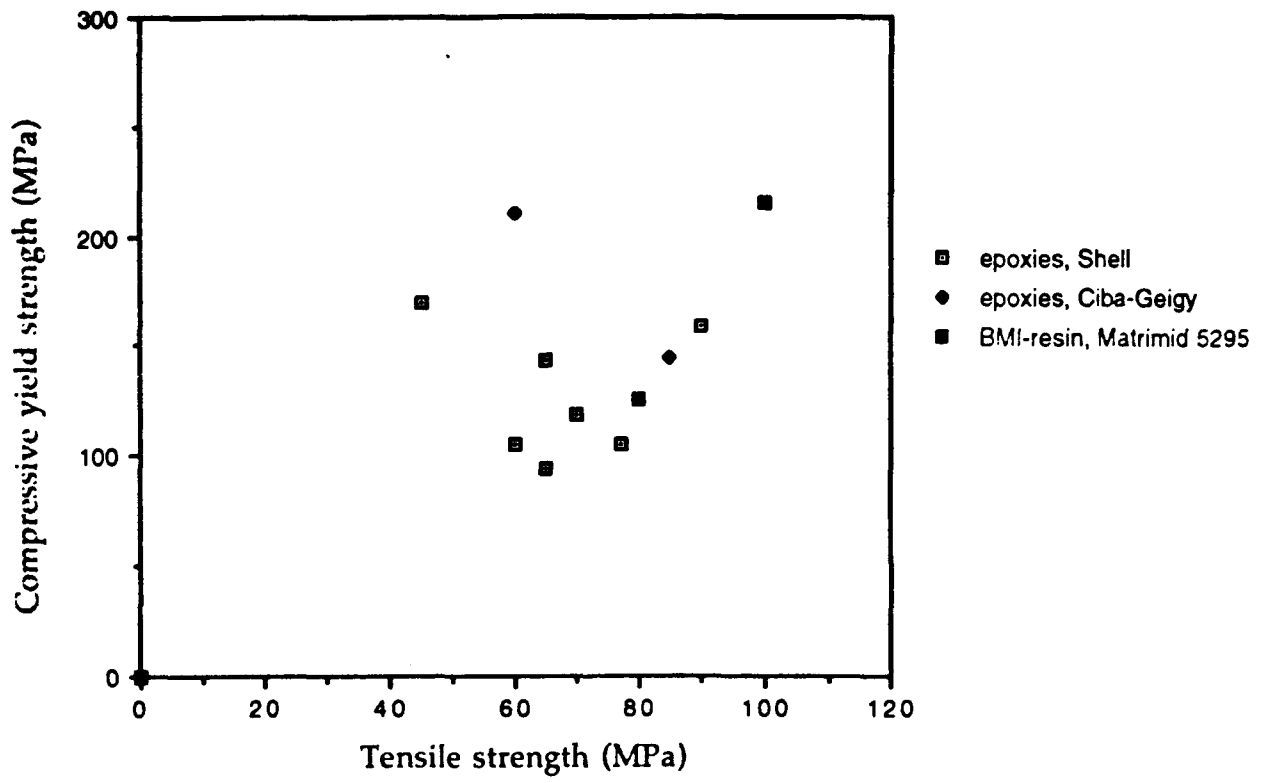
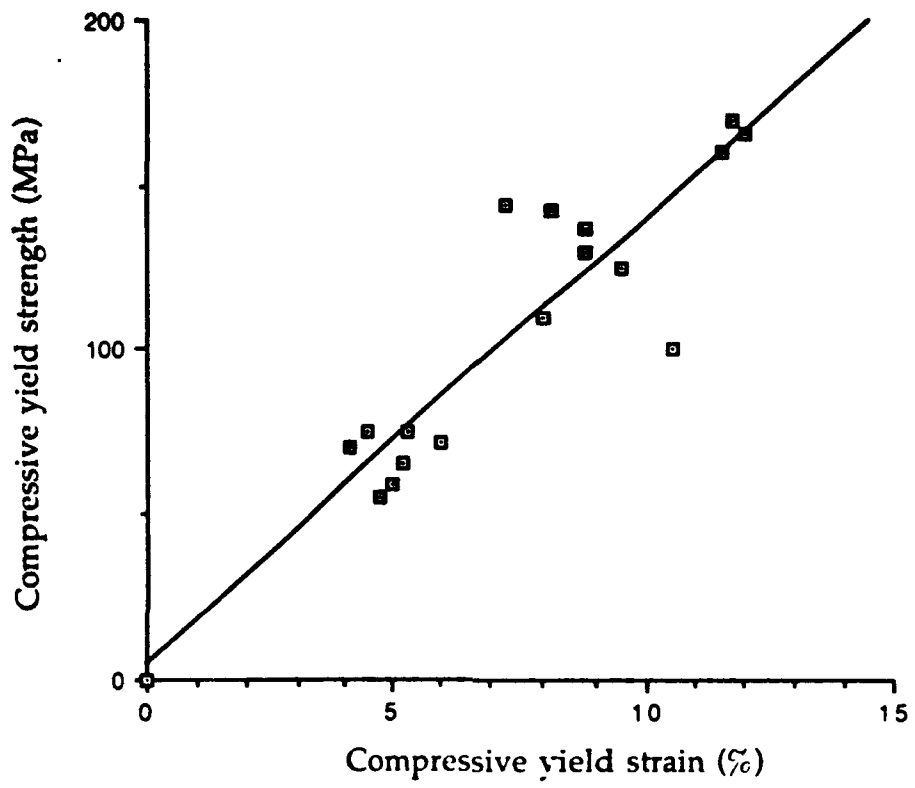
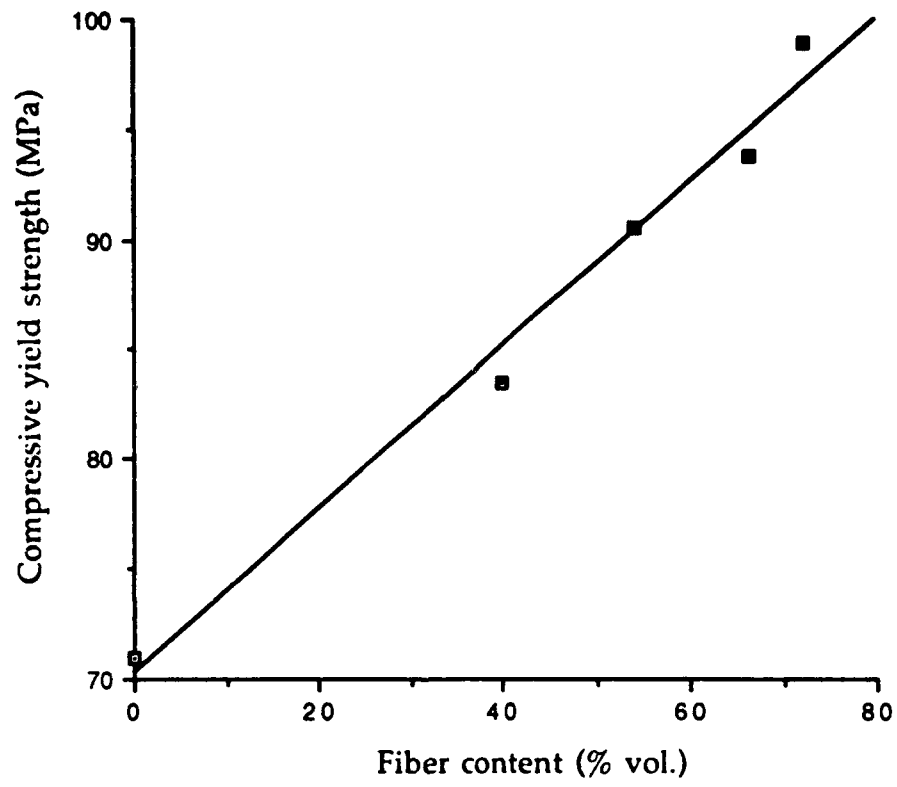


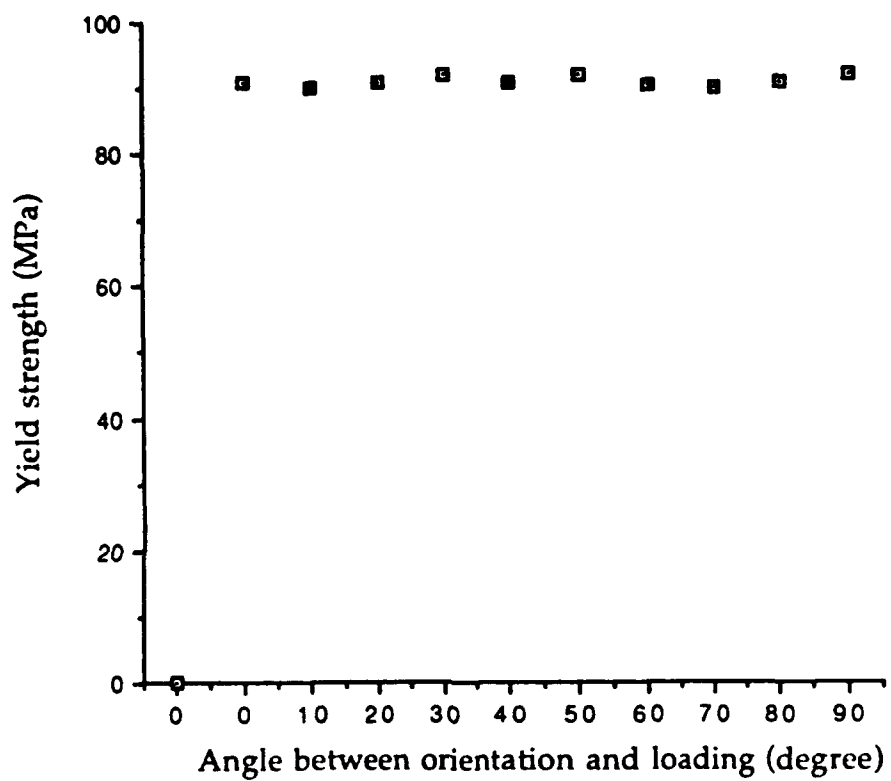
Figure 6

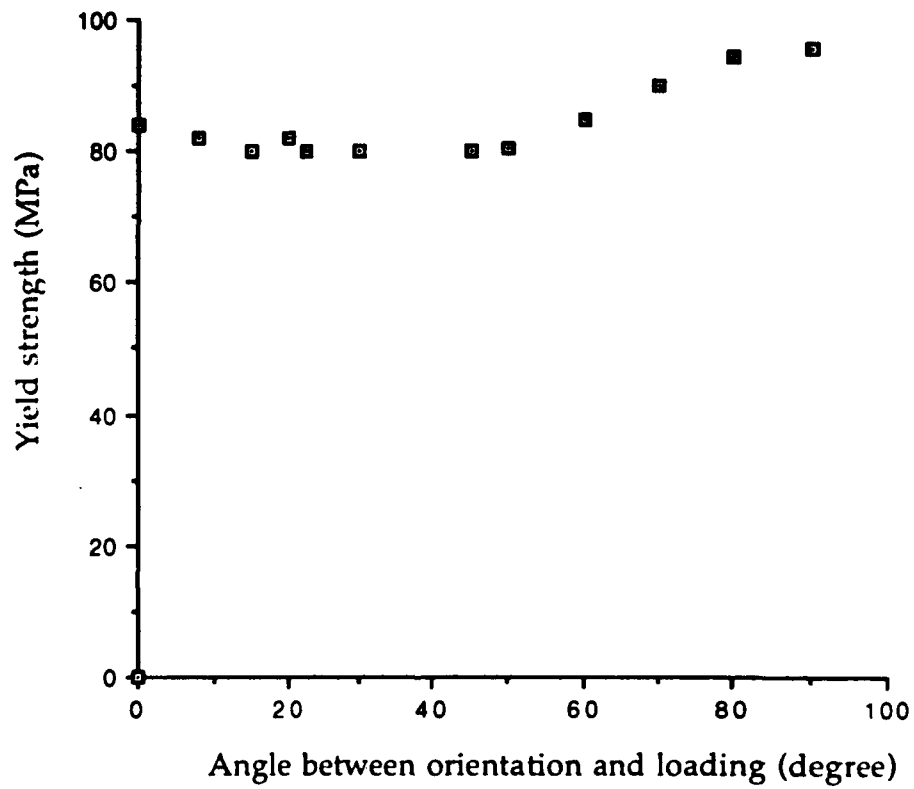












**COMPRESSIVE BEHAVIOR OF MATERIALS : HIGH-PERFORMANCE  
FIBERS**

**Victor V. Kozey, Hao Jiang, Vinay R. Mehta, & Satish Kumar**

**School of Textile & Fiber Engineering,  
Georgia Institute of Technology,  
Atlanta, GA 30332-0295, USA**

**Abstract.** The primary focus of this paper is on the axial compression behavior of high-performance polymeric and carbon fibers. Seven test methods used for determining the compressive strength of single fibers have been reviewed. Various micro-mechanical models proposed in the literature to understand the compressive failure in single filaments and in other anisotropic systems have been discussed and analyzed. The results of various approaches to influence the compressive strength of polymeric fibers have been summarized. Possible reasons for the variation in the compressive strength of pitch and PAN based carbon fibers have also been addressed .

**Key words:** compression; compressive strength; polymeric fibers; carbon fibers; compression failure modes, rigid-rod polymers.

### List of symbols used in this paper

- $d_f$  fiber diameter
- $E_f$  fiber tensile modulus - axial
- $E_{f-}$  fiber compressive modulus - axial
- $G_f$  fiber shear modulus
- $E_t$  fiber transverse tensile modulus
- $E^*$  theoretical tensile modulus
- $v_f$  fiber volume fraction in composite
- $L^*$  critical value of the major axis of loop
- $L$  major axis of the loop
- $D$  minor axis of the loop
- $h$  beam thickness in the bending beam experiment
- $R^*$  radius of curvature of the beam in the bending beam experiment
- $T_g$  glass transition temperature
- $a^*$  stress decay length at each end of the fiber
- $\sigma_c$  compressive strength of glassy polymers
- $\sigma_{f+}$  fiber tensile strength - axial
- $\sigma_{f-}$  fiber compressive strength - axial
- $\sigma_{t+}$  transverse tensile strength of the fiber
- $\sigma_{t-}$  transverse compressive strength of the fiber
- $\sigma_c$  compressive strength of the unidirectional composite along the fiber axis
- $\tau_f$  shear strength of fiber
- $\tau$  shear strength of the material failing via kinking
- $\tau^*$  "fiber-matrix" interfacial strength
- $\tau_y$  yield strength of the polymer matrix
- $\alpha^*$  &  $\beta^*$  shape and length Weibull parameters for fibers
- $\Gamma$  is the Gamma function
- $\phi$  mis-orientation angle
- $\beta$  Kink angle (refer to Figure 6)
- $\alpha$  angle of a change in orientation within a kink band (refer to Figure 6)
- $l^*$  average fiber fragment length ( + and - signs refer to tension and compression respectively)

## 1. INTRODUCTION

Early development of high performance fibers focussed on improving their tensile strength and modulus. However, the use of polymeric and high-modulus carbon fibers in composites brought attention to their poor axial compressive strength[1-3]. Mechanical properties of various high performance fibers are listed in Table 1. Despite the continuing interest and significant research efforts over last decade, compressive behavior of high-performance fibers still remains a much misunderstood subject [2-4]. In this paper various issues related to the compressive strength of high performance polymeric and carbon fibers have been reviewed.

High-performance polymeric fibers include: extended chain fibers from flexible polymers (e.g. Spectra™ fiber from ultra high molecular weight polyethylene)[5], thermotropic liquid-crystalline copolyester fibers (Vectran™)[6], fibers from semi-flexible lyotropic polymers such as poly (p-phenylene terephthalamide) (PPTA) (e.g. Kevlar™ and Terlon™)[4,7], and fibers from rigid-rod lyotropic polymers (e.g. PABI, PBZT, and PBO) [3,4,8,9]. There are three main routes to process these fibers: (a) a gel-spinning technology for polyethylene fibers[5]; (b) a melt-spinning technology for thermotropic liquid crystalline copolyester fibers[6]; (c) a dry-jet wet-spinning process for lyotropic liquid crystalline polymer solutions[3]. In the category of polymeric fibers most of the discussion on compressive strength is focussed on semi-flexible and rigid-rod polymer systems. Chemical structures of these fibers are shown in Figure 1. Carbon fibers are commonly produced either from polyacrylonitrile (PAN) or from mesophase pitch [10, 11]. Table 1 lists compressive strength of various high-performance fibers. Inorganic fibers such as alumina, boron, SiC, and glass fibers exhibit high compressive strength as compared to highly anisotropic polymeric as well as high-modulus PAN and pitch based carbon fibers[2]. Therefore, compressive behavior of the high-performance polymeric and carbon fibers is of primary interest [2-4].

## 2. COMPRESSION TEST METHODS

Very small diameter of high performance fibers (5 to 20  $\mu\text{m}$  for most polymeric and carbon fibers) makes it extremely difficult to test them directly under axial compression because of Euler buckling, however such measurements have recently been carried out on short gage length fibers[12,13]. Indirect test techniques are generally employed to measure compressive strength of fibers. The various test methods that have been used to determine the fiber compressive strength are discussed below:

**2.1 Loop Test:** Loop test was first used to determine the tensile strength of glass fibers at small gauge lengths (<1 mm) [14]. The test is of bending nature (Figure 2), and therefore stress distribution across the fiber cross-section is non-uniform and is maximum at the fiber surfaces. Sinclair [14] indicated that the ratio of major to minor axis of the loop (L/D) should remain constant at 1.34 if the loop deforms elastically. Isotropic brittle glass fibers exhibit elastic behavior in the loop up to the failure point[7,17] (Figure 2). Greenwood and Rose [15] employed the loop test to measure compressive strength of polymeric fibers. They observed that the L/D ratio begins to increase when kinks develop on compression side of the loop. Loop compressive strength is determined from the compressive strain at the fiber surface assuming that the compressive and tensile moduli are equal [15], and is given by:

$$\sigma_c = 1.43 E_f (d_f/L^*) \quad (1)$$

Nonlinear loop behavior of high-modulus PAN-based carbon fibers associated with the kinking on compression side of the loop was reported by Jones and Johnson [16], however they did not use this observation to determine the fiber compressive strength. Nonlinear loop behavior has recently been used to determine the fiber compressive strength in both PAN [17] and pitch-based [18] carbon fibers (Figure 2).

**2.2 Bending Beam (BB) Test:** In this test a single fiber[19] or a fiber strand[17] is bonded using an adhesive onto a thick (compared with the thickness of fiber or strand) beam. The beam is then subjected to 3 or 4-point bending[19,17] or cantilever [20,21,22] loading. Fiber failure is detected by optical microscopy [17,19,20,23].

Assuming perfect bonding between the sample and the beam, compressive strain in the fibers would be equal to the compressive strain on the beam surface. The strain is usually measured from the radius of curvature of the beam ( $R^*$ ), which yields compressive strength of:

$$\sigma_f = (E_f h) / (2 R^*) \quad (2)$$

The strain on compression side of the beam has also been measured using strain gauge[24] and from Raman band shift[21,22].

**2.3 Fiber Encapsulated into Polymer Block (FEPB) Test:** The idea of this test is to laterally support a small diameter fiber to avoid Euler buckling, so fiber would fail in pure compression. A single fiber or a fiber bundle is embedded in a block of polymer such as a transparent epoxy [25,26]. The block is compressed parallel to the fiber axis, and the compressive strain is usually measured using strain gauges attached to the block [26,27]. The accurate measurements can be made at strains well below the strain at which plastic yielding of the polymer block would occur. The fiber compressive failure is detected using optical microscopy [25,28]. In the case of encapsulated bundle of carbon fibers (mini-composite), the stress-strain diagram can be indicative of fiber failure[26]. Gradual compressive fracture of high-modulus carbon fibers changes the slope of stress-strain diagram while sudden fracture of high-strength carbon fibers lead to a sharp drop in stress[26]. The modifications of the FEPB test have been suggested [27-29]. The fiber was proposed to be mounted onto the side of polymer bar by attaching the fiber with spray coating [27]. Further modification of the method is based on a piezo-resistivity effect in carbon fibers [29].

**2.4 Broken Fiber Fragment Length (BFFL) Test:** This test introduced by Ohsawa et al. [30] to measure compressive strength is analogous to a technique used to determine adhesive strength between fiber and the polymer matrix[28]. Both methods are based on a "shear lag" theory of Kelly and Tyson[31]. If a sufficiently long fiber was embedded into a polymer matrix and then subjected to tensile or compressive stress greater than the fiber fracture stress, the fiber will break into many small fragments. The average fragment length ( $l_0$ ) is related to other fiber parameters as[31]:

$$l_0 = (\sigma_f d_f) / (2 \tau_0) \quad (3)$$

where  $\tau_0 = \tau_y$  if  $\tau_y < \tau^*$  or  $\tau_0 = \tau^*$  if  $\tau^* < \tau_y$ .

Compressive strength is calculated using fiber tensile strength ( $\sigma_f$ ) and the average fragment lengths in compression ( $l_{-}$ ) and in tension ( $l_{+}$ ) using the following equation [30]:

$$\sigma_f / \sigma_f^* = l_{-} / l_{+} \quad (4)$$

Since a distribution of the fragment lengths is experimentally observed, the equation (4) can be modified to reflect this distribution. For example, a Weibull statistics as applied in the case of interfacial strength measurements [28] can also be applied here. This will give the following result:

$$\sigma_f = 2 \tau_y \beta^* / \Gamma(1 - \alpha^*) \quad (5)$$

The disadvantages or limitations of this test are: (i) that it can be used only for brittle fibers; (ii) the length distributions of broken fibers (different Weibull parameters  $\alpha^*$  and  $\beta^*$ ) in compression and tension can be different [32]; (iii) early "fiber-matrix" adhesive failure may complicate interpretation of the test results.

**2.5 Tensile Recoil (TR) Test:** The observation of recoil damage after tensile fracture has been first reported in Kevlar™ fibers by Wilfong and Zimmerman [7]. It was recognized that compressive stress wave in the fiber can develop after tensile fracture during snap-back or recoil. Allen [33] used this observation to measure compressive strength of various fibers. In this technique, after stretching the fiber in tension to a pre-determined stress level, the fiber is cut at the mid-point using sharp scissors, electrical spark, or any other technique. The tensile stress wave reflects from the sample mounting clamps transforming into the compressive stress wave [33]. In the absence of energy loss in the fiber or at the stress wave reflecting boundary (e.g. clamps), the energy of tensile and compressive stress waves would be the same. Recoil compressive damage is usually observed near the clamps [33,34]. The disadvantages or limitations of this method are [33-35]: (i) this test is applicable for fibers whose tensile strength is higher than the compressive strength, (ii) possible damping of the tensile stress wave at the clamps, (iii) the possibility of bending

fracture rather than pure compression failure, (iv) the energy loss in the fiber due to visco-elastic effects.

**2.6 Direct Compression (DC) Test:** Single fibers have been tested under direct compression using a micro-tensile tester[12] and by using a nano-compression apparatus[13]. The idea of the test is to compress an unsupported fiber at very short gage length to prevent Euler buckling [36]. In the micro-tensile apparatus, a fiber is adhered to a pair of anvils, and compressive load is applied to the fiber through the anvils by rotating the micrometer. The displacement is measured by another micrometer using special adjustment system. In the nano-compression apparatus test the compressive force is introduced through a piezoelectric element while the displacement is measured by an optical probe. Non-uniform stress distribution near the clamps limits the minimal gage length that can be used in this test. A stress decay length ( $a^*$ ) along fiber axis is given by [37]:

$$a^* = d_f (E_f / G_f) \quad (6)$$

In order to provide uniform stress distribution along the length of the fiber, the minimal gage length must be more than  $2a^*$ . To prevent both Euler buckling and the end clamping effects, for 20  $\mu\text{m}$  diameter PBO and PBZT types of fibers a gage length of about 500  $\mu\text{m}$ [12], and for the 10  $\mu\text{m}$  diameter pitch based carbon fibers[13] a gage length of about 200  $\mu\text{m}$  has been used. The possible errors caused by the compliance of the machine clamps and by the polymer glue used to mount the fiber can effect the results[12,13]. The technique requires careful fiber mounting for perfect alignment.

**2.7 Composite Test:** Fiber compressive strength can be determined from compressive strength of unidirectional composite using the following relationship[2,33]:

$$\sigma_f = \sigma_c / v_f \quad (7).$$

However during compression testing, if the matrix yielding occurs, then a modified equation was proposed to account for yielding [4].

$$\sigma_f = [\sigma_c - 2 \tau_y (1 - v_f)] / v_f \quad (8).$$

Compression failure in the composites reinforced with metallic, polymeric, and pitch based carbon fibers, is due to compression failure in fibers themselves[26,38]. The composites reinforced with high-strength PAN based carbon fibers and glass fibers, may fail in compression via fiber micro-buckling or via "fiber-matrix" interface failure[26,39]. This complicates the estimation of fiber compressive strength from the composite test for the latter categories of fibers. The various issues related to the compressive strength of composites are addressed in the part III of this series of papers[40].

**2.8 Comparison of Various Compression Test Methods:** A number of difficulties are encountered in compression testing of single fibers. First, it is often difficult to precisely pinpoint initiation of compression failure. Second problem arises due to the fact that in many tests compressive strain rather than compressive strength is measured, and compressive strength is calculated using fiber tensile modulus. This may result in overestimation as fiber compressive modulus may be less than fiber tensile modulus[13,21,24,41], and fiber compressive stress-strain curve may be non-linear.

Axial compressive strength values for various carbon and polymeric fibers obtained from various tests are listed in Tables 2 & 3. It can be seen that compressive strength of the high-performance polymeric fibers are only about 5 to 15% of their tensile strength. For PBO and PBZT fibers the reported values obtained from different tests are quite similar (Table 3). For PPTA fibers the data from the recoil, encapsulated fiber and composite tests are similar (360-430 MPa). The strength of PPTA fibers measured under direct compression is about 50% lower than from other tests, probably due to poor alignment of the fibers. The loop strength of the polymeric fibers, especially PPTA and PABI, are higher than obtained from other tests[4,20]. The following effects may be responsible for this: (i) in the loop test the fiber is subjected to bending forces, and a pure compression stress develops only in thin section of the fiber near its surface. Thus only very small volume of the material is subjected to the compressive stress. Therefore, inhomogeneity through

the fiber cross-section, for example skin-core differences [42-44] can affect the loop strength. (ii) The gage length of the fiber undergoing the loop test is very small (<1 mm), much less than in other tests (usually 5-20 mm).

The loop behavior of PAN-based carbon fibers - Toray M-40J, M-50J and the Russian UKN 5000 is of the type shown for glass fibers in Figure 2b, where no deviation from the elastic limit of 1.34 is observed until fiber breaks, on the other hand loop behavior of Toray T-800 and M-40 fibers indicate deviation from non-linearity before eventual fiber breakage. The loop strengths of PAN based carbon fibers are much higher (3.5-6.6 GPa) than obtained from other tests. The microscopic observation during loop test of PAN based carbon fibers at the onset of deviation from linear elasticity and at the fiber breakage point have not been reported, and therefore it is not known whether these fiber failed in compression or in tension. Furuyama et al. in their recent work [18] have reported that the loop compressive strength of pitch based carbon fibers ranges from 1.8 to 2.6 GPa and is 60-93% of their tensile strength.

Table 2 illustrates that the compressive strength of high tensile strength (tensile strength =2.5-5.6 GPa) PAN based carbon fibers measured in the bending beam test is comparable to their tensile strength. The bending beam strength of high-modulus ( $E = 480$  GPa) PAN based carbon fiber is comparable to the compressive strength obtained from the composite test, and is only about 50% of their tensile strength.

Huh et al. [27] have reported that the compressive strength of high-strength PAN based carbon fibers (T-300) measured in the encapsulated fiber test is equal to their tensile strength ( $\approx 3.5$  GPa). Drzal[28] obtained much higher values ( $\approx 7$  GPa) for the high-strength PAN based Hercules AS-4 carbon fiber from a similar test. The latter value is about 200% of the tensile strength. High-strength PAN based carbon fibers tested in the FEPB-technique (single fiber encapsulated) has been observed by many authors to fail in a shear mode i.e at about  $45^\circ$  to the fiber axis[27-29, 32]. On the other hand, Hahn et al. [26,45] when conducting the experiments with the fiber

bundle encapsulation observed fiber micro-buckling rather than shear-like compressive fracture of the fibers.

The recoil strength of the pitch based carbon fibers is comparable to fiber compressive strength obtained from the composite compressive strength test (Table 2).

The recoil strength of the high-strength PAN based carbon fibers is lower as compared with other tests [4,34,35] (see Table 2). This is attributed to their bending failure behavior rather than pure compression during recoil[4,34,35, 46]. In the recoil test, the PAN based carbon fibers are stretched to significantly higher stress levels as compared to pitch-based carbon fibers or polymeric fibers. Thus higher stress and lower fiber diameter makes it more likely that the failure in the PAN based carbon fibers will be in the bending mode rather than compression. To circumvent this problem, two approaches have been used. (i) The recoil test has been conducted on an epoxy impregnated PAN-fiber strand having much larger bending rigidity than single fibers [47]. (ii) Recoil test was conducted on carbon fibers coated with viscous fluid[46]. In both cases recoil strength approaching the fiber tensile strength has been observed.

### 3. POLYMERIC FIBERS

**3.1 Compressive Modulus:** Tensile stress-strain plots of many high performance polymeric fibers exhibit small degree of non-linearity, resulting in a small increase in modulus with increasing stress[21,22,48]. Compressive modulus of PPTA and PABI polymeric fibers estimated from unidirectional composites is equal to their tensile modulus [7,38]. On the other hand, the decrease in modulus under compression has been reported for Kevlar™ 149 (about 28% decrease) and PBZT fibers (about 20% decrease) using the bending beam and Raman spectroscopy [21,22] and about 8% (considered within experimental error) decrease using the direct compression test [12]. It was reported that under axial compression, the birefringence of polymeric fibers decreases suggesting decreasing molecular orientation[49]. The

mis-orientation would result in decreasing compression modulus. Assuming that uniform stress model [50] is applicable for the fibers with slightly mis-oriented structural elements (crystallites or fibrils), the following equation can be used to determine the fiber compressive modulus:

$$E_f = E^* / (1 + (E^*/G_f)\phi^2) \quad (9)$$

The calculated moduli of PBZT and PPTA single crystals are 700 GPa and 320 GPa respectively[51]. According to the above equation, modulus decrease of about 5 to 10% corresponds to 2 to 3° decrease in orientation.

A gradually developing kink under compressive stress in polymeric fibers seems to be another reason for decreasing compressive modulus. The number of kinks increase with increasing axial stress [27,33]. Axial deformation is localized in the kinked regions[21,22], resulting in a decrease in the modulus. High-performance[52] and other polymeric textile fibers are often damaged during processing and handling. The kink-type of damage could affect initial fiber compressive modulus.

**3.2 Compressive strength:** Compressive failure in high-performance polymeric fibers is considered to be via formation and propagation of kinks (Fig.3) [2,7,15,19,33]. It should be mentioned that the kinking has been observed in many highly anisotropic systems such as metallic crystals [53-57], unidirectional and laminated polymer composites[58,59], carbon/carbon composites [60], anisotropic rocks[61], woods [62] etc. Significant research attempts have focussed on determining a suitable criterion for the kinking, which in turn was presumed to be a criterion for compressive failure[53,63-66]. In our opinion, the important question is whether the kinking and the compressive strength criteria coincide. For example, it has been established that the kinking in fibrous unidirectional composites under compression can result from other micro-failure processes such as fiber micro-buckling, fiber fracture, fiber mis-orientation, or due to fiber/matrix interface failure[17,47,26,59]. These examples suggest that the kinking could be just a post-

effect. A consequence of the kinking process is the localization of axial deformation. This effect has been observed experimentally in a compressed Kevlar™ 49 fiber using Raman spectroscopy [67]. Polymeric fibers allow the development of many kinks without brittle fracture. As a result, these materials exhibit very high energy-dissipation capacity and fracture toughness.

It has been reported that the variation in tensile modulus ( $E_t$ ) of PPTA fibers from 78 GPa to 184 GPa, and for PABI and PABI/PPTA fibers from 110 to 150 GPa, does not result in significant compressive strength variation[2-4]. However increasing compressive strength in PPTA with increasing modulus has been reported by one group of researchers[68,69]. Use of different coagulants and the variation in spin draw ratio for PBO fiber processing leads to the variation of tensile modulus of Heat-Treated (HT) PBO fibers from 130 to 210 GPa [2]. The compressive recoil strengths of all these HT PBO fibers was reported to be in the 200 to 300 MPa range. The compressive strength of heat-treated PBZT fibers was also reported to be independent of fiber modulus and fiber diameter[73]. In general, As-Spun (AS) PBZT and PBO fibers have much lower moduli (90-110 GPa) than fibers heat-treated under tension (200-300 GPa) [70]. It is of interest that the compressive strength of as-spun PBZT fibers has been reported to be lower (140-170 MPa) than that for the heat-treated PBZT fibers (200-300 MPa) [20,23,27], however according to one report, the compressive strength of both the as spun and heat treated PBZT fibers are similar[71]. On heat-treatment under tension molecular orientation, crystallite size, and overall order improves. For instance, the average crystallite mis-orientation angle in as spun PBZT fiber measured by WAXS azimuthal spreads of equatorial reflections is about  $\lambda=15-18^\circ$  which corresponds to a Hermans orientation factor of about 0.87[70]. In PBZT fibers heat-treated at different temperatures (300-650°C), the observed value of  $\lambda$  is typically  $5-7^\circ$  [70,72]. On the other hand, crystallite size significantly increases on heat treatment (as much as a factor of 5, typical transverse crystallite dimension in HT PBZT fiber is 10 to 12 nm)[70,72].

It has been observed that compressive strength of HT PABI and PABI/PPTA

fibers does not change as their tensile strength increases from 3.2 to 5.1 GPa[4]. The compressive strength of HT PABI fibers is not affected either with varying Weibull  $\beta^*$ -parameter (responsible for the tensile defect distribution) from 12 to 20 [4]. Compressive strength of PBO and PBZT fibers also does not vary with the tensile strength variations from 1.5 GPa to 3.5 GPa[2]. These facts point out that if compressive strength of polymeric fibers was controlled by defects, then these defects are of different nature than the defects controlling their tensile strength. Compressive strength may be affected by rather weak intermolecular or interfibrillar interactions, while theoretical tensile strength is due to breakage of covalent bonds in highly oriented polymer. Various types of defects can reduce the experimentally achievable values of tensile strength. Often polymeric fibers when tested in tension, for example PBZT, exhibit significant fiber splitting along the fiber axis [70,73]. This can be attributed to easy crack propagation along polymer crystallites/fibrils.

The following relationship between compressive strength and shear modulus for Kevlar™, PBZT, PE and liquid crystalline copolyester fibers has been obtained[74]:

$$\sigma_f \approx 0.25 G_f \quad (10).$$

Kozey & Berlin[4] have compared axial compressive strength and transverse tensile strength for different polymeric fibers (Fig.4). In the Terlon B and C fibers rigid comonomer chains are introduced into main PPTA chain (Fig.1). The fiber transverse tensile strength was obtained from transverse tensile testing of unidirectional polymeric fiber/epoxy tubes[75], using the data from the samples where failure was due to fiber splitting (for further discussion of intrafiber failure in transverse tensile and shear testing of polymeric fiber/epoxy matrix composite system see also refs.[28,76,77]). Figure 4 shows that axial compressive strength of the polymeric fibers linearly increases with transverse tensile strength.

### 3.3 Theoretical models :

3.3.1 Micro-buckling models: (i) Cooperative micro-buckling: The model has been

introduced for fibers in ref.[19], and is similar to the one developed in 60's for fiber composites [78,79]. In the model, compressive failure is assumed to be due to elastic micro-buckling of polymer chains. Cooperative "in phase" buckling of many closely spaced chains would take place in small region of a fiber (Fig.5), and hence the term "microbuckling". This term should be distinguished from Euler buckling of an unsupported fiber as a whole. According to the microbuckling model:

$$\sigma_f = G_f \quad (11)$$

Equation (11) was derived for microbuckling failure propagating normal to the fiber axis. Such type of microbuckling was observed experimentally in unidirectional composites based on soft polymer matrices[17,38]. However, compressive failure in polymeric fibers is due to kink formation at angles other than 90°, and usually a kink propagation angle  $\beta$  ranges from 45 to 60° (Figs.3,6). In such case the microbuckling strength is given by [80]:

$$\sigma_f = G_f + E_t \tan^2 \beta \quad (12)$$

The transverse modulus,  $E_t$ , of the Kevlar™ fibers is about 2.4 GPa [81]. Based on the kink propagation angle of about 45°, the compressive strength predicted according to equation 12 would be about 4.0 GPa. However, the measured compressive strength value for this fiber is only about 10% of the value estimated from equation 12. A plot of compressive recoil strength vs fiber shear modulus for various polymeric fibers is given in Fig.7 (experimental data are taken from refs.[2,73,82-85]), indicating lack of correlation between  $\sigma_f$  and  $G_f$ . However when the compressive strength and the shear modulus data was compared for Kevlar™ 49 as a function of temperature, it yields one to one correspondence between the two properties [85].

McGarry and Moally [86,87] suggest compressive failure via fibril microbuckling originating at the fiber surface, they further suggest that the application of hard ceramic coatings on the fiber surface can delay the microbuckling. Theoretical calculations suggest that the microbuckling strength falls by 20-30% if buckling fibrils were unsupported from one side i.e located on the fiber

surface [88]. On application of 700 nm thick  $\text{Al}_2\text{O}_3$  coating, compressive strength of PBO fibers was reported[86,87] to increase from 80 MPa (without coating) to 180 MPa (with coating). Both these values are lower than the normally reported recoil strength (210 to 400 MPa) for uncoated PBO fibers[2,3,12,33].

**(iii) Microbuckling of supported chains.** According to this model [47] compressive failure in polymeric fibers is attributed to microbuckling of a critical number of single chains encapsulated into elastic media of other chains responding like elastic springs with the stiffness equal to the transverse modulus of the fiber. The compressive strength in the supported fibril model is given by [47]:

$$\sigma_f = (E_f E_t / \pi)^{1/2} \quad (13)$$

Using the typical experimental values for Kevlar™ 49 ( $E_f = 120$  GPa and  $E_t = 2.40$  GPa [81]), one estimates the microbuckling strength from eq.(13) of about 10 GPa.

**3.3.2 Misorientation model:** Unlike the microbuckling models which consider that a fiber has perfectly aligned structure, a misorientation model [4,105] takes into account structural imperfections such as crystallite/fibril misorientations, as well as low transverse and shear properties of highly anisotropic polymeric fibers. An average misorientation measured by WAXS in high-performance polymeric fibers such as heat-treated PPTA, PBZT, and PBO range from 4 to 7° [70,72]. Local crystallite misorientation observed using TEM lattice imaging in these fibers is 3 to 5° [89]. The misorientation seems to play important role in compression behavior of highly anisotropic materials. For example, it was observed that if the angle between a zinc crystal axis and the compressive loading axis was small ( $< 2-3^\circ$ ) the crystal failed in buckling mode, and at angles greater than 2 - 3° the kinking failure occurred [54,56]. Argon[63] using an analogy with compressive behavior of crystals has proposed a misorientation model for a unidirectional composite (Fig.5a). He pointed out the importance of regions of local misorientation inside the composite, and used a dislocations approach to calculate the energy of nucleus consisting of misoriented

fibers. Gilman [56] and Argon[63] gave a similar formula for compressive strength of a material with small misorientation between the loading axis and the main axis of material symmetry (basal plane in a crystal and fiber axis in a composite):

$$\sigma_c^- = \tau/\phi \quad (14)$$

This represents the stress when structural elements (basal planes in a crystal, fibers in a composite or crystallites/fibrils in a fiber) start to slip under resolved shear stress, forming a kink. The kink initiation at fiber misoriented sites has experimentally been observed in unidirectional fibrous composites[47] and is discussed in part 3 of this series of papers. Based on the empirical relationship between the fiber shear strength and the transverse tensile strength, the misorientation model can be written as[4]:

$$\sigma_f = \tau_f/\phi = (1.4 \sigma_{t^+})/\phi \quad (15)$$

The misorientation model is consistent with the linear relationship between  $\sigma_f$  and  $\sigma_{t^+}$  illustrated by Fig.4. The typical experimental values of  $\sigma_{t^+} = 25$  MPa and  $\tau_f = 35$  MPa for Kevlar™ 49 (estimated from a composite test as well as from a single filament transverse compression test [81]) can be used to obtain the misorientation necessary to achieve the typical compressive strength value of 400 MPa for Kevlar, and yields  $\phi = 50^\circ$ . This predicted misorientation angle compares well with the average misorientation in the polymeric fibers measured by WAXS [90,91,69,70] as well as with the local misorientation measured by TEM lattice imaging [89].

**3.3.3 Crystallographic twinning:** The axial compressive failure in a polydiacetylene single crystal is reported to be due to crystallographic twinning [92]. The existence of a single (212) twin in the crystal is probably associated with its chain structure i.e. planar backbone and bulky side groups make it difficult to bend a molecule in a certain direction[92]. Compressive strain to twinning was determined by the shift in the Raman spectroscopy band, and was reported to be about 0.22%, which based on the experimental tensile modulus, translates to the compressive strength of about 100 MPa. The experimental procedure used in reference [92] allows the fiber

orientation to be accurate only within  $\pm 5^\circ$ .

Earlier studies of kinking in metallic crystals showed that kinks were formed by slip and bending of basal planes, and not by twinning [53-57]. Using WAXS, electron diffraction, and dark field imaging in TEM, different slip systems responsible for the formation of kink bands in various high-performance polymeric fibers (PBZT, PPTA, polyethylene, copolyester) have been investigated [72,93-95]. It was found that inter-crystalline and interfibrillar slips play a role in compressive failure of these fibers. The main crystallographic slip systems in various fibers are presented in Table 5. In addition to the inter-crystalline slip, interfibrillar slip was also observed in the polymeric fibers [93].

### **3.4 Perspectives on compressive strength of high-performance polymeric fibers:**

Various approaches that have been explored in an attempt to influence the compressive strength of high performance polymeric fibers are summarized below: (i) Chemical Modification and crosslinking[71,82,96-103]: Intermolecular crosslinking is one of the attempted approaches to improve the compressive strength of rigid-rod and semi-flexible polymer systems. Modified chemical structures along with the original structures that have been made to influence the compressive strength are given in Figure 1. Table 4 indicates that terphenyl PBZT, methyl pendant PBZT, and PBZT with fluorene moiety gives compressive strength values of up to 500 MPa, while on the other hand the values obtained from di-hydroxy PBZT are as low as 140 MPa. It should be noted that no direct evidence of crosslinking has yet been reported in these fibers. Swelling studies are currently carried out to monitor crosslinking [96], however swelling may be affected by increased crystallographic order and the skin core formation[73,100].

Sweeny's crosslinking approach[82] is based on thermal elimination of an activated aryl halogen, followed by combination of aryl free radicals to yield intermolecular crosslinking. The degree of crosslinking was estimated indirectly, by the amount of aryl halogen loss. Sweeny's data on recoil compressive strength of the

crosslinked PBZT fibers as a function of degree of crosslinking is presented in Figure 8. There is significant data scattering, which makes it difficult to draw unequivocal conclusion on the effect of crosslinking on compressive strength. The possibility of degradation which may lead to variations in properties can not be ruled out, and in fact there is spectroscopic evidence[100] to suggest degradation in methyl pendant PBO fibers on extended heat treatment. The recent efforts to crosslink the PPTA based fibers have not resulted in significant compressive strength improvements, and this is reported to be due in part at least to chain degradation [102, 103].

The various chemical modifications proposed above may only lead to a two dimensionally (2-D) crosslinked structure, resulting at best in a fiber structure akin to pitch based carbon fibers. Even carbon fibers having sheetlike graphitic order are weak in compression (e.g. pitch-based P100, PAN-based GY-70). Development of rigid-rod chemical structures capable of forming three dimensionally (3-D) cross-linked structures appears desirable and is the subject of current research[104].

The 17% increase (up to 560 MPa) in the recoil compressive strength has been observed for commercial PABI fibers when these fibers were exposed to X-ray irradiation dosage of 50 Mrad, while no compressive strength increase was observed at 10 Mrad dose [4]. Ion implantation of PBO fibers has also been attempted, however no compressive strength data was reported on the ion implanted fibers[105].

(b) Polymeric fibers infiltrated with silica glass[106]: This method was reported to have enhanced the compressive recoil strength of PBO fibers by 30%, from 210 MPa to 280 MPa[106].

(c) Fibril morphology modification [3,83,107]: In order to influence the fibrillar dimensions, fiber spinning was carried out with varying coagulation conditions [3, 83,107]. The recoil compressive strength of heat treated PBO fibers coagulated in water (at room temperature, 60°C, 90°C), steam at atmospheric pressure, methanol, and in 5% and 12% ammonium hydroxide was reported to be between 200 and 300 MPa[3]. Rakas and Farris [83] observed that the compressive recoil strength of as spun PPTA fibers decreases by 38-60% if ethanol or aqueous solution of potassium

iodide were used as coagulants instead of water. The WAXS studies of these low-strength PPTA fibers suggested no change in crystalline structure, although the average degree of misorientation increased considerably. The misorientation model appears to explain the observed low values. Bubeck et al. [107 ] report that the compressive strength of PBO fibers spun using slow coagulation was significantly higher (about 300 MPa) than the PBO fiber coagulation in water at room temperature (about 100 MPa).

The various approaches that have been pursued to influence the compressive strength of high performance polymeric fibers have at best yielded a compressive strength of about 600 MPa. The lower limit of compressive strength in these fibers has been about 150 MPa. This represents a four fold variation in compressive strength. And still one is not able to precisely pinpoint the factors responsible for this change. This has been due to difficulties in (i) accurate compressive strength measurement, (ii) determining the degree of crosslinking, (iii) measurement of fibril/microfibril dimensions, and (iv) studying the intermolecular and interfibrillar interactions (e.g differences between PBZT and di-hydroxy PBZT). The most influence on compressive strength has been reported with chemical modifications which possibly resulted in molecular crosslinking. The di-hydroxy PBZT resulted in lowest compressive strength fiber. The influence of variations in coagulation condition and of silica glass infiltration to prevent or delay microfibrillar buckling, have been moderate at best.

**3.5 Kinking in Polymeric Fibers:** Development of kink bands in polymeric fibers is considered to be the criterion for their compressive failure [15,19,33,20,27]. The feature of kinking is a sharp change in molecular orientation within a kink band (Fig.6). The kinking also occurs in shear, bending and twisting of polymeric fibers[109,110] and oriented polymers[111]. It appears that shear stresses developed in various loading conditions are responsible for the kinking process.

Some authors working mostly with metallic crystals, confirm that the kinking is the kind of plastic deformation in crystals [53,64,65]. In these papers

different slip systems responsible for kinking in the crystals are discussed. Other authors [55-57,66] consider the kinking as separate mechanism of plasticity in crystals which differs from slipping and twinning. It should be pointed out that the kinking is often observed in anisotropic materials failing in brittle rather than plastic manner. The examples of such systems include pitch-based carbon fibers [35], carbon/epoxy composites [17], carbon/carbon composites [60], anisotropic rocks [61] etc. Kinking was also observed in many non-crystalline materials such as rocks [61], wood [62], and various fibrous composites [15,17,38,58-60]. High morphological and mechanical anisotropy seems to be the main cause for kink development in all these systems. Therefore a global approach is needed to understand the kinking phenomenon in different anisotropic materials.

In our opinion, the important questions about the kinking process in polymeric fibers are: (i) Is the kinking primary failure mode or just post-effect; (ii) What causes the kink initiation and propagation under compression; (iii) What mechanical or morphological parameters affect kink geometry (Fig.6).

As mentioned earlier, a crystallite/microfibril slip near misoriented region inside fibers or local microbuckling are considered to trigger the kinking in polymeric fibers. Then crystallite/microfibril begin to slip as well as move away from the compression axis producing the region of instability. This region transforms into a kink band propagating approximately along the direction of maximum shear stresses in a sample i.e at about  $45^{\circ}$  to the compressive axis [63]. The stress concentration ahead the tip of kink band is responsible for its propagation across the fiber. Martin and Thomas [112] working on bright field (BF) and dark field (DF) TEM, HR- SEM, and TEM lattice images, have observed in a PBZT fiber a very small size kinks with the thickness of the order of 30 to 50 nm. It seems that such small kinks develops at the level of crystallites or microfibrils rather than large fibrils. After the kinking at the level of crystallites/microfibrils, the kinking process appears to repeat at the level of large fibrils resulting in a formation of more large-scale kink bands with thickness from 200 to 1000 nm or more [27,87]. The thickness

and density (that is number of kinks per unit fiber length) of these large-scale kinks increases with increasing strain [27,69,109].

Table 6 lists the reported kink boundary angles  $\beta$  (Figure 6) for various high-performance polymeric fibers. The values of  $\beta$  in Table 6 indicate that in general the direction of kink propagation differs from  $45^\circ$ . The angle  $\beta$  can be estimated using Budiansky's model [80] which is based on the analysis of initial instability caused by misorientation in an elastic anisotropic system under compression, and is given by:

$$(\sqrt{2}-1)[G_f/E_t][1-\sigma_f/G_f]^{1/2} < \tan \beta < [G_f/E_t][1-\sigma_f/G_f]^{1/2} \quad (16)$$

The typical parameters for Kevlar™ 49 are:  $(G_f/E_t) \approx 0.6$ ;  $(\sigma_f/G_f) \approx 0.25$ . According to equation 16, the calculated values of  $\beta$  range from  $18^\circ$  to  $38^\circ$ . Comparison of these values with the experimental data listed in Table 6 suggests that the Budiansky's model gives reasonable estimations for  $\beta$ . The values of  $G_f$ ,  $E_t$  and  $\sigma_f$  for Kevlar™ 29, 49, and 149 are quite similar [81,113]. Therefore, according to the Budiansky's model, the  $\beta$  values for these three fibers must also be similar, this is in agreement with the experimental data reported in Table 6.

Studies of kink propagation in oriented polymers [111] and in unidirectional composites [15,47] showed that after initial propagation of a kink band, its width increases while  $\beta$  remains constant. The similar observation has also been reported for Kevlar™ fibers [109].

The following relationship between  $\beta$  and an angle of change in orientation within kink band,  $\alpha$ , has been predicted to minimize a volume change within a kink band [58,60]:

$$\alpha = 2 \beta \quad (17)$$

The value of  $\alpha$  increases under stress in polymeric fibers while the angle  $\beta$  does not vary significantly [109,112]. This observation is not consistent with equation (17), and typically  $\alpha < 2 \beta$ . This indicates that total volume within a kink band increases during its propagation, sometimes leading to formation of micro-voids [105].

#### 4. CARBON FIBERS

**4.1 Compressive Modulus:** In contrast to compressive behavior of unidirectional composite reinforced with glass fibers, pitch and PAN based carbon fiber composites exhibit non-linear compressive response, that is attributed to non-linear compressive behavior of the carbon fibers themselves[13,41,114]. The non-linearity in compression is significantly more in pitch-based carbon fibers than in PAN-based carbon fibers[41]. Non-linear response in compression has also been observed for pyrolytic graphite[115]. For the measurement of compressive modulus, direct compression (DC) [15] and composite [41,114] tests were used. Both tests have disadvantages. In the DC test misalignment of a fiber could contribute to the modulus non-linearity [12,13]. In the composite test, carbon fibers (especially pitch based fibers) break at many points prior to final failure of the composite sample [26]. This effect could also contribute to the observed drop in compressive modulus.

**4.2 Compressive Strength of Graphite Crystal:** Compressive strength along graphitic planes of a pyrolytic graphite having structure approaching that of a single crystal graphite, is reported to be in the range of 100 to 210 MPa[115,116]. The experimental value of shear modulus between the basal planes in pyrolytic graphite is reported to be in the 130 to 350 MPa range[115-118]. These values overlap with the reported compressive strength for single crystal graphite, suggesting that the graphite crystal in compression may fail due to microbuckling. However twinning in single crystals has also been considered a possible compression failure mechanism[119, 120].

**4.3 Compressive Strength of Pitch-based Carbon Fibers:** For pitch-based carbon fibers the compressive strength values obtained from different test methods (TR, DC, composite test) are comparable [13,18,121,122] (see also Table 2). Figure 9 illustrates that the compressive strength of both pitch and PAN based carbon fibers decreases with increasing modulus [2,120,123]. This is, despite the fact that the low-modulus fibers have much higher void content (10-15%) than the high-modulus fibers (2 - 4%) [2].

In order to understand relatively low compressive strength of pitch-based carbon fibers as compared with the PAN based fibers (Table 1), their microstructure have to be taken into account. SEM observations indicate sheet-like morphology of pitch based carbon fibers (Fig.10) [120,124]. TEM lattice image analysis of pitch based carbon fibers show graphite-like sheet structures well-oriented along the fiber axis [10,44]. Average misorientation in various pitch-based fibers measured from WAXS as full width at half-maximum of the azimuthal (002) scan are presented in Table 8[120]. TEM lattice image analysis of the pitch fibers, especially high-modulus ones, indicates poor interlinkage of the graphite sheets [10,44]. The following can be taken as a measure of degree of this physical interlinkage: (a) ratio of D-line to G-line in Raman Spectroscopy [10] of carbon fibers, or (b) deviation of (002) d-spacing for a given fiber from the pure graphite spacing of 0.335 nm [2,125]. Low degree of interlinkage results in high mechanical anisotropy of the pitch-based carbon fibers (i.e. high value for  $E_{\text{long}}/E_{\text{trans}}$  or  $E/G$ ), and their low shear strength ( $\tau_f$ ) (Table 8). The shear strength of single carbon fibers ( $\tau_f$ ) presented in Table 7 is estimated from the data in reference [81] on transverse compression testing of single fibers, as transverse compression failure in carbon fibers is due to shear at  $45^\circ$ , like other brittle solids [126,127]. Thus  $\tau_f = 1/2\sigma_f \sin(2 \times 45^\circ) = \sigma_f/2$ . It should be noted that the lower limit of shear strength of anisotropic pitch based carbon fibers (0.04 - 0.17 GPa) approaches the shear strength of polymeric fibers ( $\approx 0.03-0.04$  GPa). On the other hand, the shear strength of less anisotropic PAN based carbon fibers (0.5-1.7 GPa) and of isotropic glass fibers (1.4 GPa) are relatively higher.

The kinking has been observed during axial compression of pitch based carbon fibers[35,105,123,125]. The best way to observe kinks in pitch-based carbon fibers is by following fiber shrinkage in selected polymer matrix [105]. In the composite test and in the recoil test it is rather difficult to observe the kinking in the pitch based carbon fibers as development of kink is soon followed by brittle failure along kink boundaries. Some authors however have observed kink formation in pitch based carbon fibers during the recoil test [35,123,125].

The theoretical models used for understanding compression behavior of polymeric fibers could also be employed to explain compression failure in pitch based carbon fibers. The microbuckling theory predicts that compressive strength (eq.11) would not depend on the type of reinforcement i.e. chains/fibrils-rods or sheets [79]. Figure 11 presents compressive strength vs shear modulus for pitch and PAN based carbon fibers [128]. As evident,  $\sigma_f$  does not correlate with  $G_f$ , and this is particularly true for PAN based carbon fibers. Besides, the magnitudes of shear moduli for pitch based carbon fibers (5-9 GPa) are much higher than their compressive strength values (0.5-1.8 GPa). According to the misorientation model, compressive strength is governed by misorientation angle and the fiber shear strength (see eq.14). Table 7 lists the calculated compressive strength based on the average misorientation angle and the fiber shear strength. The strength calculated based on the misorientation model agrees well with the experimental data.

**4.4 Compressive Strength of PAN based Carbon Fibers:** High strength PAN based carbon fibers fail in compression via shear-like (at approximately  $45^\circ$ ) brittle cracking rather than kinking [20,27-29,32,47] (see Fig.12). This type of compressive failure is also characteristic of brittle isotropic solids such as rocks and ceramics [126]. The distinction between such brittle shear fracture and the kinking in more anisotropic systems (high modulus pitch based carbon fibers and polymeric fibers) is that the shear fracture is not accompanied with change in orientation in the fractured region.

The shear modulus of PAN based carbon fibers, 15-17 GPa [128] as well as their shear strength, 0.5 - 1.8 GPa (estimated from single fiber transverse compression test [81,127]), are much higher as compared with pitch-based carbon fibers. Fitzer [10] has reported that the ratio of D-line to G-line measured in Laser Raman Spectroscopy in the PAN based carbon fiber (T-300) is four times that of the pitch based P-55 fiber, suggesting high structural disorder (interlinkage) in the high-strength PAN based carbon fibers.

Accurate determination of compressive strength in high strength PAN based

carbon fibers has not been without problems (see section 2.7 and Table 2). The compressive and tensile strengths from the loop test were measured to be the same for high-strength PAN Toreyaca M 40J, M 50J fibers [129] and Russian UKN 5000 fibers [17]. The compressive strength of unidirectional epoxy composites reinforced with high-strength PAN based carbon fibers such as AS4 or T-300 is comparable with their tensile strength, and therefore some authors assume that the compressive strength of the fibers is equal to their tensile strength [130,131]. The data from the bending beam [22,47] or the composite mini-sandwich test [132] also indicate that the compressive strength of high-strength PAN based carbon fibers are very close to their tensile strength (Table 2). Compressive strength of various high-strength PAN based carbon fibers has also been measured using the "fiber encapsulated block" test [26-29]. Authors reported very high values of compressive strain for such fibers (1.4-3.5%), which is 100-250% of their tensile failure strain.

The tensile strength of some PAN based carbon fibers was found to be gage length-dependent, indicating that defects such as voids could affect the tensile strength [10,44]. But recently developed high-strength PAN based carbon fibers, for example Toreyaca M 50, M 50J, M40J, M60J etc., have strength in loop (very small gauge length, < 1 mm) equal to the tensile strength measured at higher gauge lengths (10-40 mm) [129]. This suggests that fiber microstructure (crystallite sizes, crystallite misorientation etc.) rather than large defects affect fracture of such high-strength PAN based carbon fibers. Sharp-Reynold's model[50] describes tensile failure in carbon fibers as originating from shear-induced microcracks in misoriented ( $\approx 45^\circ$ ) graphite-like crystallites. The comparable values of compressive and tensile strengths for high-strength PAN based carbon fibers, as well as "shear" type of compressive failure in these fibers suggest that the Sharp-Reynold's mechanism may also be applicable in compression. If a crack propagated perpendicular to the fiber axis, tensile and compressive strengths would be different. This is due to the fact that in tension the axial stress opens the crack tip of such cracks, while the compressive stress would close tend to close such a tip, producing

different stress concentrations at the crack tip. In the case of a shear-induced microcrack inclined at about 45°, the stress concentrations and consequently strengths in tension and compression would be equal.

## **REFERENCES**

1. **Advanced Composite Materials. Products & Manufacturers.,** edited by D.J. DeRenzo (Noyes Data Corp.Publ., Park Ridge N.J., 1988).
2. S. Kumar, T.E.Helminiak, in *Mater. Res. Soc. (MRS) Symp. Proceed.,v.134* , edited by W.W.Adams, R.K.Eby,, D.E.McLemore (MRS Publ., Pittsburgh, 1989) p.363-374.
3. S.Kumar in *Intern. Encyclopedia of Composites, v.4*, edited by S.M.Lee (VCH Publ., N.Y., 1990) p.51.
4. V.V.Kozey, A.A.Berlin, Paper N 22-P from 3 Japan-USSR joint Symp. on advanced composites materials, edited Y.M.Tovmasyan, (ICP Publ., Moscow, 1991).
5. P. Smith andP. J. Lemstra, *J. Mater. Sci.* **15** (1980) 505.
6. W. R. Krigbaum in "Handbook of Fiber Science and Technology: Vol III, High Technology Fibers - Part B" M. Lewin and J. Preston editors, Marcel Dekker inc. (1989).
7. R.E.Wilfong, J.Zimmerman, *J.Appl.Polym. Sci. Polym. Symp.* **31**,1-19 (1977).
8. W.W. Adams, R.K.Eby, D.E. McLemore editors, *MRS Proc, Vol 134* (1989).
9. J. F. Wolfe, " *Encyclopedia of Polymer Sci. & Engr.*" Vol 11 (1988) 601.
10. E.Fitzer, *Carbon* **27**, 621 (1989).
11. J. B. Donnet and R. C. Bansal, "Carbon Fibers", Marcel Dekker Inc. (1984).
12. S.A.Fawaz, A.N.Palazotto, C.S.Wang, *Mater. Res. Soc. Symp. Proceed., v.134*, edited by W.W.Adams, R.K.Eby, D.E.McLemore D.E., (MRS Publ., Pittsburgh, 1989) p.381-388.
13. K.S.Masturk, R.K.Eby, W.W.Adams, *Polymer* **32**, 1782-1789 (1991).
14. D.Sinclair, *J.Appl. Phys.* **21**, 380-389 (1950).

15. J.H.Greenwood, P.G.Rose, *J. Mater. Sci.* 9, 1809-1815 (1974).
16. W.R.Jones, J.W.Johnson, *Carbon* 9, 645-651 (1971).
17. S.L.Bazhenov, V.V.Kozey, *J.Mater.Sci.* 26, 6764-6771 (1991).
18. M.Furuyama, M.Higuchi, K.Kubomura, H.Sunago, H.Jiang, S.Kumar, *J Mater. Sci.* 28, 1611-1618 (1993).
19. S.J.DeTeresa, AFWAL-TR-85-4013, (1985).
20. S.Fidan, M.S. Thesis, Air Force Institute of Technology, WPAFB, (1988).
21. C.Vlattas, C.Galiotis, *Polymer* 32, 1788-1795 (1991).
22. N.Melanitis, C.Galiotis, *J.Mater.Sci.* 25, 5081-5089 (1990).
23. M.E.Hunsaker, G.E.Price, S.J.Bai, *Polymer* 33, 2128-2133 (1992).
24. Mrse A.M., Piggott M.R., in *Proceed. of 35-th Intern. SAMPE Symp.*, (SAMPE Publ., Covina CA, 1990), pp.2236-2240.
25. H.M.Hawthorne, P.Teghsoonian, *J. Mater.Sci.* 10, 41-51 (1975).
26. H.T.Hahn, M.Sohi, S.Moon, NASA Contractor Report 3988, (June 1986).
27. W.Huh, S.Kumar, T.E.Helminiak, W.W.Adams, in *Proceed. of SPE Annual Tech. Conf.*, (1990), pp.1245-1247.
28. L.T.Drzal, AFWAL-TR-86-4003, (1986).
29. S.J.DeTeresa, *Carbon* 29, 397-405 (1991).
30. T.Ohsawa, M.Miwa, M.Kawade, E.Tsushima, *J.Appl.Polym. Sci.* 39, 1733-1741 (1990).
31. A.Kelly, W.R.Tyson, *J.Mech.Phys.Solid* 13, 329-336 (1965).
32. D.J.Boll, R.M.Jensen, L.Cordner, W.Bascom, *J. Comp.Mater.* 24, 208-213 (1990).
33. S.R.Allen, *J. Mater. Sci.* 22, 853-860 (1987).
34. H.Jiang, S.Damodaran, P.Desai, S.Kumar, A.S.Abhiraman, in *Amer. Chemic. Soc (ACS) Proceed., Polym. Sci.&Eng.*, 64, 383-387 (1991).
35. M.G.Dobb, D.J.Johnson, C.R.Park, *J.Mater.Sci.* 25, 829-834 (1990).
36. A.Pytel, L.L.Singer, *Strength of materials.* (Harper and Row Publ., N.Y.,1987).
37. C.O.Horgan, *Int.J. Solid Struct.* 10, 837-843 (1974).
38. S.L.Bazhenov, V.V.Kozey, A.A.Berlin, *J.Mater.Sci.* 24, 4509-4517 (1989).

39. V.V.Kozey, *J.Mater.Sci.Lett.* 12, 48-54 (1993).
40. V. V. Kozey and S. Kumar, Part III
41. A.S.Crasto, R.J.Kim, in *Proceed. of 36 Intern.SAMPE Conf.*, (SAMPE Publ., Covina CA, 1991), pp.1649-1654.
42. J.Nic, J.Yang, Z.Hu, Y.Zheng, in *Proc. of 7-th Intern Conf. on Compos.Mater.- ICCM 7, v.2*, (Pergamon Press Publ., N.Y., 1989), pp.133-137.
43. M.Panar, P.Avakian, R.C.Blume, K.H.Gardner, T.G.Gierke, H.H.Yang, *J. Polym. Sci. Polym.Phys.* 21, 1955-1962 (1983).
44. D.J.Johnson, in *Carbon Fiber Filaments and Composites*, edited by G.Figueiredo, C.A.Bernardo, R.T.K.Baker, K.J.Huttinger, (Kluwer Academic Publ.,1990), pp.119-146.
45. J.M.Prandy, H.T.Hahn, *SAMPE-Quart.* 22, 47-52 (1991).
46. A.S.Crasto, S.Kumar, in *Proceed. of 35-th SAMPE Intern. Symp.*, (SAMPE Publ., Covina CA, 1990), pp.318-324.
47. V.V.Kozey, Ph.D. Dissertation, *Polymers &Composites Program, Moscow Institute of Physics & Technology*, (Moscow, 1990).
48. H.Jiang, R.K.Eby, W.W.Adams, G.Lenhart, in *Mater. Res. Soc. (MRS) Symp. Proceed.*, v.134, 341-350 (1989).
49. P.E.Klunzinger, R.G.Ramirez, D.A.Thomas, R.K.Eby, *Amer. Phys. Soc. Bulletin* 37, 508-512 (1992).
50. W.N.Reynolds, J.V.Sharp, *Carbon* 12,105-112 (1974).
51. K.Tashiro, M.Kobayashi, Sen-I, *Gakkaishi* 43, 78-82 (1987).
52. S.R.Allen, *AFWAL-TR-83-4065*, (1983).
53. E.Orowan in *Dislocations in Metals*, edited by M.Cohen, (AIME Publ., N.Y., 1954).
54. J.B.Hess, C.S.Barrett, *Trans. AIME J.Metals* 185, 599-606 (1949).
55. J.B.Hess, C.S.Barrett, *Trans. AIME J.Metals* 188, 1022-1029 (1950).
56. J.J.Gilman, *Trans. AIME J.Metals* 192, 621-629 (1954).
57. J.J.Gilman, *Trans. AIME J.Metals* 194, 205-214 (1955).

58. C.R.Chaplin, *J.Mater.Sci.* 12, 347-353 (1977).
59. E.G.Guynn, W.L.Bradley, *J.Comp.Mat.* 23, 479-488 (1989).
60. A.G.Evans, N.F.Adler, *Acta Metallurgica* 26, 725-732 (1978).
61. F.A.Donath, *American Scientist* 58, 54-58 (1970).
62. F. F. Wangaard, "The Mechanical Properties of Wood", John Wiley, (1950).
63. A.S.Argon, in *Treatise on Materials Sci.&Techn.*, (Academic Press Publ., N.Y., 1972), pp.79-93.
64. D.A.Zaukelies, *J.Appl.Phys.* 33, 2797-2804(1962).
65. P.B.Bowden, R.J.Young, *J.Mater.Sci.* 9, 2034-2045 (1974).
66. "Mechanical behaviour of materials", edited by F.A.McClintock and A.S.Argon, (Addison-Wesley Publ., Reading MA,1966).
67. H.Jahankhani, C. Galiotis, in *Interfaces in polymer, ceramic and metal matrix composites*, edited by H.Ishida, (Pergamon Publ.,N.Y., 1988), pp.107-114.
68. S.Van der Zwaag, G.Kampschoer, in *Integration of Fundamental Polym.Sci.&Techn*, v.2, (Elsevier Appl.Sci.Publ., London, 1988), pp.545-551.
69. S.Van der Zwaag, S.J.Picker, C.P.Van Sluijs, in *Integration of Fundamental Polym.Sci.&Techn*, v.3, (Elsevier Appl.Sci., London, 1989), pp.199-205.
70. S.R.Allen, R.Porter, R.Farris, *J.Mater.Sci.* 20, 4588-4593 (1985).
71. U.Santhosh, M.H.Dotrong, H.H.Song, C.Y.-C.Lee, *Amer. Chemic. Soc. (ACS) Proceed., Polym. Sci.&Eng.*, v.65, 40-47 (1991).
72. E.J.Roche, T.Takahashi, E.L.Thomas, *ACS Symp. Fiber Diffraction Methods* v.141, 303-309 (1980).
73. M. Sahafeyan and S. Kumar, to be published in *Macromol Chem. and Phys.*
74. S.J.DeTeresa, R.J.Farris, in *Mater. Res. Soc. (MRS) Symp. Proced.v.134* , edited by W.W.Adams, R.K.Eby,, D.E.McLemore (MRS Publ., Pittsburgh, 1989) pp.375-380.
75. Y.M.Tarnopolskii, T.A.Kintsis, *Static methods of testing reinforced plastics*, (Van Nostrand Reinhold Publ., N.Y., 1985).
76. B.V.Perov, A.M.Skudra, G.P.Mashinskaja, F.J.Bulavs, in *Proceed. of I USA-*

- USSR Symp. on composites, edited by G.S.Sih, V.P.Tamuzs, (Van Nostrand Reinhold Publ., N.Y.,1978), pp.291-298.
77. O.P.Lebedeva, Ph.D. Dissertation, Institute of Chemical Physics, (Moscow, 1989).
  78. B.W.Rosen, in Fiber composite materials, (Amer.Soc. Metals, Metals Park, 1964).
  79. A.L.Rabinovich, in Proceed. of Moscow Inst. of Physics & Technology, edited by V.Petrov, (Oborongiz Publ., Moscow, N 7, 1961).
  80. B.Budiansky, Computers & Structures 16, 3-11 (1983).
  81. S.Kawabata, J.Textile Instit. 81, 432-439 (1990).
  82. W. Sweeny, J. Polym. Sci. Pt.A. 30, 1111-1119 (1992).
  83. M.R.Rakas, R.J.Farris, in Mater. Res. Soc. (MRS) Symp. Proceed.v.134 , edited by W.W.Adams, R.K.Eby,, D.E.McLemore (MRS Publ., Pittsburgh, 1989) pp.277-282.
  84. C.R.Hwang , M.F.Malone, R.J.Farris, D.C.Martin, E.L.Thomas, in Mater. Res. Soc. (MRS) Symp. Proceed.v.134 , edited by W.W.Adams, R.K.Eby,, D.E. McLemore (MRS Publ., Pittsburgh, 1989) pp.547-552.
  85. V. R. Mehta and S. Kumar, to be published in J. Mater. Sci.
  86. F.J.McGarry, J.E.Moalli, SAMPE-Quart. 23, 35-40 (1992).
  87. F.J.McGarry, J.E.Moalli, Polymer 32, 1816-1822 (1991).
  88. Y.N.Lapusta, Mechanics of composites 4, 739-742 (1990).
  89. D.C.Martin, WL-TR-91-4011 (1991).
  90. E.M.Sanford, G.M.Prilutski, in Mater. Res. Soc. (MRS) Proceed., v.171, 147-152 (1990).
  91. W.C.Uy, E.R.Perusich E., in Mater. Res. Soc. Proceed., (MRS) Proceed., v.171, 153-156 (1990).
  92. I.M.Robinson, P.H.J.Yeung, C.Galotis, R.J.Young, D.N.Batchelder, J.Mater. Sci. 21, 3440-3446 (1986).
  93. T.Takahashi, M.Miura, K.Sakurai, J.Appl. Polym. Sci. 28, 579-585 (1983).

94. T.Takahashi, K.Suzuki, K.Sakurai, J.Macrom.Sci. Phys. B 30, 101-107 (1990).
95. T.Takahashi, C.-F.Xiao, K.Sakurai, Sen -I Gakkaishi 47, 397-402 (1991).
96. (a) S.Bhattacharya, H.H.Chauh, M.Dotrong, K.H.Wei, C.S.Wang, A.Vezie, A.Day, W.W.Adams, Amer. Chemic. Soc. (ACS) Proceed., Polym. Sci.&Eng. v.60, 512-519 (1989). (b) M. Dotrong and R. C. Evers, Polym Mater. Sci. & Engr. V 60 (1989) p. 507.
97. C.S.Wang, J.Burkett, S.Bhattacharya, H.H.Chauh, F.E.Arnold, Amer Chemic. Soc Proceed., Polym. Sci.&Eng. v.60, 767-772 (1989).
98. H.H.Chauh, S.S.Tsai, C.S.Wang, F.E.Arnold, Amer. Chemic. Soc Proceed., Polym. Sci.&Eng. v.60, 517-522 (1989).
99. T.D.Dang, L.S.Tan, K.H.Wei, H.H.Chauh, F.E.Arnold, Amer. Chemic. Soc. Proceed., Polym. Sci.&Eng. v.60, 424-428 (1989).
100. V. R. Mehta and S. Kumar, to be published.
101. D.C.Martin, T.Jiang, J.Rigney, M.-C.Jones, L.Markoski, J.S.Moore, Polymer Preprints (ACS), 34(2) (1993) 720.
102. C. Rickert, P. Neuenschwander, U. W. Suter, Macromol Chem. and Phys. Vol 195 (1994) p. 511
103. B. Gloom, C. Rickert, P. Neuenschwander, U. W. Suter, Macromol Chem. and Phys. Vol 195 (1994) p. 525.
104. X. Hu, M. B. Polk, and S.Kumar, "Three dimensionally crosslinkable rigid-rod polymer systems", paper presented at the spring MRS meeting, San Fransisco, (1994).
105. Vezie D., Ph.D. thesis, MIT, (1993).
106. R.F.Kovar, R.R.Hagghat, R.W.Lusignea, in Mater. Res. Soc. (MRS) Symp. Proceed.v.134 , edited by W.W.Adams, R.K.Eby,, D.E.McLemore (MRS Publ., Pittsburgh, 1989) pp.389-394.
107. J.K.Gillie, M.Newsham, S.J.Nolan, V.S.Jear, R.A.Bubeck, Amer. Phys. Soc. Bulletin v.38 , 292 (1993).
108. V.V.Kozey, S.Kumar S., "Compressive behavior of materials. Part 1-Glassy

polymers", to be published.

109. M.G.Dobb, D.J.Johnson, B.P.Saville, *Polymer* 22, 960-965 (1981).
110. J.J.DeTeresa, S.R.Allen, R.J.Farris, R.S.Porter, *J.Mater.Sci.* 19, 57-65 (1984).
111. R.E.Robertson, *J.Polym Sci. A-2*, v.7, 1315-1322 (1969).
112. D. C. Martin, E.L.Thomas, *J. Mater.Sci.* 26, 5171-5177 (1991).
113. V.Mehta, S.Kumar, *Amer. Phys. Soc. Bulletin*, v.38, 280 (1993).
114. K.Kubomura, T.Tsuji, in *Proceed. of 36 Intern.SAMPE Con.f.*, (SAMPE Publ., Covina CA, 1991), pp.1664-1670.
115. E.J.Seldin, *Carbon* 4, 177-185 (1966).
116. W.H.Smith, D.H.Leeds, in "Modern Materials- Advances in Development and Applications", v.7, edited by B.W. Gonser, (Academic Press Publ., 1970), pp.166- 174.
117. D.E.Soule, C.W.Nezbeda, *J.Appl.Phys.* 39, 5122-5131 (1968).
118. O.L.Blakslee, *J.Appl.Phys.* 41, 3373-3380 (1970).
119. L.M.Gillin, A.Kelly, in *Proceed. of Intern.Conf. on Electron Diffraction & Crystal Defects*, p.II L-4, (Melbourne, 1965).
120. S.Kumar, P.Anderson, A.S. Crasto, *J.Mater.Sci.* 28, 423-439 (1993).
121. T.A.Doyne, A.N.Palazotto, T.Schuppe, C.Y.-C.Lee, C.S.Wang , *Amer. Chemic. Soc (ACS) Proceed., Polym. Sci.&Eng.*, v.63, 982-987 (1990).
122. G.J.Hayes, D.D.Edie, T.Stephan, Abstract presented to Carbon Conf. in Buffalo, 1993.
123. G.J.Hayes, D.D.Edie, J.M.Kennedy, *J.Mater.Sci.* 28, 3247-3257 (1993).
124. M.Endo, *J.Mater.Sci.* 23, 598-603 (1988).
125. C.R.Park, Ph.D thesis, University of Leeds, UK, (1990).
126. L.Obert, in *Fracture of nonmetals and composites*, edited by H.Liebowitz, (Academic Press Publ., N.Y., 1972), pp.60-95.
127. K.Fujita, Y.Sawada, Y.Nakanishi, in *Proceed. of 37th Intern.SAMPE Symp.*, (SAMPE Publ, Covina CA,1992), pp.593-605.
128. S.Kumar, V.Mehta, P.Anderson, A.S.Crasto,in *Proceed. of 37 Intern. SAMPE*

- Symp., (SAMPE Publ, Covina CA,1992), pp.967-976.
129. A.Sumida, K.Ono, Y.Kawaru, in Proceed. of 34 Intern. SAMPE Symp., (SAMPE Publ, Covina CA, 1989), pp.2579-2585.
  130. J.H.Sinclair, C.C. Chamis, in ASTM STP 808, (Americ.Soc. for testing @ materials, Philadelphia, 1983), pp.155-169.
  131. R.K.Clark, W.B.Lisagor, in ASTM STP 734, (Americ.Soc. for testing @ materials, Philadelphia, 1981), pp.34-49.
  132. A.S.Crasto, R.Y.Kim, in Proceed. of 22-nd SAMPE Techn. Conf., (1990), pp.264-272.

## Figure Captions:

- Figure 1.** Chemical structures of various high performance polymers (i) poly (paraphenylene benzobisthiazole) (PBZT)[3, 8, 9], (ii) poly (paraphenylene benzobisoxazole) (PBO) [3, 8, 9], (iii) poly (paraphenylene terephthalamide) (PPTA) [7], (iv) poly (amide benzimidazole) (PABI)[4], (v) Terlon B[4], (vi) Terlon C[4], (vii) methyl pendant PBZT[98], (viii) PBZT modified with fluorene moiety[96], (ix) di-hydroxy PBZT[99], (x) Brominated PBZT[82], (xi) modified PPTA[101], (xii) modified PPTA[102,103], (xiii) terphenyl PBZT[ Arnold in ref 8]. For polymer structures (vii) through (xiii) random copolymers with PBZT (where modification is based on PBZT) or with PPTA (where modification is based on PPTA) have also been made.
- Figure 2.** (a) Loop test, typical loop test data for (b) glass fiber[17] and (c) high strength PAN based carbon fiber(T-800)[17].
- Figure 3.** Kink under compression in polymeric fibers. (a) Kevlar 49 fiber tested in recoil, (b, c, d) HT-PBZT fiber tested in recoil[73], and (e) HT-PBO fiber under compression in FEPB test - compressed fiber removed from the matrix and peeled for SEM observation[27].
- Figure 4.** Axial compressive strength vs transverse tensile strength for high performance polymeric fibers [4].
- Figure 5.** Compressive failure models in high performance fibers (a) misorientation model, and (b) microbuckling model.
- Figure 6.** Kink Geometry.
- Figure 7.** Compressive recoil strength vs shear modulus for high performance polymeric fibers. Data from references [2, 73, 82-84].
- Figure 8.** Compressive strength vs degree of chemical crosslinking in modified PBZT fiber[data from reference 82]. Amount of halogen loss has been taken as a measure of the degree of crosslinking[82].
- Figure 9.** Compressive strength vs fiber tensile modulus for pitch and PAN based carbon fibers[120].

Figure 10. Scanning electron micrograph of (a) pitch based and (b) PAN based carbon fiber[120].

Figure 11. Compressive strength vs shear modulus of various carbon fibers[128].

Figure 12. Shear like failure in high strength PAN based carbon fiber[47].

Table 1. Properties of various high-performance fibers.

Fiber	Density (g/cm <sup>3</sup> )	Modulus (GPa), longitudinal <sup>1</sup> , transversal <sup>2</sup> , shear <sup>3</sup>	Tensile strength (GPa), longitudinal <sup>1</sup> , transversal <sup>2</sup>	Compressive strength(GPa) longitudinal <sup>1</sup> , transversal <sup>2</sup>
Alumina (Al <sub>2</sub> O <sub>3</sub> )	3.7	350 <sup>1</sup> , 12-26 <sup>2</sup>	1.7 <sup>1</sup>	6.9 <sup>1</sup> , 2.3 <sup>2</sup>
Boron	2.5	415 <sup>1</sup>	3.5 <sup>1</sup>	5.0 <sup>1</sup>
SiC	2.8	200 <sup>1</sup> ,	2.8 <sup>1</sup>	3.1 <sup>1</sup> ,
E-glass	2.58	76 <sup>1</sup> , 68 <sup>2</sup>	3.4 <sup>1</sup>	4.2 <sup>1</sup> , 2.7 <sup>2</sup>
Pitch based carbon fibers				
P 25	1.9	159 <sup>1</sup> , 9.95 <sup>2</sup>	1.4 <sup>1</sup>	1.15 <sup>1</sup> , 0.6 <sup>2</sup>
P 55	2.0	380 <sup>1</sup> , 6.75 <sup>2</sup> , 6.6 <sup>3</sup>	1.7 <sup>1</sup>	0.8 <sup>1</sup> , 0.3 <sup>2</sup>
P 75	2.05	517 <sup>1</sup> , 4.85 <sup>2</sup> , 8.0 <sup>3</sup>	2.1 <sup>1</sup>	0.7 <sup>1</sup> , 0.2 <sup>2</sup>
P 100	2.15	724 <sup>1</sup> , 4.1 <sup>2</sup> , 4.7 <sup>3</sup>	2.2 <sup>1</sup>	0.5 <sup>1</sup> , 0.13 <sup>2</sup>
P 120	2.18	827 <sup>1</sup> , 3.1 <sup>2</sup>	2.2 <sup>1</sup>	0.45 <sup>1</sup> , 0.08 <sup>2</sup>
PAN based carbon fibers				
GY 70	1.96	517 <sup>1</sup>	1.86 <sup>1</sup>	1.06 <sup>1</sup>
T 300	1.79	230 <sup>1</sup> , 6.0 <sup>2</sup> , 15.0 <sup>3</sup>	3.2 <sup>1</sup>	2.7 <sup>1</sup> -3.2 <sup>1</sup> , 2.7 <sup>2</sup>
AS 4	1.80	230 <sup>1</sup> , 17.0 <sup>3</sup>	3.6 <sup>1</sup>	2.7 <sup>1</sup>
T 800	1.80	300 <sup>1</sup>	5.6 <sup>1</sup>	2.8 <sup>1</sup> -5.6 <sup>1</sup>
Russian UKN 5000 A	1.74	230 <sup>1</sup>	2.5 <sup>1</sup>	2.5 <sup>1</sup>
UKN 5000 B	1.75	240 <sup>1</sup>	3.2 <sup>1</sup>	3.0 - 3.2 <sup>1</sup>
UKN 5000 C	1.74	230 <sup>1</sup>	4.5 <sup>1</sup>	2.2 - 4.5 <sup>1</sup>
Courtauld's Grafil XA	1.78	240 <sup>1</sup>	3.5 <sup>1</sup>	1.75 - 3.5 <sup>1</sup>
M40	1.84	400 <sup>1</sup>	2.8 <sup>1</sup>	1.4 <sup>1</sup>
Russian HM	1.86	480 <sup>1</sup>	1.4 <sup>1</sup>	0.7 <sup>1</sup>
Polymeric Fibers				
Kevlar <sup>TM</sup> 49	1.45	125 <sup>1</sup> , 2.5 <sup>2</sup> , 1.4 <sup>3</sup>	3.5 <sup>1</sup>	0.35 - 0.45 <sup>1</sup> , 0.06 <sup>1</sup>
Kevlar <sup>TM</sup> 149	1.47	185 <sup>1</sup> , 2.5 <sup>2</sup> , 1.2 <sup>3</sup>	3.4 <sup>1</sup>	0.32 - 0.46 <sup>1</sup> , 0.07 <sup>2</sup>
Terlon <sup>TM</sup> A	1.45	135 <sup>1</sup>	3.8 <sup>1</sup> , 0.022 <sup>2</sup>	0.40 <sup>1</sup>
Terlon <sup>TM</sup> B	1.32	133 <sup>1</sup>	3.2 <sup>1</sup> , 0.013 <sup>2</sup>	0.30 <sup>1</sup>
Terlon <sup>TM</sup> C	1.46	184 <sup>1</sup>	3.6 <sup>1</sup> , 0.013 <sup>2</sup>	0.31 <sup>1</sup>
PABI	1.45	122 <sup>1</sup>	4.0 <sup>1</sup> , 0.024 <sup>2</sup>	0.42 <sup>1</sup>
PABI/PPTA	1.45	150 <sup>1</sup>	5.2 <sup>1</sup> , 0.026 <sup>2</sup>	0.43 <sup>1</sup>
PBO	1.58	200 - 320 <sup>1</sup> , 1.0 <sup>3</sup>	3.0 - 5.0 <sup>1</sup>	0.20 - 0.40 <sup>1</sup>
PBZT	1.58	200 - 300 <sup>1</sup> , 1.2 <sup>3</sup>	2.6 - 3.9 <sup>1</sup>	0.3 - 0.4 <sup>1</sup>

References: Longitudinal Tensile modulus [2,4], transverse compressive modulus[81], shear axial modulus[85], longitudinal tensile strength[2,4], transverse tensile strength[4], longitudinal compressive strength[2,4], transverse compressive strength[81].

Kevlar<sup>TM</sup> and Terlon<sup>TM</sup> A are both PPTA fibers.

Table 2. The ratio of compressive to tensile strength for various carbon fibers.  
Compressive strength values obtained from different tests.

Fiber\Test	Loop	Bending beam	Reco <sup>1</sup>	Encapsulated into block	From composite
<b>PAN-based, high-strength</b>					
Russian UKN 5000	1.0 [47]	1.0 [47]	0.65 [47];	-	0.97 [20]
UKN 5000B	1.0 [47]	1.0 [47]	-	-	0.75 [20]
Toreyca T300	1.03 [18]	-	-	1.0 [27]	0.9-1.0 [130]
Courtaulds Grafil XA	-	1.0 [22]	0.50 [35]	-	-
UKN 5000C	0.91 [47]	1.0 [47]	0.40 [47];	-	0.53 [47]
Toreyca T800	0.42 [47]	1.0 [47]	-	-	0.44 [47]
<b>PAN-based, high-strength high-modulus:</b>					
Toreyca M40	0.66 [47]- 0.85 [18]	0.90 [47]	0.44 [18]	-	0.38 [47]
<b>PAN-based, ultra-high modulus:</b>					
Russian HM	-	0.47 [47]	-	-	0.50 [47]
BASF GY 70	-	-	-	0.58 [30]	0.60 [30]
<b>Pitch-based</b>					
P 55	-	-	0.30 [35]- 0.44 [123]	-	0.50 [120]
P 75	-	-	0.25 [35]- 0.36 [123]	0.53 [33]	0.33 [120]
P100	-	-	0.22 [35]- 0.24 [123]	-	0.21 [120]

Table 3. Influence of various test techniques on compressive strength of high-performance polymeric fibers

Test/Fiber	PPTA	PBO	PBZT
Loop	510-790 (MPa) [4,20]	430 [20]	390 [20]
Bending beam	380-690 [9,20,21]	320 [20]	300 [20]
Encapsulated into block	310-430 [27,28]	380 [27]	330-420 [28,27]
Recoil	360 [33]	200-350 [2,33]	200-300 [73]
Direct compression	210 [12]	300 [12]	-
From composite	400 [2,33]	200-345 [33,12]	340 [33]

Table 4. Recoil compressive strength of modified PBZT fibers.

Fiber	Tensile modulus (GPa)	Tensile strength (GPa)	Compressive strength (GPa)
PBZT, control	240	2.3	200-300 [73]
F-PBZT	240	2.1	320-550[96]
T-PBZT	220	2.4	210-490[98]
M-PBZT	200	2.3	300-400[71]
H-PBZT	180	2.1	140-410[99]

F-fluorene moiety in PBZT ; T- terphenyl PBZT; M-methyl pendant PBZT; H-hydroxy PBZT. Chemical structures of PBZT and modified PBZT are given in Figure 1.

Table 5. Crystal slip systems for different polymeric fibers.

Fiber	Slip system
Ultra-high-molecular-weight polyethylene	(110)<001> and (100)<001> [94]
PPTA	(200)<001> [97]
PBZT	(010)<001> [72]
Aromatic polyester	(110)<001> and (100)<001> [95]

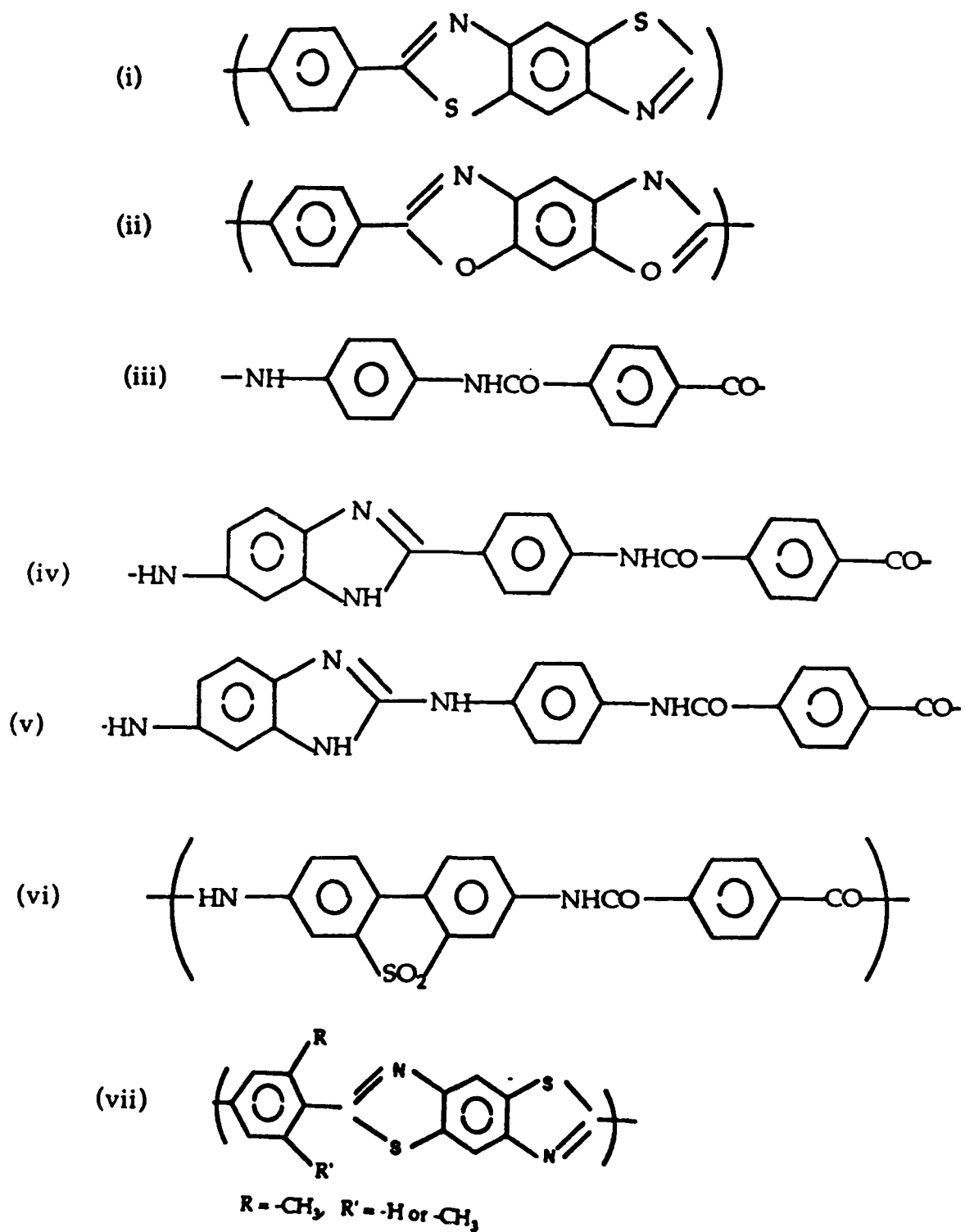
Table 6. The kink band angles in various polymeric fibers.

Kevlar™ 29	36° [27]
Kevlar™ 49	36° [74], 40-50° [109], 30° [7,68], 20-30° [94]
Kevlar™ 149	38° [27]
AS PBZT	22° [27]
HT PBZT	17° [27]
AS PBO	22° [27], 15° [89]
HT (600° C) PBO	22° [27], 21° [89]
HT (665° C) PBO	24° [89]

Table 7. Morphological and mechanical properties of pitch-based carbon fibers.

Fiber/ property	P 55	P 75	P 100	P 120
Average misorienta- tion <sup>1</sup>	14.1 <sup>0</sup>	11 <sup>0</sup>	6.0 <sup>0</sup>	5.6
Modulus anisotropy <sup>3</sup>	56	107	178	270
Shear strength <sup>4</sup> (MPa)	170	110	65	40
Compressive strength (MPa)	800	690	480	450
Calculated compressive strength <sup>5</sup> (MPa)	710	580	650	420

1- measured by WAXS, 3- ratio of longitudinal to transversal moduli, 4- shear strength = 1/2 of transversal compression strength, experimental data are taken from ref.[81]; 5- compressive strength= shear strength/ average misorientation.



AD-A284 959

STUDY OF THE COMPRESSION BEHAVIOR OF HIGH PERFORMANCE  
FIBERS(U) GEORGIA TECH RESEARCH INST ATLANTA S KUMAR  
25 AUG 94 AFOSR-TR-94-0560 AFOSR-91-0194

2/2

UNCLASSIFIED

NL



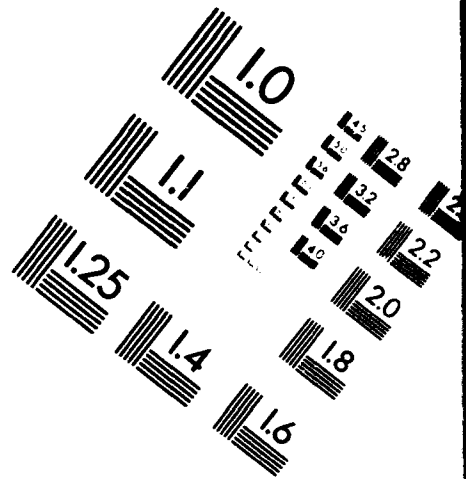
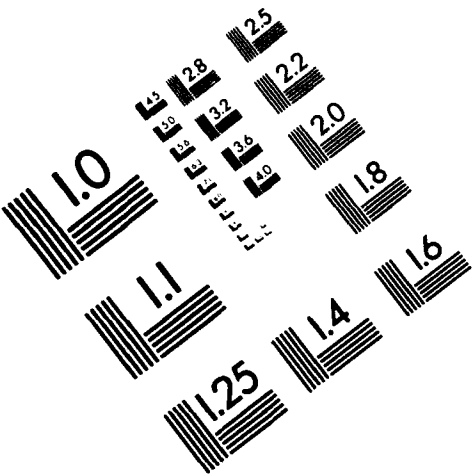


**AIM**

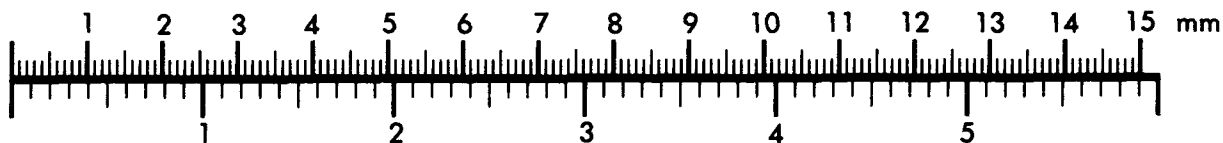
**Association for Information and Image Management**

1100 Wayne Avenue, Suite 1100  
Silver Spring, Maryland 20910

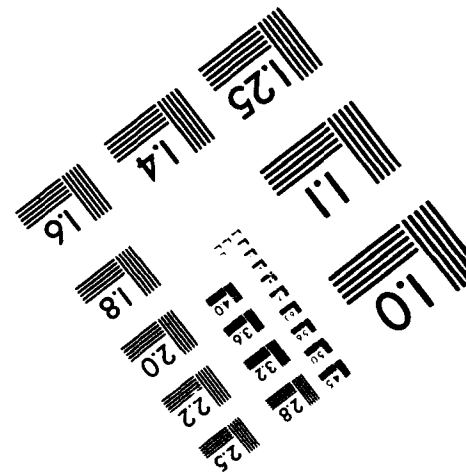
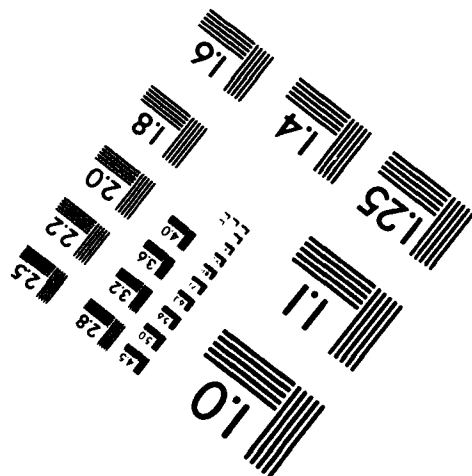
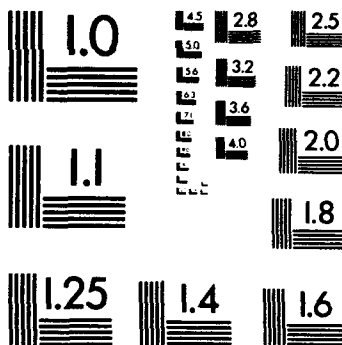
301/587-8202



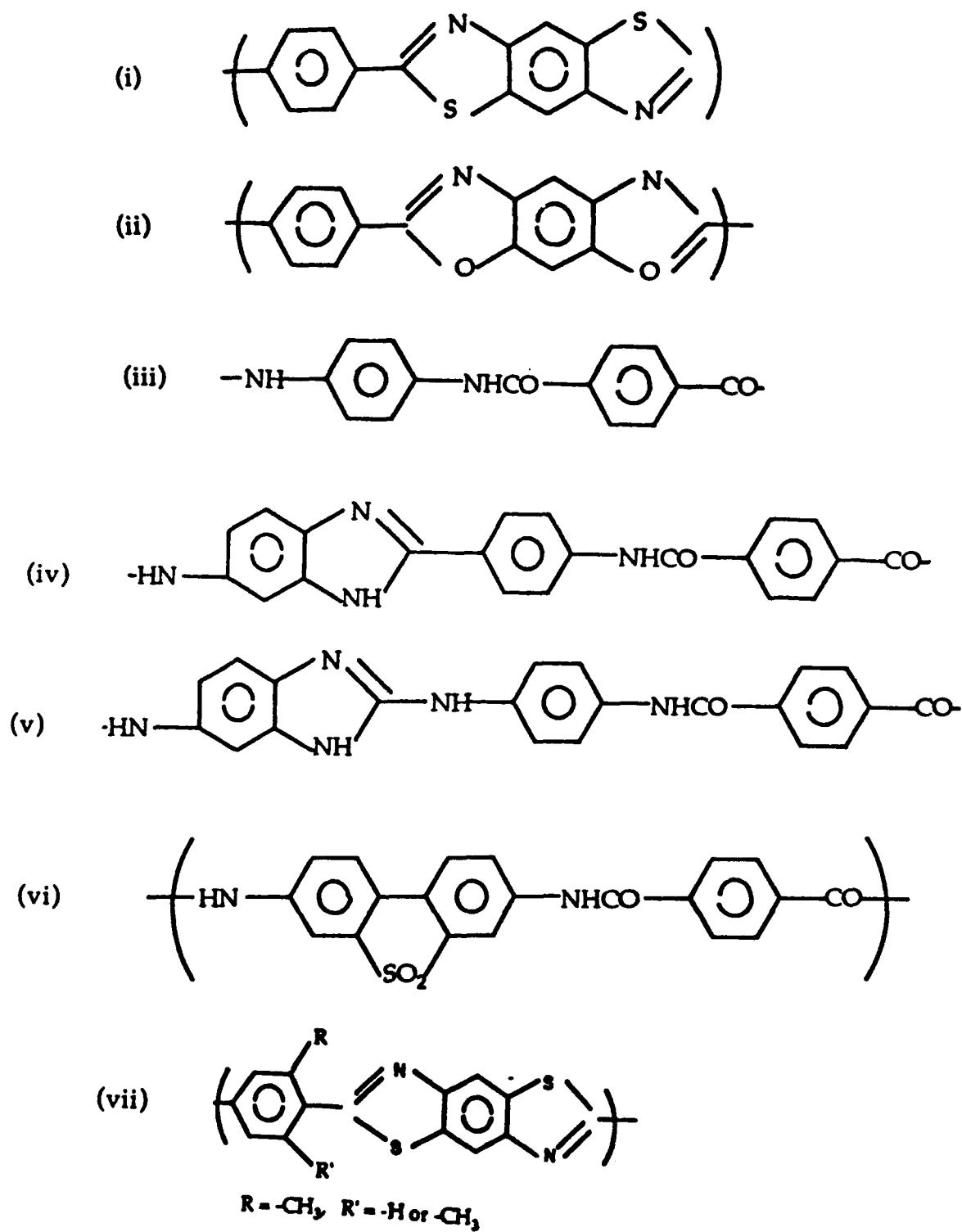
**Centimeter**

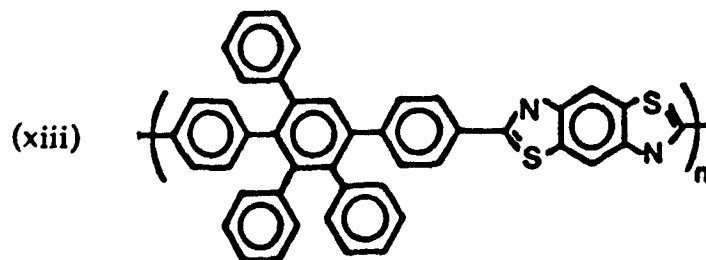
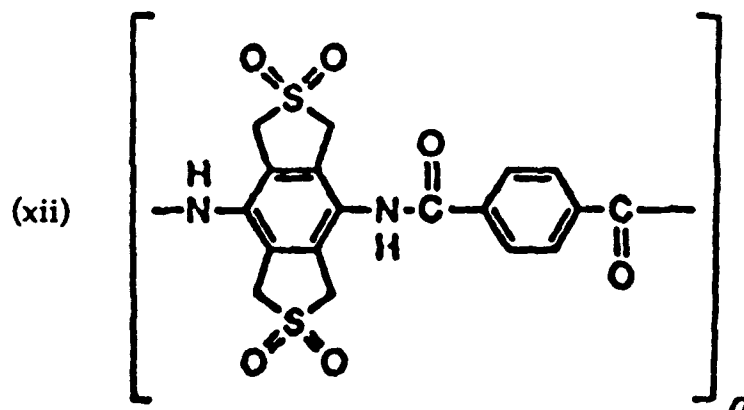
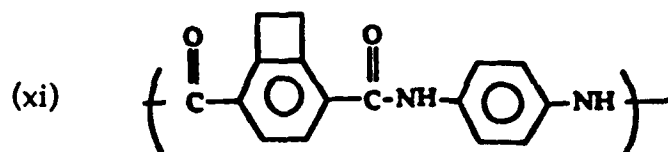
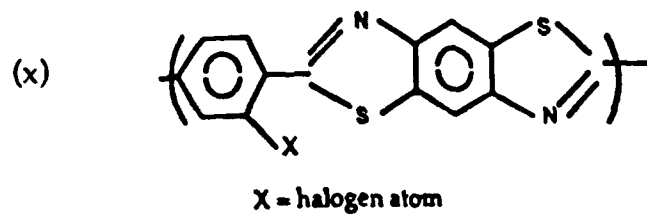
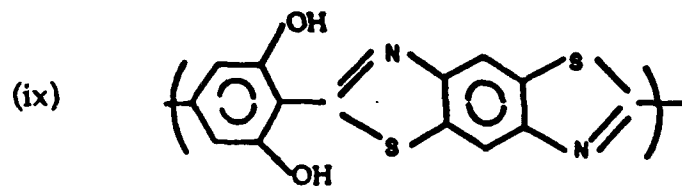
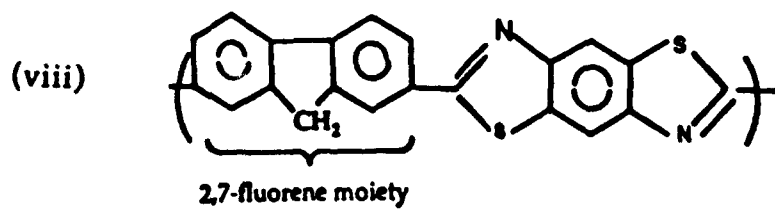


**Inches**

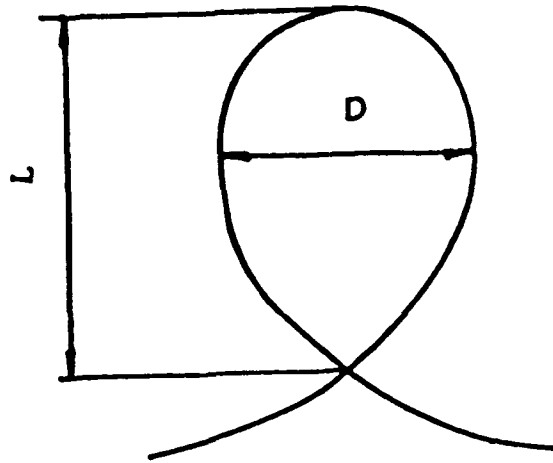


MANUFACTURED TO AIM STANDARDS  
BY APPLIED IMAGE, INC.

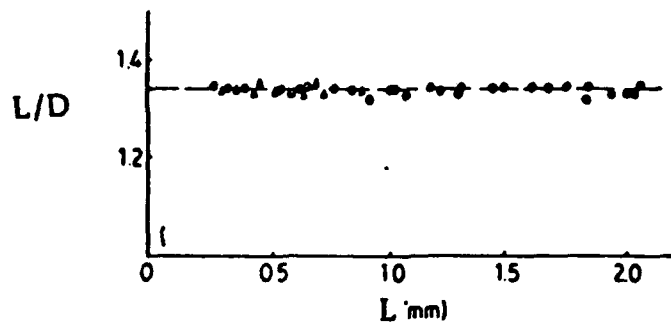




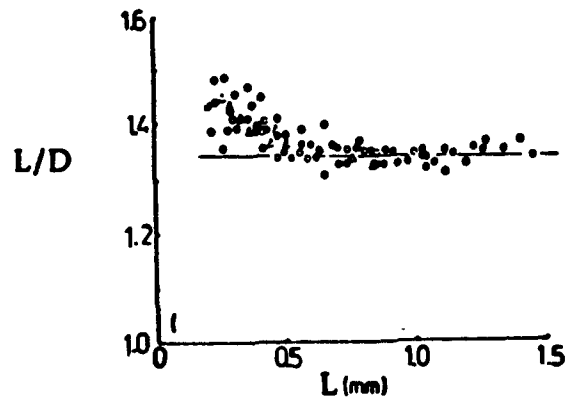
(a)

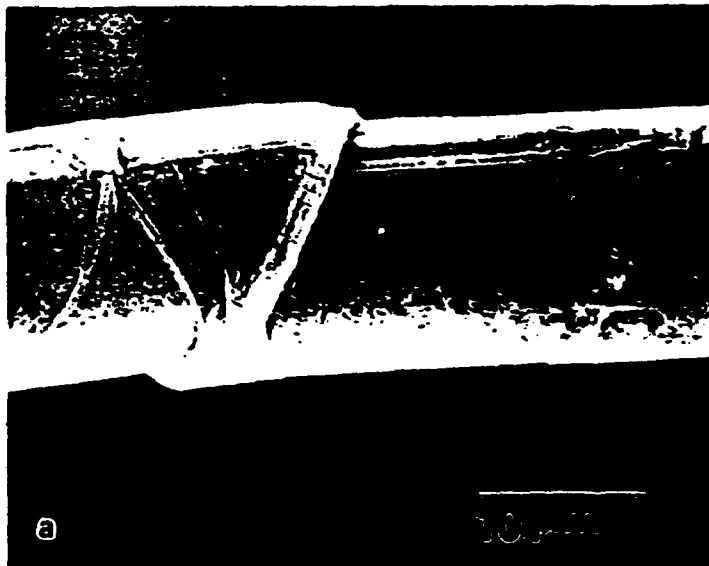


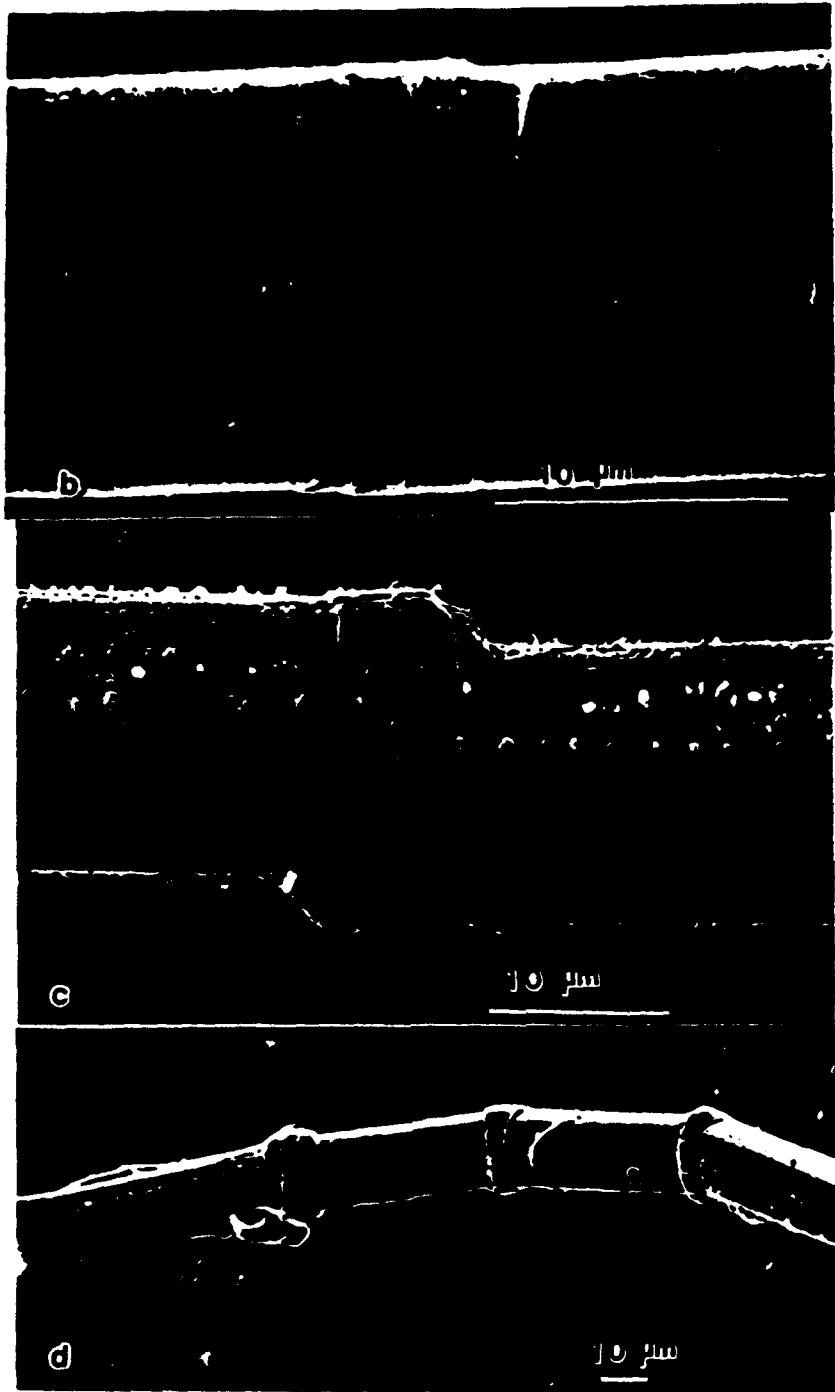
(b)

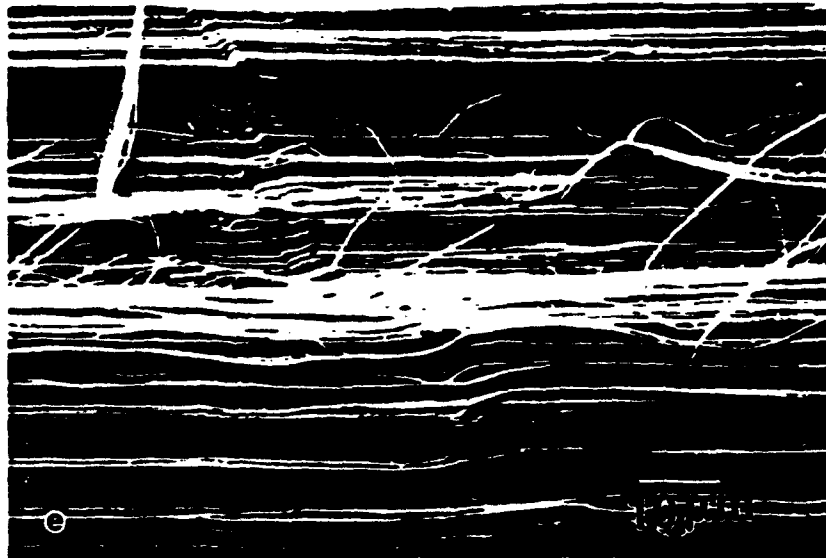


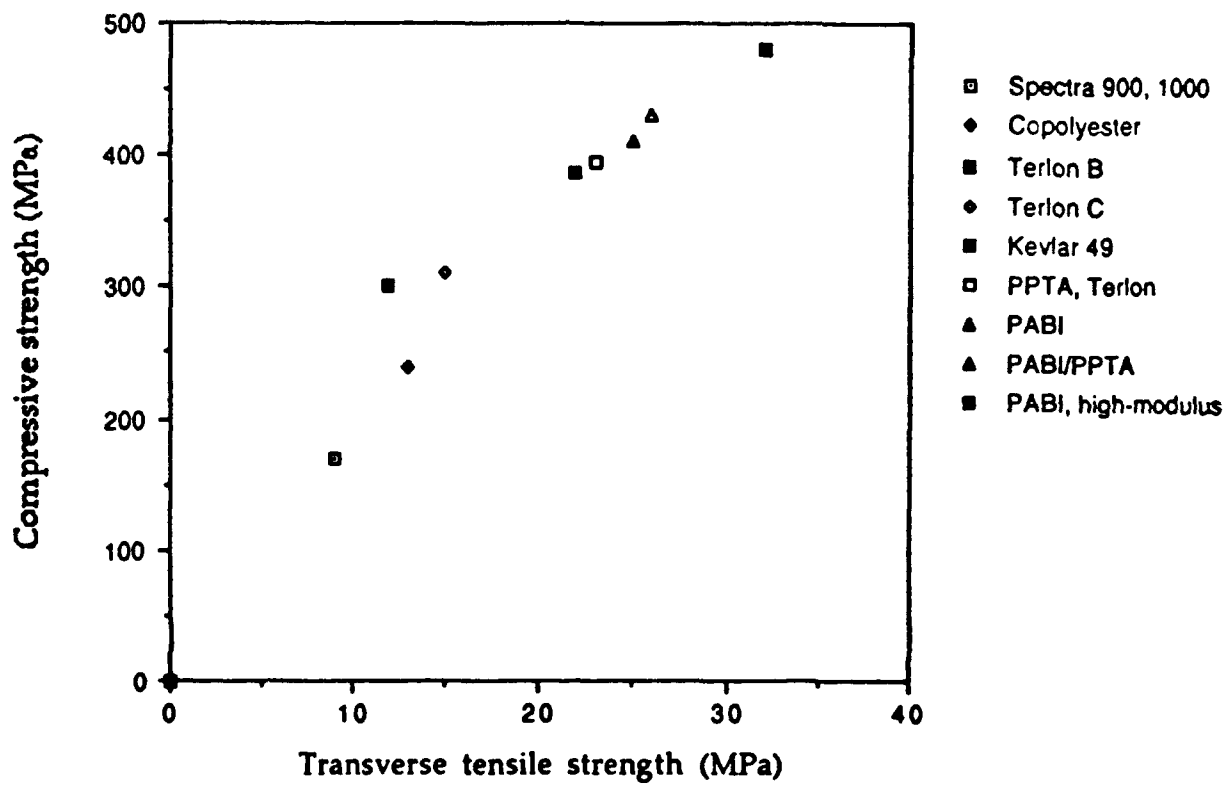
(c)

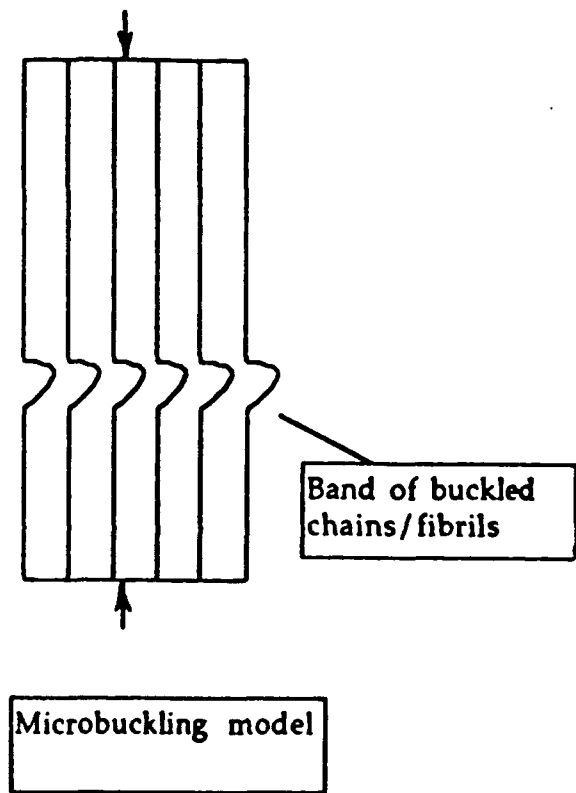
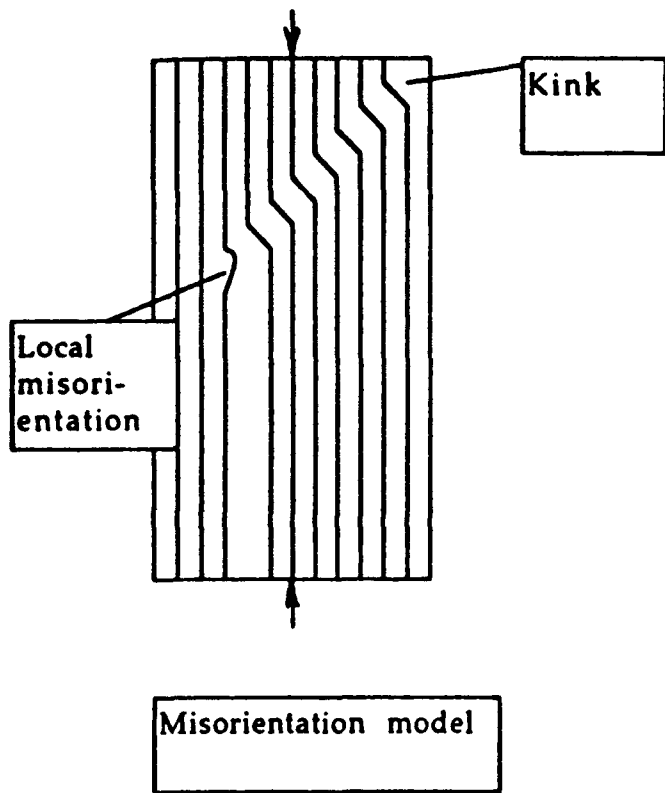


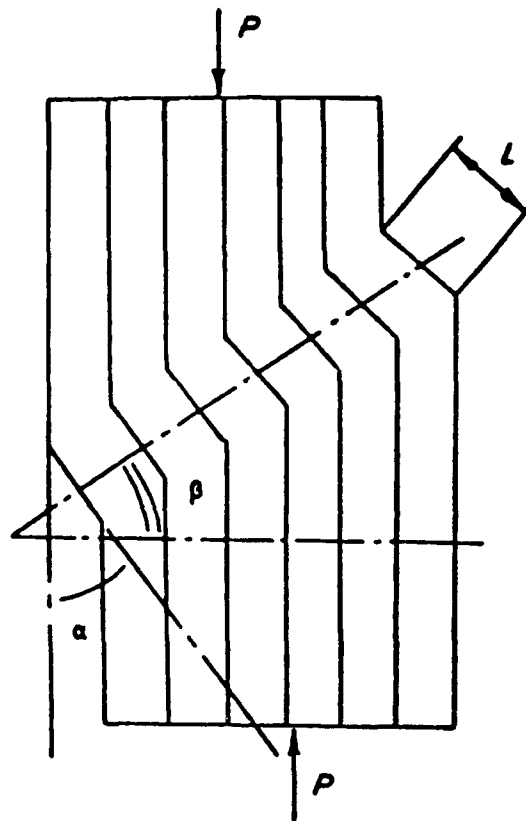












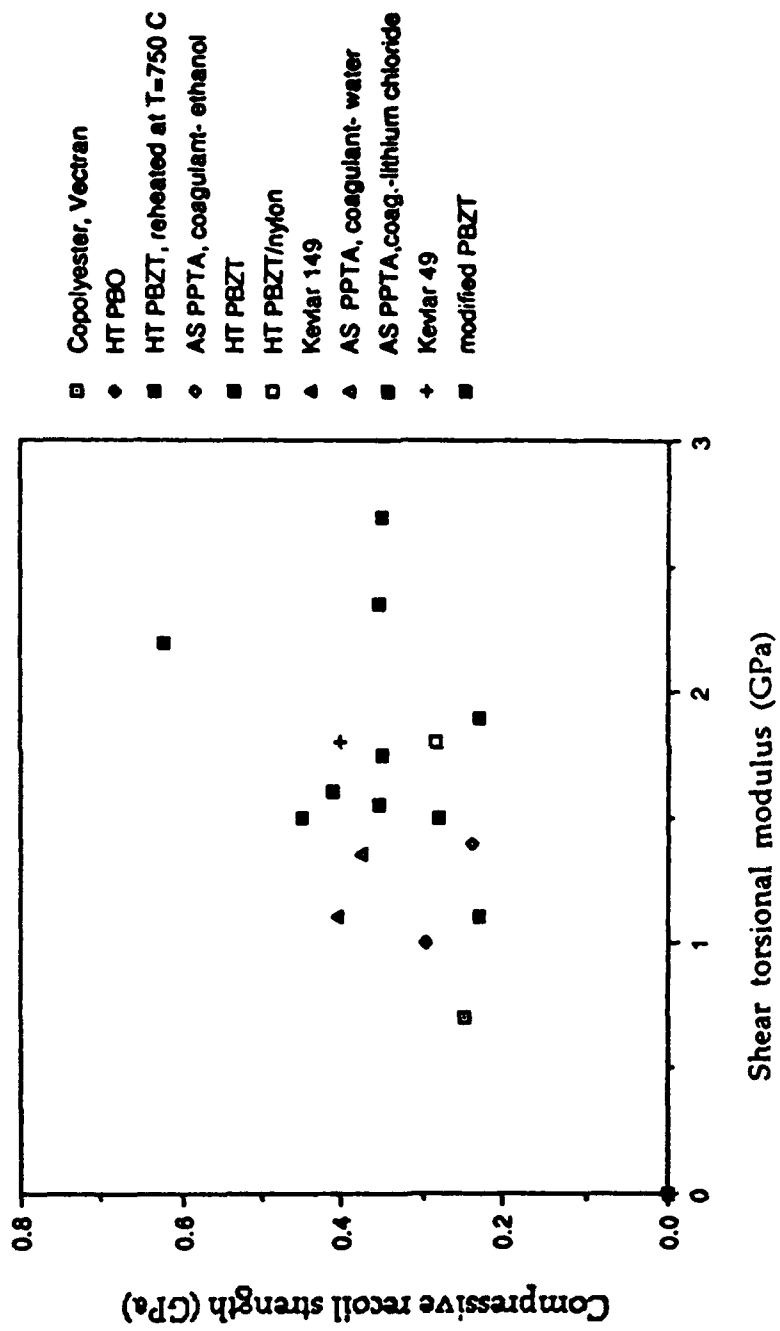


Figure 7.

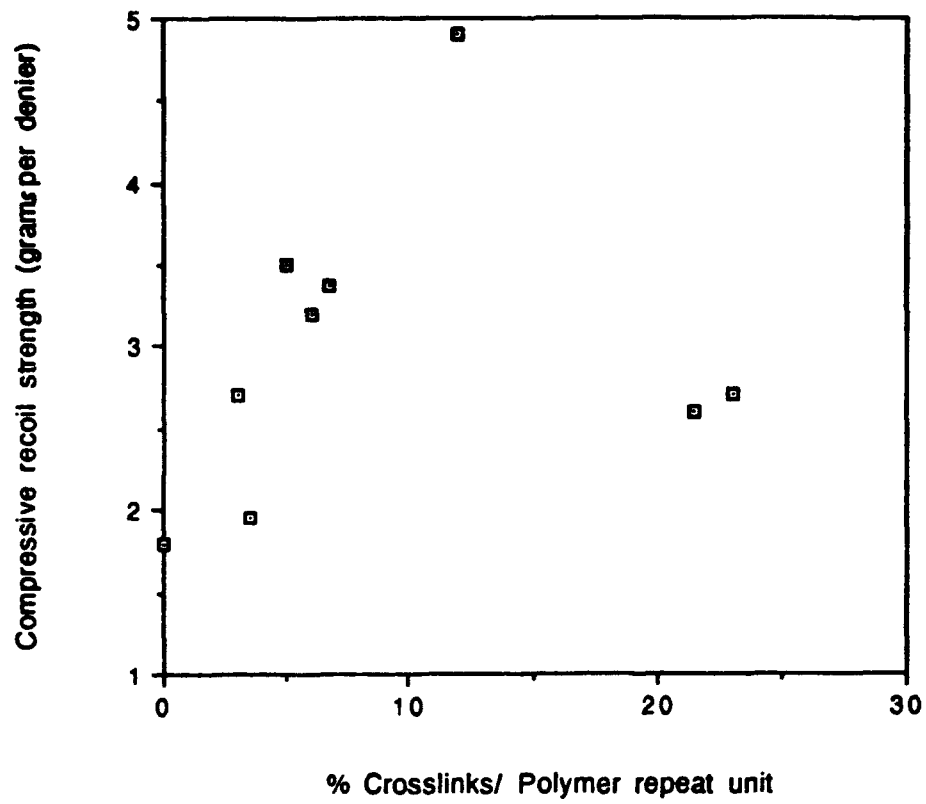


Figure 8.

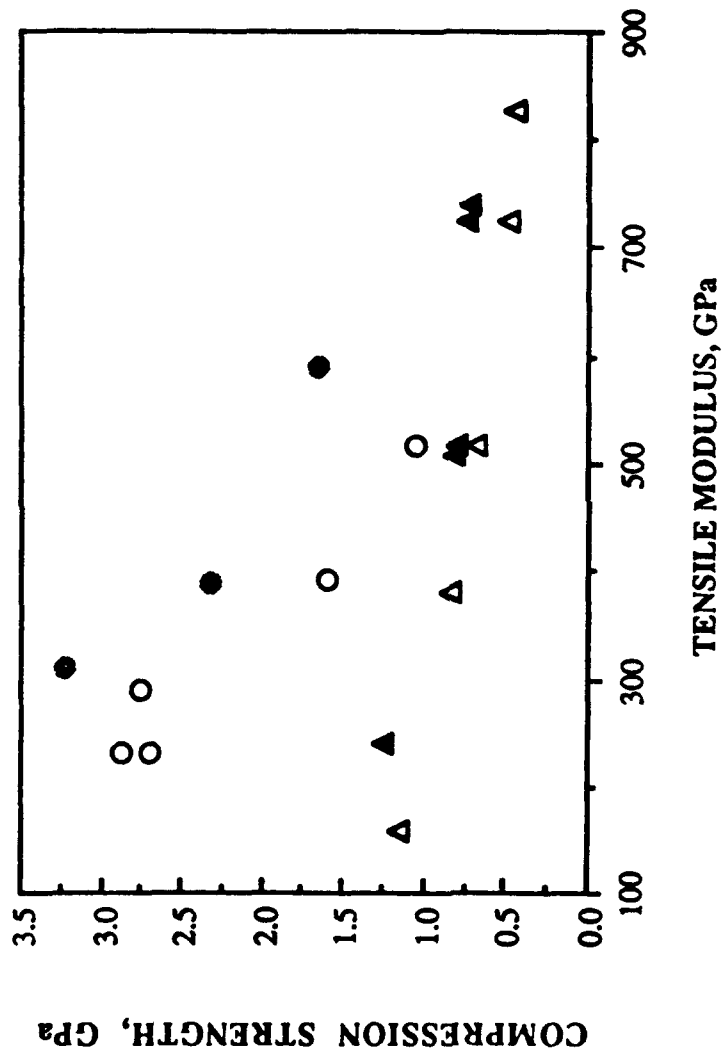
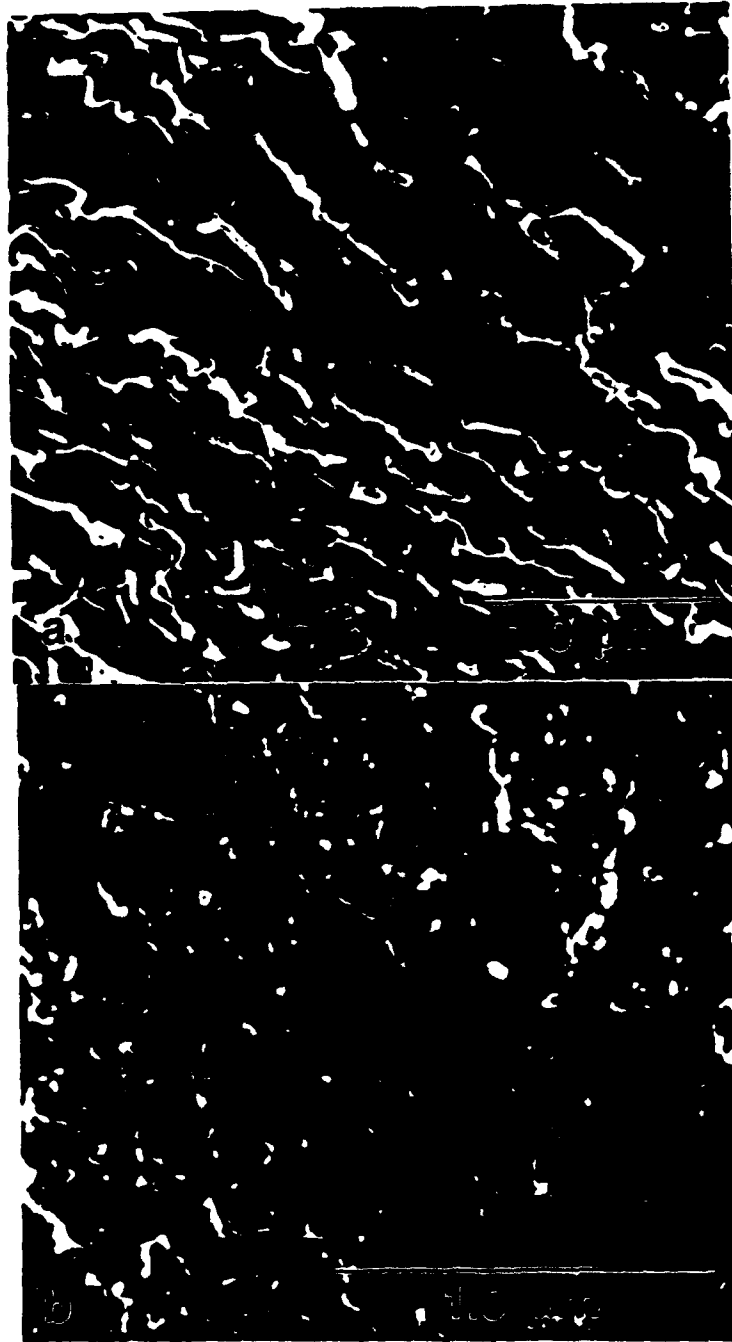


Figure 9.



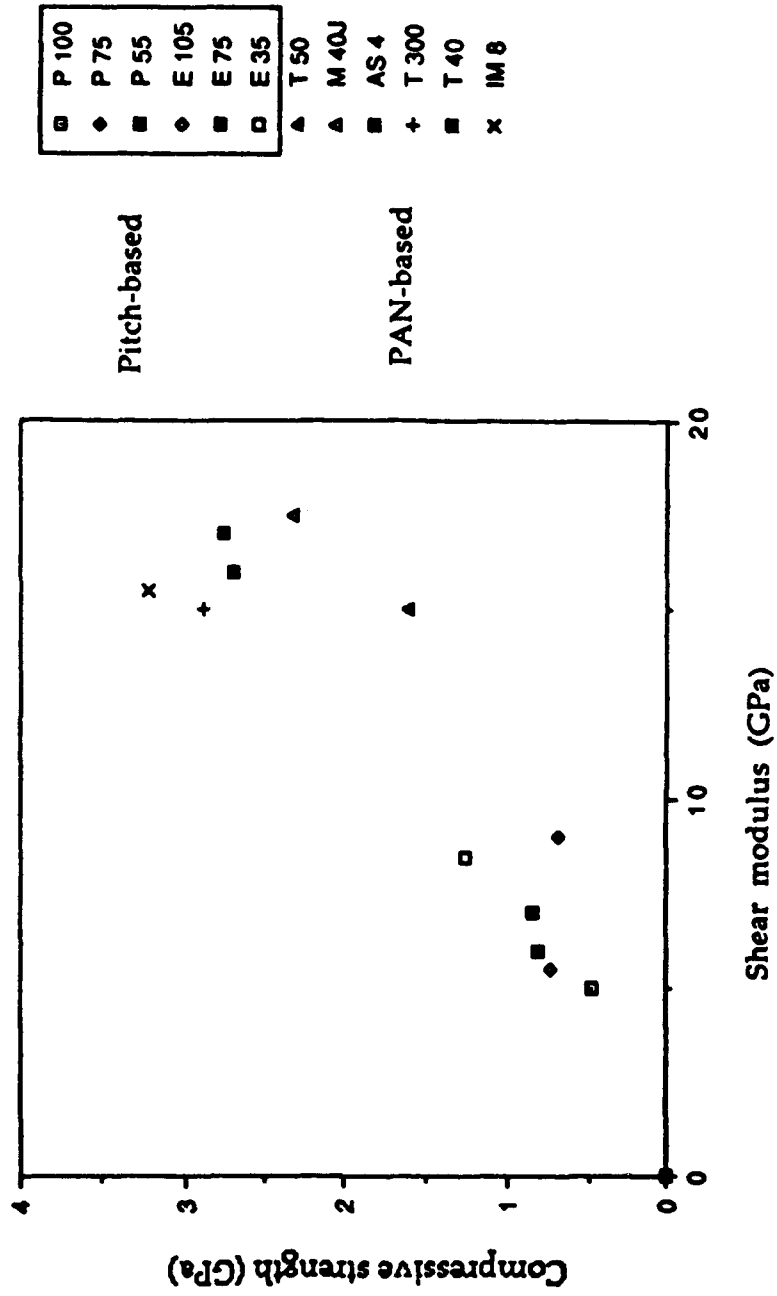


Figure 11.



Part VI  
PBO/SULFURIC ACID INTERACTION

Heat treated PBO fibers were soaked in excess of as received (96%) sulfuric acid. The PBO fibers soaked in excess of sulfuric acid were dried in vacuum oven at 160°C for three hours. TGA scans of PBO and the sulfuric acid exposed PBO samples are given in Figure 1. From the weight loss analysis in specimen 2 in Figure 1, it can be seen that on vacuum drying at 160°C, one sulfuric acid molecule is present in the fiber, per PBO repeat unit. X-ray diffraction data present in the enclosed Table on PBO and PBO/sulfuric acid sample show the presence of additional strong equatorial, meridional, and off-axis reflections in the sample containing sulfuric acid. This clearly suggest that the sulfuric acid forms a co-crystal with the PBO. <sup>13</sup>C NMR spectra of various samples are given in Figure 2. A comparison of the unprotonated carbon spectra for untreated cis PBO and cis PBO/sulfuric acid clearly shows that the field at the carbons attached to the nitrogen is affected, while the carbon attached to the oxygen is not effected. This suggest that sulfuric acid interacts with nitrogen and not with oxygen. A detailed research paper is being written on this work.

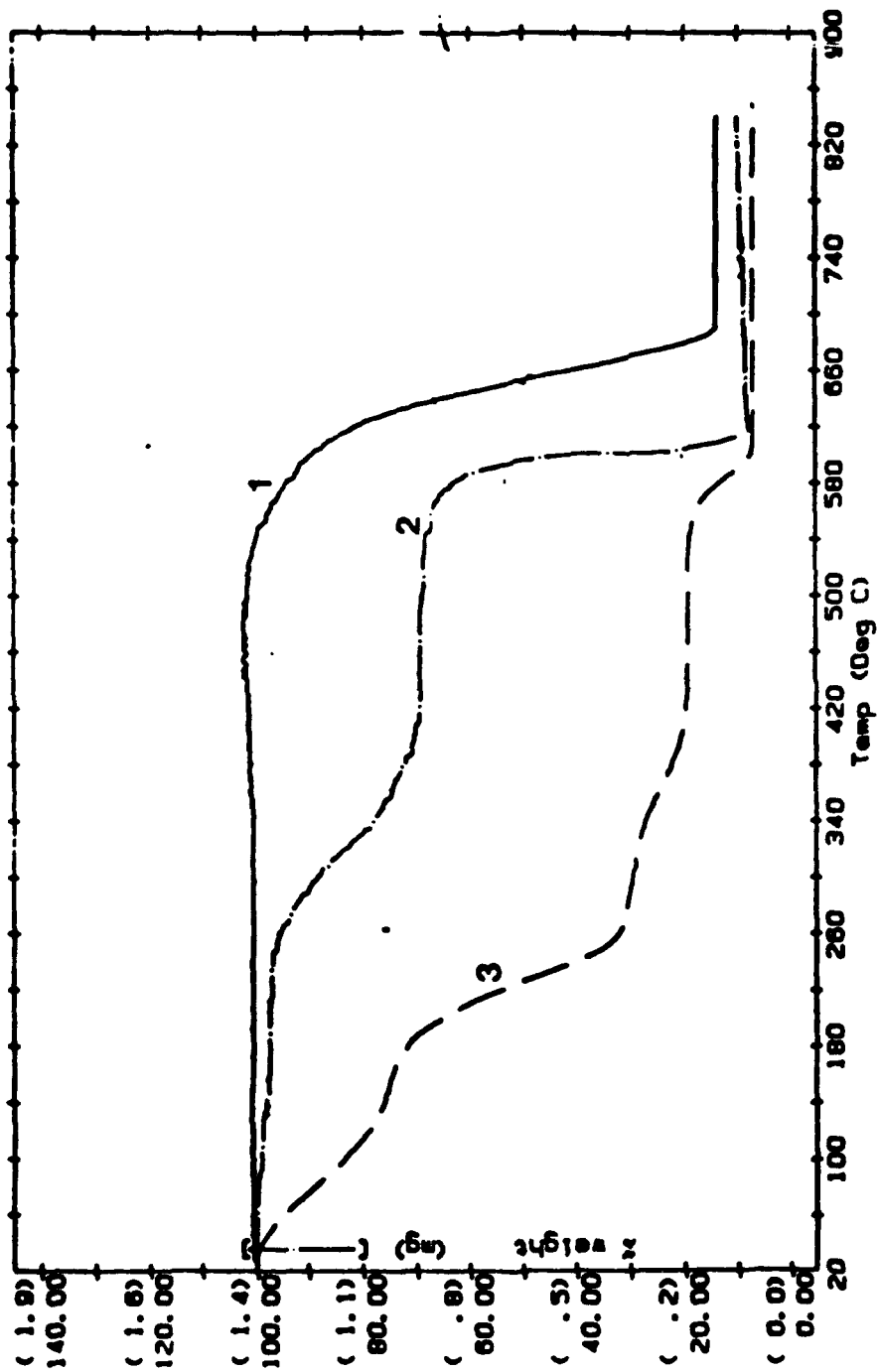


Figure 1. Thermogravimetric analysis of (1) cis-PBO (2) cis-PBO/H<sub>2</sub>SO<sub>4</sub> (vacuum dried at 160°C for three hours, and (3) cis-PBO/H<sub>2</sub>SO<sub>4</sub> (not dried, may contain moisture and excess sulfuric acid).

Table

# X-ray Diffraction Data

## Interatomic Spacings (Å)

Scattering Plane	PBO	Acid-Treated PBO
-----	-----	-----
Equatorial		
(200)	5.59 s	5.59 s 4.72 s
(010)	3.59 s	3.59 s
(210)	3.30 s	3.30 s
(400)	2.75 w	
Meridional		
(001)	12.20 m	12.01 m
(002)		6.05 vs 4.76 w
(003)	4.00 m	4.00 w
(004)	2.92 w	2.92 w
Off-Axis		
	3.16 w	4.60 m

(w, m, s, vs = weak, moderate, strong, very strong intensity)

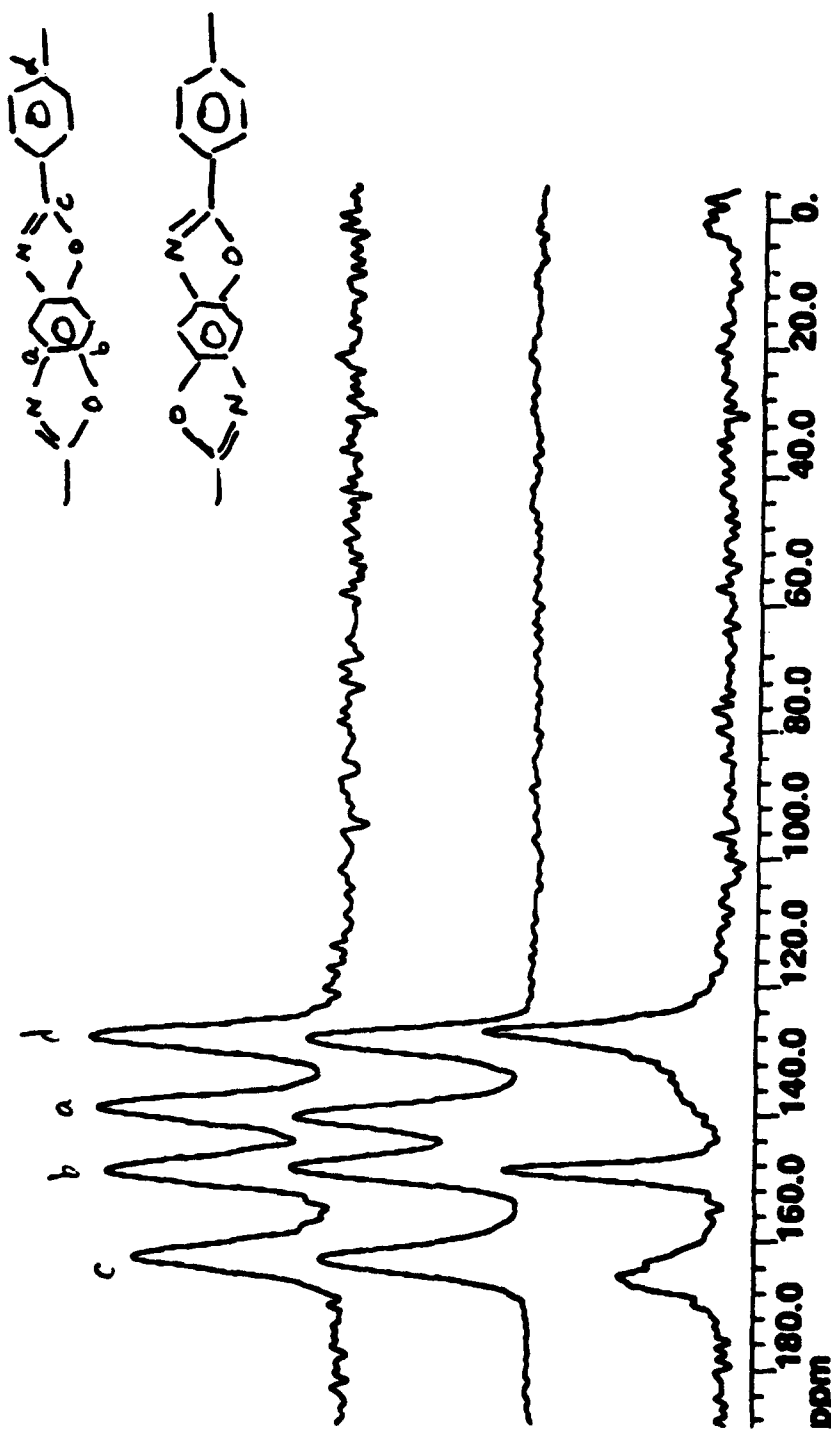


Figure 2a  
**COMPARISON OF 25 MHZ CP SPECTRA (UNPROTONATED CARBONS ONLY) FROM  
 VARIOUS PBO SAMPLES:**  
**TOP = CIS-PBO UNTREATED**  
**MID = TRANS-PBO UNTREATED**  
**BOT = CIS-PBO, SATURATED WITH H<sub>2</sub>SO<sub>4</sub> AND DRIED AT 200 C FOR 3 H.**

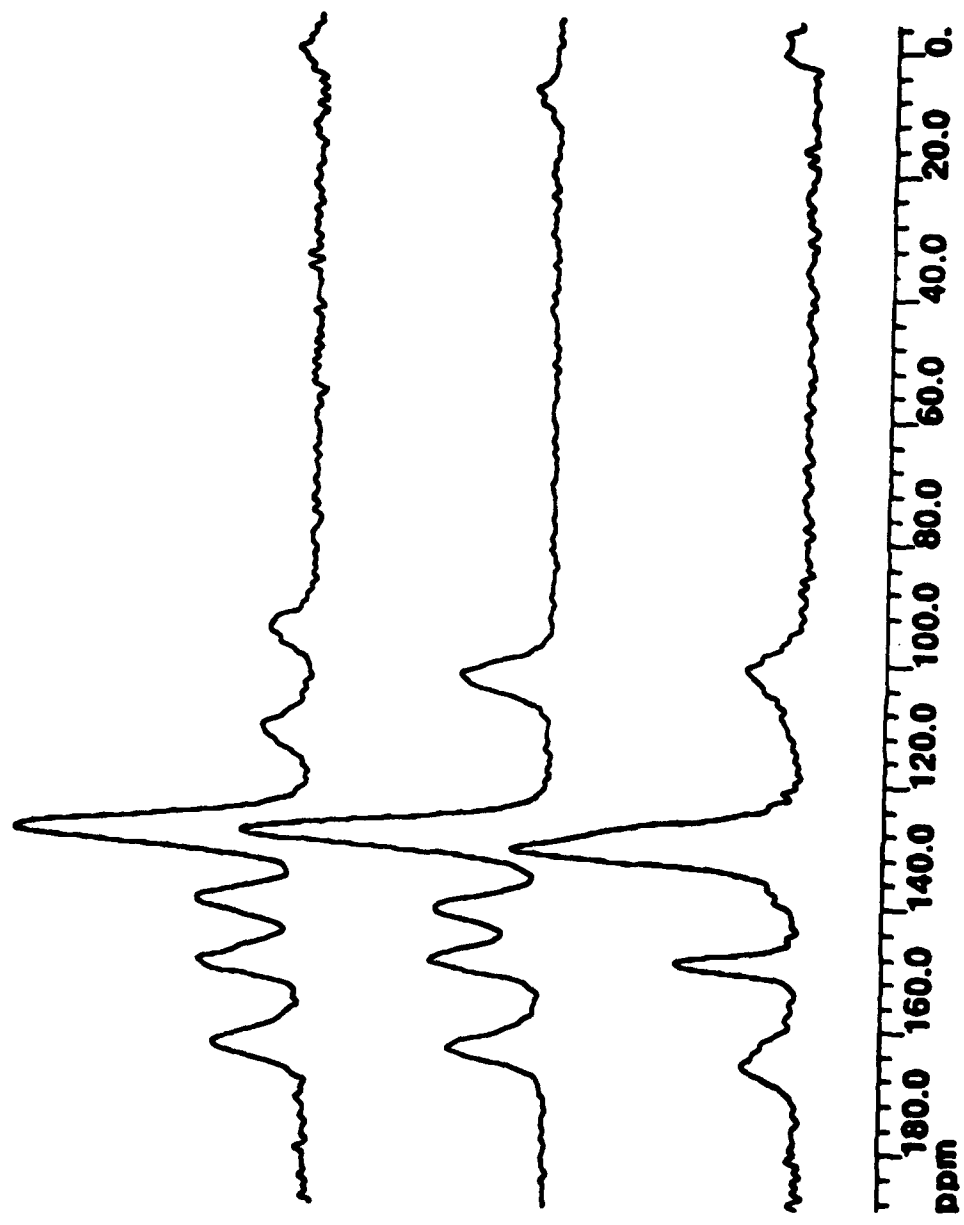


Figure 2b

**COMPARISON OF 25 MHZ CP SPECTRA (1.5 MS CP TIME) FROM VARIOUS PBO SAMPLES:  
TOP = CIS-PBO UNTREATED  
MID = TRANS PBO UNTREATED  
BOT = CIS-PBO, SATURATED WITH H<sub>2</sub>SO<sub>4</sub> AND DRIED AT 200 C FOR 3 H.**